Paleobiology, Biostratigraphy, and Taphonomy of Neoproterozoic Eukaryotes and Cambrian Animals with Carbonaceous Preservation

Qing Tang

Dissertation submitted to the faculty of the Virginia Polytechnic Institute and State University in partial fulfillment of the requirements for the degree of

Doctor of Philosophy
In
Geosciences

Shuhai Xiao
Sterling Nesbitt
Benjamin C. Gill
Brian Romans

October 10, 2018
Blacksburg, Virginia

Keywords: Paleobiology, Biostratigraphy, Taphonomy, Carbonaceous preservation

Paleobiology, Biostratigraphy, and Taphonomy of Neoproterozoic Eukaryotes and Cambrian Animals with Carbonaceous Preservation

Qing Tang

ABSTRACT

Carbonaceous fossil preservation is an important taphonomic window that provides critical perspectives on the evolutionary history of life. However, phylogenetic interpretation of carbonaceous fossils is not straightforward. This is largely because critical biological information is usually lost during fossilization and three-dimensional morphologies are flattened into two-dimensional compressions. Hence, innovative techniques and methods are required in order to better understand the evolutionary significance of these fossils. To achieve this goal, this dissertation is focused on using an array of innovative research techniques to investigate the paleobiology, biostratigraphy, and taphonomy of carbonaceous fossils in critical times of early life evolution, including Neoproterozoic and Cambrian. Chapters 2–5 in this dissertation present original research that helps to decipher hidden biological structures of various carbonaceous fossils using a series of research methods. An improved understanding of these carbonaceous remains will ultimately advance our knowledge regarding the early evolutionary history of life on Earth.

Chapter two describes new cellular structures of the carbonaceous compression macrofossil *Chuaria* using backscattered electron scanning electron microscopy. The data show that *Chuaria*, which is one of the most common fossils in Neoproterozoic and whose phylogenetic interpretation has been uncertain, is likely a multicellular eukaryote. Chapter three is aimed to resolve a long debate on the depositional age of the Gouhou Formation in the Huaibei region of North China and to constrain the Precambrian-Cambrian (P-C) boundary in this area. Using a low manipulation maceration technique, this study reveals a diverse assemblage of organic-walled microfossils from the lower Gouhou Formation, suggesting that the lower Gouhou Formation is Tonian in age and the P-C boundary may be located within the Gouhou Formation. Chapter four reports a group of problematic carbonaceous compression macrofossils from the Hetang Formation in South China. Taphonomic analysis using optical and electron microscopy tentatively suggests that these carbonaceous macrofossils are probably carapaces of bivalved arthropods. The last chapter describes a group of sponge fossils with carbonaceous preservation from the early Cambrian Hetang Formation in South China. Using an array of electron microscopy techniques, this study reveals that siliceous spicules of the Hetang sponges have large axial filaments and large proportions of organic material, suggesting early sponge in the Precambrian and Cambrian may have had weakly mineralized or entirely organic skeletons. Results from this study helps to reconcile the apparently conflicting molecular clocks, biomarker fossils, and spicular fossils of early sponges.

GENERAL AUDIENCE ABSTRACT

Carbonaceous fossils can provide important information about the life on Earth in deep time. However, biological interpretation of carbonaceous fossils is not always straightforward, largely because critical biological information is usually lost during fossilization. To address this matter, this dissertation presents original research that helps to decipher hidden biological structures of various carbonaceous fossils using a series of innovative research techniques and methods. Specifically, Chapter two describes new cellular structures of the carbonaceous compression macrofossil *Chuaria* using backscattered electron scanning electron microscopy. The data show that *Chuaria*, which is one of the most common fossils in Neoproterozoic and whose biological interpretation has been uncertain, is likely a multicellular eukaryote. Chapter three is aimed to resolve a long debate on the depositional age of the Gouhou Formation in the Huaibei region of North China and to constrain the Precambrian-Cambrian (P-C) boundary in this area. Using a low manipulation maceration technique, this study reveals diverse organic-walled microfossils from the lower Gouhou Formation, suggesting that the lower Gouhou Formation is Tonian in age and the P-C boundary may be located within the Gouhou Formation. Chapter four reports a group of problematic carbonaceous compression macrofossils from the Hetang Formation in South China. This study, using optical and electron microscopy, suggests that these carbonaceous macrofossils are probably carapaces of bivalved arthropods. The last chapter describes a group of sponge fossils with carbonaceous preservation from the early Cambrian Hetang Formation in South China. Using an array of electron microscopy techniques, this study reveals that the Hetang sponges developed spicules with large proportions of organic material, suggesting early sponge in the Precambrian and Cambrian may have had weakly mineralized or entirely organic skeletons. Therefore, an improved understanding of these carbonaceous remains presented in this dissertation will ultimately advance our knowledge regarding how the early life on Earth evolved through time.

DEDICATION

I dedicate this work to my mother, father, wife, and brother, who have been tremendously supportive to me and keep me mindful of the past and present, and more importantly, hopeful about the future.

ACKNOWLDEGEMENTS

I would like to thank those who have supported my pursuit of education; contributed to my development as a scientist; and played a role in my personal establishment. Certainly, it is impossible to acknowledge all the help I have received through the years. Still, I would like to take this opportunity to acknowledge and thank, in no particular order, the following exceptional people for their support:

- My mother, Lianxiu Chen, who dedicated all her life to her family.
- My farther, Cunde Tang, who taught me to be a good person with patience, diligence, and perseverance.
- My wife, Yuli Yang. I feel so lucky and thankful to meet her and marry with her on the campus.
- My little brother, Li Tang, who I spent memorable childhood with and takes more responsibility than me to take care of our parents ever since I studied abroad.
- My fellow graduate students—particularly those in paleontology, including Andrew (Drew 1) Hawkins, Anthony (Drew 2) Muscente, Natalia Bykova, Chris Griffin, Caitlin Colleary, Candice Stefanic, Krista Koeller, Mitchell Riegler, Kiersten Formoso, Dana Korneisel, Devin Hoffman, Brenen Wynd, Morrison Nolan, as well as visiting scholars in the paleo-group Zhou Wang, Wei Wang, Junfeng Guo, Ke Pang, Bin Wan, Qin Ye, Fanfan Kong, and Juliana Okubo—for fun conversations, scientific discussions, constructive feedbacks, and good, peaceful times.
- The teachers, professors, and mentors who were instrumental in my education from primary school to college.
- My PhD committee: Sterling Nesbitt, Ben Gill, and Brian Romans.
- My co-authors and collaborators—Ke Pang, Bin Wan, Xunlai Yuan, Chuanming Zhou, Jie Hu, Guwei Xie, Leimin Yin, Jinlong Wang, Zhe Chen, and Anthony Drew Muscente—who contributed to the work in this dissertation.
- The faculty and staff in the Virginia Tech Department of Geosciences, particularly Michelle Stocker, Connie Lowe, and April Newcomer.
- Xunlai Yuan, who introduced me to the world of Precambrian paleontology, encouraged my pursuit of PhD abroad, and has continued to support my professional development.
- Last but not least, my advisor Shuhai Xiao, who led me to the geobiology world, gave me the opportunity of studying abroad, and has been extremely generous, particularly with his time and knowledge, as an academic adviser, professional mentor, and respected friend.

ATTRIBUTIONS

Chapter Two, or "Electron microscopy reveals evidence for simple multicellularity in the Proterozoic *Chuaria*", was published in *Geology*, 2017, volume 45, pages 75–78, by Q. Tang, K. Pang, X. Yuan, and S. Xiao. Q. Tang and S. Xiao conceived the project. Q. Tang, K. Pang, and X. Yuan collected materials. Q. Tang collected all data. Q. Tang and S. Xiao developed the manuscript with contributions from K. Pang and X. Yuan.

Chapter three is an updated version of the paper "Organic-walled microfossils from the Tonian Gouhou Formation, Huaibei region, North China Craton, and their biostratigraphic implications", which was published in *Precambrian Research*, 2015, volume 266, page 296–318, by Q. Tang, K. Pang, S. Xiao, X. Yuan, and B. Wan. X. Yuan, S. Xiao, and Q. Tang conceived the project, Q. Tang, K. Pang, B. Wan, and X. Yuan collected materials, Q. Tang collected all data, Q. Tang and S. Xiao developed the manuscript with contributions from K. Pang, X. Yuan, and B. Wan.

Chapter four has been submitted and is under review in *Journal of Paleontology*. The initial title of the publication is "A problematic animal fossil from the early Cambrian Hetang Formation, South China". Co-authors in the manuscript include J. Hu, G. Xie, X. Yuan, B. Wan, C. Zhou, X. Dong, G. Cao, and S. Xiao. S. Xiao and Q. Tang conceived the project, Q. Tang, J. Hu, G. Xie, X. Yuan, B. Wan, and C. Zhou collected materials, Q. Tang, X. Dong, and J. Hu collected data. Q. Tang and S. Xiao developed the manuscript with contributions from G. Cao, X. Dong.

Chapter five has been submitted for publication. Tentative title for the manuscript is "Spiculogenesis and biomineralization in early sponge animals" and my co-authors in the manuscript are B. Wan, X. Yuan, A.D. Muscente, and S. Xiao. Q. Tang and S. Xiao conceived the project, Q. Tang, B. Wan, and X. Yuan collected materials. Q. Tang collected all data. Q. Tang and S. Xiao developed the manuscript with contributions from B. Wan and X. Yuan, and A.D. Muscente.

TABLE OF CONTENTS

LIST OF FIGURES

Chapter 2

Chapter 3

LIST OF TABLES

Chapter 5

GRANT INFORMATION

Chapter 2

This work was supported by the U.S. National Science Foundation (grant EAR-1528553), the National Natural Science Foundation of China (grants 41272011, 41602007), the Geological Society of America, Sigma Xi, the Chinese Ministry of Science and Technology (grant 2013CB835000), the Chinese Academy of Sciences (grant KZZD-EW-02, KZCX2-YW-153), the Science Foundation of Jiangsu Province of China (grant BK20161090), and the State Key Laboratory of Palaeobiology and Stratigraphy (grant 20162109).

Chapter 3

This research was supported by National Natural Science Foundation of China (41272011 and 41130209), Chinese Ministry of Science and Technology (2013CB835000), Chinese Academy of Sciences (KZZD-EW-02 and KZCX2-YW-153), U.S. National Science Foundation (EAR-1250800), and American Association of Stratigraphic Palynologists.

Chapter 4

This research was supported by National Science Foundation (EAR 1528553), NASA Exobiology and Evolutionary Biology (NNX15AL27G), National Natural Science Foundation of China (41502010), Geological Society of America, Paleontological Society, and Society for Sedimentary Geology.

Chapter 5

This research was supported by National Science Foundation (EAR 1528553), NASA Exobiology and Evolutionary Biology Program (NNX15AL27G), National Natural Science Foundation of China (41130209), and Chinese Academy of Sciences (QYZDJ-SSW-DQC009).

CHAPTER 1

Overview of Neoproterozoic eukaryotes and Cambrian animals preserved as carbonaceous compressions

QING TANG

Department of Geosciences, Virginia Tech, Blacksburg, VA 24060, USA

1.1 Introduction

All organisms on Earth contain organic biomolecules, making organic matter the most common fossil material (Muscente et al., 2017a). This organic matter can be preserved and often compressed as kerogen films in various fossils of micro- and macroscopic protists, algae, plants, and animals. Therefore, carbonaceous compression fossils provide important perspectives on the evolutionary history of life on Earth, particularly on the rise of eukaryotes and the radiation of animals (Muscente et al., 2017b).

Exploration of carbonaceous fossils and their taphonomic mechanism are active research topics in the study of early eukaryotes and animals. Carbonaceous fossil preservation is particularly common in early Neoproterozoic (Tonian, 1000 Ma to ca. 720 Ma) when eukaryotes consisted predominantly of unicellular/multicellular protists and algae that have not yet evolved mineralized skeletons (Jankauskas et al., 1989; Xiao and Tang, 2018). The majority of these organisms were decomposed soon after their death, but recalcitrant organic matter could evade complete degradation. The surviving organic remains were transformed to kerogen via *in situ* diagenetic polymerization (also known as kerogenization) (Briggs, 2003; Cai et al., 2012), resulting in carbonaceous compression fossils. Even in the Cambrian, after many animals evolved mineralized skeletons (Erwin and Valentine, 2013), many animal fossils are preserved as carbonaceous compressions, e.g. in Burgess Shale-type assemblages (Holmes et al., 2018). This is because their hard skeletons were easily demineralized in early diagenesis with only carbonaceous residue left behind and transformed into a cohesive and stable carbonaceous compression by way of diagenetic polymerization (Muscente and Xiao, 2015; Muscente et al., 2017a).

Although the taphonomic processes responsible for carbonaceous fossil preservation have not been fully understood, biological interpretation of two-dimensionally compressed carbonaceous fossils is a greater challenge, hampering our ability to take full advantage of the rich paleontological record of carbonaceous compression fossils. This is largely because critical biological and anatomic information may be modified or lost during burial diagenesis, including bacteria decomposition, sediment compaction, metamorphic alteration, and demineralization. The phylogenetic affinities of morphologically simple carbonaceous fossils, such as organic-walled leiospheres and chuariids, are even more difficult to interpret (Xiao et al., 2002; Tang, 2013; Ye et al., 2015). In addition, organic-walled acritarchs preserved in fine grained siliciclastics (e.g. shale and mudstone) are usually vulnerable to fragmentation when extracted using traditional palynological maceration techniques (Grey and Sugitani, 2009), further adding to the difficulty of their phylogenetic interpretation.

Therefore, in order to unlock the hidden biological information from Neoproterozoic–Cambrian carbonaceous compression fossils, innovative methods for studying the paleobiology, biostratigraphy, and taphonomy of these carbonaceous fossils must be applied or developed. The four research projects of this dissertation are case studies on fossil eukaryotes and animals with traces of carbonaceous preservation. Specifically, the work in chapter 2, published as "Electron microscopy reveals evidence for multicellularity in the Proterozoic fossil *Chuaria*" in Geology (Tang et al., 2017), pertains to new evidences, as revealed by backscattered electron scanning electron microscopy (BSE-SEM), for the multicellular eukaryote affinity of the Tonian problematic fossil *Chuaria*, which is one of the most ubiquitous Proterozoic carbonaceous fossils. Although simple multicellularity have evolved no later than the Paleoproterozoic (Hofmann, 1976; Schirrmeister et al., 2013), complex multicellular organisms with cellular and tissue

differentiation did not appear until the Mesoproterozoic (Butterfield, 2000), and did not become ecologically important until the Ediacaran (635−541 Ma) (Yuan et al., 2011; Xiao et al., 2014a). In the intervening Tonian Period, however, multicellular organisms are poorly documented in fossil record. To address this knowledge gap, we investigated *Chuaria* and associated carbonaceous compression fossils from the Tonian Liulaobei Formation in North China. Our analysis using BSE-SEM revealed direct evidence of simple multicellularity in some of these fossils and indicates that *Chuaria* may have had a multicellular vegetative stage in its life cycle. This investigation demonstrates that BSE-SEM has the potential to unveil the hidden diversity of multicellular organisms in the Tonian Period, thus enriching our knowledge on the multiple origins of multicellularity before Cryogenian glaciations.

The study reported in chapter 3 is focused on biodiversity and biostratigraphy of the Gouhou Formation in North China, using a low manipulation maceration technique which is effective in recovering organic-walled microfossils with minimal damage. In particular, the work in chapter 3—an updated version of our paper published as "Organic-walled microfossils from the Tonian Gouhou Formation, Huaibei region, North China Craton, and their biostratigraphic implications" in Precambrian Research (Tang et al., 2015)—explores the biodiversity and biostratigraphy of organic-walled microfossils from the lower Gouhou Formation. The depositional age of the Gouhou Formation has been a matter of controversy, and this stratigraphic unit has been variously interpreted as Cambrian (Xing, 1989; Zang and Walter, 1992), Cryogenian−Ediacaran (Cao, 2000), or Tonian in age (Xiao et al., 2014b). This ambiguity hinders our ability to take full advantages of the rich geological and paleontological history record in the Gouhou Formation. To address this controversy, we carried out a systematic study of organic-walled microfossils from the Gouhou Formation. Our study revealed a diverse

assemblage of organic-walled microfossils from the Gouhou Formation. Importantly, the co-occurrence of *Trachyhystrichosphaera*, *Valeri*a, and *Dictyosphaera* from the lower Gouhou Formation suggests a likely Tonian age. However, a depositional hiatus has been identified between the lower and middle-upper members of the Gouhou Formation, and recent detrital zircon geochronology has shown that the middle Gouhou Formation is probably early Cambrian in age (He et al., 2017). Hence, integrated biostratigraphic, geochronologic, and sedimentological data indicate that the Precambrian-Cambrian boundary may be placed between the lower and middle-upper members of the Gouhou Formation with an infra-Cambrian depositional gap of >200 myr, perhaps driven by a major tectonostratigraphic event.

Because carbonaceous remains of metazoans (e.g. Burgess Shale-type assemblages) comprise a major source of the Cambrian fossils (Holmes et al., 2018), the hidden biological and anatomic information of these carbonaceous fossils is key to understand the early evolutionary history of eukaryotes and animals. The research projects described in chapter 4 and 5 were designated to focus on carbonaceous animal fossils from the early Cambrian Hetang Formation in South China. Specifically, the study in chapter 4 is focused on a problematic animal fossil with carbonaceous preservation from the Hetang Formation, which is well-known for its preservation of the earliest articulated sponge fossils (Chen et al., 2004; Xiao et al., 2005). However, metazoan fossils other than sponges are poorly documented from this stratigraphic interval, resulting in an incomplete picture of the Hetang biota and limiting its contribution to the understanding of the early evolution of animals. Our study describes a new animal taxon, *Cambrowania ovata* new genus new species, from the middle Hetang Formation in the Lantian area, South China. A comprehensive analysis using reflected light microscopy, scanning electron microscopy, energy dispersive X-ray spectroscopy, and micro-CT reveals that the new species is

characterized by a fusoidal to ovoidal truss-like structure consisting of rafter-like crossbar, and is interpreted as a spherical vesicle or more likely a carapace of bivalve arthropods. Although the phylogenetic affinity remains problematic, the new species adds to the taxonomic diversity of the Hetang biota that is otherwise dominated by benthic sponges.

As mentioned above, the Hetang biota is predominately comprised of sponge fossils, many of which are preserved as demineralized carbonaceous compressions. The work in chapter 5 is focused on these organic remains from the Hetang Formation. As sponges are among the earliest animals with biomineralized skeletons, they have the potential to provide critical implications on the early evolution of metazoans. However, the development of biomineralized spicules in early sponges is poorly understood so far. This is largely because fine organic structure of spicules and particularly the axial filament that catalyzes biomineralization in siliceous sponges are rarely preserved in the fossil record. Our study reveals that some early Cambrian sponges developed spicules that contain disproportionately large amount of organic material. We infer that early sponges may have had only weakly mineralized spicules and thus poor fossilization potential. Out study indicate that, although sponge classes may have diverged in the Cryogenian Period (Gold et al., 2016), biomineralized spicules likely evolved later and independently among sponge classes.

1.2 References

Briggs, D.E.G., 2003, The role of decay and mineralization in the preservation of soft-bodied fossils: Annual Review of Earth and Planetary Sciences, v. 31, p. 275–301.

Butterfield, N.J., 2000, *Bangiomorpha pubescens* n. gen., n. sp.: Implications for the evolution of sex, multicellularity, and the Mesoproterozoic/Neoproterozoic radiation of eukaryotes: Paleobiology, v. 26, p. 386–404.

Cai, Y., Schiffbauer, J.D., Hua, H., and Xiao, S., 2012, Preservational modes in the Ediacaran Gaojiashan Lagerstätte: Pyritization, aluminosilicification, and carbonaceous compression: Palaeogeography Palaeoclimatology Palaeoecology, v. 326–328, p. 109–117.

Cao, R., 2000, Discussion on some problems in the Mesoproterozoic and Neoproterozoic stratigraphical study in China: Journal of Stratigraphy, v. 24, p. 247–254.

Chen, Z., Hu, J., Zhou, C., Xiao, S., and Yuan, X., 2004, Sponge fossil assemblage from the Early Cambrian Hetang Formation in southern Anhui: Chinese Science Bulletin, v. 49, p. 1625–1628.

Erwin, D.H., and Valentine, J.W., 2013, The Cambrian Explosion: The Construction of Animal Biodiversity. Roberts and Company Publishers, Greenwood Village, 416 p.

Gold, D.A., Grabenstatter, J., de Mendoza, A., Riesgo, A., Ruiz-Trillo, I., and Summons, R.E., 2016, Sterol and genomic analyses validate the sponge biomarker hypothesis: Proceedings of the National Academy of Sciences of the United States of America, v. 113, p. 2684–2689.

Grey, K., and Sugitani, K., 2009, Palynology of Archean microfossils (c. 3.0 Ga) from the Mount Grant area, Pilbara Craton, Western Australia: Further evidence of biogenicity: Precambrian Research, v. 173, p. 60–69.

He, T., Zhou, Y., Vermeesch, P., Rittner, M., Miao, L., Zhu, M., Carter, A., Pogge von Strandmann, P.A.E., and Shields, G.A., 2017, Measuring the ‘Great Unconformity’ on

the North China Craton using new detrital zircon age data: Geological Society, London, Special Publications, v. 448, p. 145–159.

Hofmann, H.J., 1976, Precambrian Microflora, Belcher Islands, Canada: Significance and Systematics: Journal of Paleontology, v. 50, p. 1040–1073.

Holmes, J.D., García-Bellido, D.C., and Lee, M.S.Y., 2018, Comparisons between Cambrian Lagerstätten assemblages using multivariate, parsimony and Bayesian methods: Gondwana Research, v. 55, p. 30–41.

Jankauskas, T.V., Mikhailova, N.S., and Hermann, T.N., 1989, Precambrian Microfossils of the USSR. Nauka, Leningrad, 190 p.

Muscente, A.D., Czaja, A.D., Riedman, L.A., and Colleary, C., 2017a, Organic Matter in Fossils. *In* White, W.M., eds., Encyclopedia of Geochemistry: A Comprehensive Reference Source on the Chemistry of the Earth. Springer International Publishing, Cham, p. 1–5.

Muscente, A.D., Schiffbauer, J.D., Broce, J., Laflamme, M., O'Donnell, K., Boag, T.H., Meyer, M., Hawkins, A.D., Huntley, J.W., McNamara, M., MacKenzie, L.A., Stanley, G.D., Hinman, N.W., Hofmann, M.H., and Xiao, S., 2017b, Exceptionally preserved fossil assemblages through geologic time and space: Gondwana Research, v. 48, p. 164–188.

Muscente, A.D., and Xiao, S., 2015, New occurrences of *Sphenothallus* in the lower Cambrian of South China: Implications for its affinities and taphonomic demineralization of shelly fossils: Palaeogeography, Palaeoclimatology, Palaeoecology, v. 437, p. 141–164.

Schirrmeister, B.E., de Vos, J.M., Antoelli, A., and Bagheri, H.C., 2013, Evolution of multicellularity coincided with increased diversification of cyanobacteria and the Great Oxidation Event: Proceedings of the National Academy of Sciences of the United States of America, v. 110, p. 1791–1796.

Tang, Q., 2013, Organic-walled microfossils from the early Neoproterozoic Liulaobei Formation in the Huainan region of North China and their biostratigraphic significance: Precambrian Research, v. 236, p. 157–181.

Tang, Q., Pang, K., Yuan, X., Wan, B., and Xiao, S., 2015, Organic-walled microfossils from the Tonian Gouhou Formation, Huaibei region, North China Craton, and their biostratigraphic implications: Precambrian Research, v. 266, p. 296–318.

Tang, Q., Pang, K., Yuan, X., and Xiao, S., 2017, Electron microscopy reveals evidence for simple multicellularity in the Proterozoic fossil *Chuaria*: Geology, v. 45, p. 75–78.

Xiao, S., Hu, J., Yuan, X., Parsley, R.L., and Cao, R., 2005, Articulated sponges from the Lower Cambrian Hetang Formation in southern Anhui, South China: their age and implications for the early evolution of sponges: Palaeogeography, Palaeoclimatology, Palaeoecology, v. 220, p. 89−117.

Xiao, S., Muscente, A.D., Chen, L., Zhou, C., Schiffbauer, J.D., Wood, A.D., Polys, N.F., and Yuan, X., 2014a, The Weng'an biota and the Ediacaran radiation of multicellular eukaryotes: National Science Review, v. 1, p. 498–520.

Xiao, S., Shen, B., Tang, Q., Kaufman, A.J., Yuan, X., Li, J., and Qian, M., 2014b, Biostratigraphic and chemostratigraphic constraints on the age of early Neoproterozoic carbonate successions in North China: Precambrian Research, v. 246, p. 208–225.

Xiao, S., and Tang, Q., 2018, After the boring billion and before the freezing millions: evolutionary patterns and innovations in the Tonian Period: Emerging Topics in Life Sciences. doi:10.1042/etls20170165.

Xiao, S., Yuan, X., Steiner, M., and Knoll, A.H., 2002, Macroscopic carbonaceous compressions in a terminal Proterozoic shale: A systematic reassessment of the Miaohe biota, South China: Journal of Paleontology, v. 76, p. 347–376.

Xing, Y., 1989, The Upper Precambrian of China, Volume 3 of "The Stratigraphy of China". Geological Publishing House, Beijing, 314 p.

Ye, Q., Tong, J., Xiao, S., Zhu, S., An, Z., Tian, L., and Hu, J., 2015, The survival of benthic macroscopic phototrophs on a Neoproterozoic snowball Earth: Geology, v. 43, p. 507–510.

Yuan, X., Chen, Z., Xiao, S., Zhou, C., and Hua, H., 2011, An early Ediacaran assemblage of macroscopic and morphologically differentiated eukaryotes: Nature, v. 470, p. 390–393.

Zang, W., and Walter, M.R., 1992, Late Proterozoic and Early Cambrian microfossils and biostratigraphy, northern Anhui and Jiangsu, central-eastern China: Precambrian Research, v. 57, p. 243–323.

CHAPTER 2

Electron microscopy reveals evidence for multicellularity in the Proterozoic fossil *Chuaria*

QING TANG[1], KE PANG[2], XUNLAI YUAN[2,3], AND SHUHAI XIAO[1]

[1]*Department of Geosciences, Virginia Tech, Blacksburg, Virginia 24061, USA*

[2]*State Key Laboratory of Palaeobiology and Stratigraphy, Center for Excellence in Life and Paleoenvironment, Nanjing Institute of Geology and Palaeontology, Chinese Academy of Sciences, Nanjing, 210008*

[3]*University of Chinese Academy of Sciences, Beijing 100039, China*

2.1 Abstract

Multicellularity arose multiple times in the evolutionary history of eukaryotes and simple multicellularity may have a deep history tracing back to the Paleoproterozoic. However, complex multicellular organisms with cellular and tissue differentiation did not appear in the fossil record until the Mesoproterozoic, and it is not until the Ediacaran Period (635–541 Ma) when diverse assemblages of complex multicellular eukaryotes evolved. In the intervening Tonian Period (ca. 1000–720 Ma), the fossil record of multicellular organisms is poorly documented. To address this knowledge gap, we investigated *Chuaria* and associated carbonaceous compression fossils from the Tonian Liulaobei Formation in North China. These fossils have been variously interpreted as unicellular or multicellular organisms. Our analysis using backscattered-electron scanning electron microscopy (BSE-SEM) revealed direct evidence for simple multicellularity in some of these fossils and suggests that *Chuaria* may have had a multicellular vegetative stage in its life cycle. This study demonstrates that BSE-SEM has the potential to unveil the hidden diversity of multicellular organisms in the Tonian Period, thus enriching our knowledge about the multiple origins of multicellularity in this critical geological period before Cryogenian glaciations.

2.2 Introduction

The rise of multicellularity represents one of the major transitions in the evolutionary history of cellular life (Maynard Smith and Szathmary, 1997). However, in notable contrast to the rise of eukaryotes, which is also regarded as a major evolutionary transition, the development of multicellularity is not an evolutionary singularity. According to phylogenetic and paleontological data, the evolutionary march toward multicellularity occurred convergently in

many clades and took extraordinarily protracted paths. Simple multicellularity—characterized by clusters, filaments, or sheets of cells that arise via mitotic cell division from a single progenitor and that have limited cell differentiation and cell-to-cell communication (Knoll, 2011)—evolved independently at least 25 times among eukaryotes alone (Bonner, 2000; Grosberg and Strathmann, 2007; Herron et al., 2013). In contrast, complex multicellularity—characterized by intercellular communication and tissue differentiation—has occurs in only a handful of eukaryotic groups (Knoll, 2011). Both the fossil record and molecular clocks indicate that simple multicellularity, as represented by cellularly preserved colonial coccoids and filamentous fossils (Butterfield, 2009), evolved no later than the early Paleoproterozoic (Hofmann, 1976; Herron et al., 2013). However, complex multicellularity appeared in the fossil record only in the middle Mesoproterozoic (Butterfield, 2000) and did not become ecologically significant until the Ediacaran Period or 635–541 Ma (Yuan et al., 2011; Xiao et al., 2014a).

A literal reading of the fossil record, however, should be taken with caution because of problems about the preservation of soft-bodied organisms, the interpretation of morphologically simple forms, and the incomplete understanding of life cycles. Those problems are conspicuously prominent in Proterozoic carbonaceous compression fossils, which often do not preserve any traces of cellular structures or a complete life cycle. For example, the carbonaceous compression fossil *Chuaria*, which is diagnosed as submillimeter- to millimeter-sized thick-walled spherical vesicles and is common in the Proterozoic Eon (particularly in the Tonian Period, ca. 1000–720 Ma), has been variously interpreted as a unicellular or multicellular organism. *Chuaria* has been regarded as a unicellular/coenocytic eukaryote because of its similarity to acritarchs (Vidal and Ford, 1985), which are often uncritically treated as resting cysts of unicellular eukaryotes. It has also been interpreted as a colonial cyanobacterium based

on its putative association with *Nostoc*-like filaments (Sun, 1987), or as a multicellular eukaryote because of its excystment structures and a potentially complex life cycle (Kumar, 2001; Sharma et al., 2009). These interpretations are difficult to resolve because *Chuaria* fossils are morphologically simple, apparently lack cellular preservation, and do not record a complete life cycle.

Recently, variable-voltage backscattered-electron scanning electron microscopy (BSE-SEM) has been proven as an effective method with which to study carbonaceous compressions and to bring to light hidden morphological details that are otherwise invisible in reflected light microscopy (RLM) and secondary-electron scanning electron microscopy (SE-SEM). Briefly, by adjusting the accelerating voltage in BSE-SEM and thus allowing the primary electrons to penetrate to different depths, it is possible to illuminate subsurface structures in carbonaceous compressions (Orr et al., 2002; Pang et al., 2013; LoDuca et al., 2015; Muscente and Xiao, 2015). This technique offers an immense opportunity to test whether *Chuaria* and associated fossils are multicellular organisms, because it has the potential to elucidate cellular structures preserved in carbonaceous compressions.

2.3 Materials and Methods

Fossils were collected from the Tonian Liulaobei Formation at the Diangeda-Baieshan section (116°46′0.19”E, 32°37′51.52”N) near Shouxian, Anhui Province, North China (Fig. 2.1). The geologic and stratigraphic setting of the Liulaobei Formation was described elsewhere (Dong et al., 2008). The fossiliferous strata were deposited in offshore ferruginous environments (Guilbaud et al., 2015). The age of the Liulaobei Formation is loosely constrained by K–Ar and

Rb–Sr radiometric dates to be 900–750 Ma (summarized in Dong et al., 2008), consistent with chemostratigraphic and biostratigraphic correlations (Tang et al., 2013; Xiao et al., 2014b).

Fossils analyzed in this study are carbonaceous compressions preserved on the bedding surface of shales and mudstones. A subset of these carbonaceous compressions represent submillimeter- to millimeter-sized, thick-walled, spherical vesicles that fit the diagnosis of and have been described as *Chuaria* (Sun, 1987). Other fossils have multicellular structures and are referred to as multicellular aggregates. Both *Chuaria* fossils and multicellular aggregates were imaged using RLM, SE-SEM, and BSE-SEM. All illustrated specimens are reposited at the Virginia Polytechnic Institute Geosciences Museum (VPIGM, Blacksburg, Virginia, USA).

2.4 Results

Under RLM, *Chuaria* specimens from the Liulaobei Formation conform to the diagnosis of *Chuaria circularis* (Walcott, 1899). They are spherical vesicles compressed into two-dimensional discoidal to subdiscoidal structures, often with concentric compressional folds (Fig. 2.2A), V-shaped ruptures (Fig. 2.2A, B), and radial splits (Fig. 2.2C). Their vesicle size varies from 0.5 mm to 5 mm. They are often randomly disseminated on bedding planes (Figs. 2.2D and 2.3A).

In total, 103 discoidal fossils among ~578 examined specimens were found to preserve multicellular structures (Figs. 2.2E, F, and 2.3); sometimes, the multicellular nature of the fossils was visible under BSE-SEM but invisible under RLM or SE-SEM (Fig. 2.3B–F), suggesting that the multicellular structures are preserved within the compressed fossils. Twenty of them were observed to have a modest number of loosely packed cells (mostly 50–300 μm in cell diameter, with rare outliers) within a common envelope (0.8–5.7 mm in diameter) that often displayed

concentric compressional folds (Figs. 2.2E, F); hereafter, these are referred to as enveloped cell aggregates. The others were observed to have tightly packed cell aggregates without a distinct common envelope (Fig. 2.3), and they are hereafter referred to as naked cell aggregates. The tightly packed cells in naked aggregates became increasingly visible as the accelerating voltage increased from 5 keV to 25 keV, again suggesting that these cells are embedded within the carbonaceous compression, which is estimated to be 2–3 μm in thickness based on Monte Carlo simulations (Muscente and Xiao, 2015). Cells in the periphery are often better discernable than those in the center, where they are obscured (Fig. 2.3G–I). Cells are 70–110 μm in diameter (average = 85 μm; n = 934), and their size was relatively constant regardless of aggregate size (Fig. 2.4).

2.5 Interpretation and Discussion

The naked aggregates with tightly packed cells are interpreted as spherical multicellular colonies (i.e., simple multicellularity). The variable-voltage BSE-SEM observations indicate that the cellular structures are embedded within the carbonaceous compression. The fact that they are most discernible in the periphery of the aggregate, but are obscured toward the center, suggests that the colonies were three-dimensional structures filled with a solid mass of cells. Thus, when compressed, the central part of a colony became more obscured than the periphery due to greater compaction. The naked aggregates may each contain 36–10,232 cells, assuming close packing, which has a packing density of ~74%, or 32–8849 cells, assuming random packing with a packing density of ~64% (Schiffbauer et al., 2012). The lack of morphological differentiation among the cells suggests that the aggregates represent colonies, and the lack of a common envelope indicates that these colonies represent vegetative growth stages.

The enveloped aggregates with loosely packed cells (Figs. 2.2E, F), on the other hand, may represent a stage entering into or exiting from an encystment stage. The presence of concentric folds indicates that the envelopes were thick walled and resistant, a likely sign for dormant cysts or hypnospores (Coleman, 1983). The more variable cell sizes (Fig. 2.2E), in comparison with cells in naked cell aggregates, may be related to the more dynamic cytoplasm growth or condensation during encystment or excystment. Alternatively, such variations in cell size may in part be a taphonomic artifact. Similarly, it is uncertain whether the sparse numbers of cells in most enveloped aggregates resulted from a taphonomic loss of cells or a biologically programmed reduction of cell numbers.

The compressed vesicles of *C. circularis* from the Liulaobei Formation are interpreted as relatively thick-walled cysts. The lack of cellular content within the cysts could be due to taphonomic loss or biological excystment; indeed, some *C. circularis* specimens show well-defined V-shaped ruptures (Figs. 2A and 2B; Butterfield et al., 1994, their figure 13F; Sharma et al., 2009, their figures 6k, 6l, and 6n) that may represent excystment openings through which cells were released from germinating cysts.

One may choose to name the naked aggregates, enveloped aggregates, and *Chuaria* vesicles as distinct taxa. However, based on their coexistence and overlapping size range, we propose that they represent different stages of the same organism, and when considered together, they can illuminate the life cycle of *Chuaria*. The enveloped aggregates provide a key morphological intermediate between the naked aggregates and *Chuaria* vesicles. If these forms do indeed represent different stages of the same organism, we speculate that *Chuaria* had a biphasic (planktonic-benthic) life cycle involving (1) a benthic encystment stage and (2) a planktonic colonial stage that grew out of spores released during excystment (Fig. 2.5). The

planktonic phase was likely vegetative, characterized by rapid cell growth and division, which could involve fast cell cycles with rapid alternation of S (synthesis) and M (mitosis) phases, or rapid hypotrophic growth and karyokinesis to form multinucleate cells that subsequently underwent palintomic cytokinesis (Cross and Umen, 2015); many modern green algae such as *Chlamydomonas*, *Scenedesmus*, and *Chlorella* share these types of cell growth and division to develop a simple multicellular stage (Bišová and Zachleder, 2014). The benthic phase was largely dormant and enclosed within thick vesicles, much like resting cysts of modern green algae (Coleman, 1983). From a taphonomic point of view, it is not surprising that the benthic phase with thick-walled cysts would leave a much better fossil record. Thus, *Chuaria* is often represented by empty vesicles only, and the planktonic multicellular vegetative stages are rarely preserved (e.g., in the Liulaobei Formation). On the other hand, it is also possible that the multicellular stages have been neglected because BSE-SEM has not been widely applied to investigate all *Chuaria* assemblages, as our study shows that RLM and SE-SEM are inadequate techniques with which to visualize the hidden multicellularity in some specimens.

It is intriguing that the cyst-forming *Chuaria* commonly occurs in predominantly anoxic Proterozoic basins, including the Liulaobei Formation (Guilbaud et al., 2015), Chuar Group (Johnston et al., 2010), and the Lantian Formation (Yuan et al., 2001; Guan et al., 2014). It is worth exploring in the future whether anoxic conditions led to fluctuating environments (e.g., nutrient availability) that facilitated the prevalence of encystment in *Chuaria* and other Proterozoic organisms.

Regardless, *Chuaria* from the Liulaobei Formation is suggested to be a simple multicellular organism, and possibly a multicellular eukaryote, considering the combination of characters such as large vesicle size, thick vesicle wall, possible encystment, and a biphasic life

cycle. Although it is possible that fossils described as *Chuaria* may encompass a wide range of organisms, including bacteria and unicellular organisms (Steiner, 1997), the present study suggests that the Proterozoic diversity of multicellular organisms is probably underestimated and that a systematic investigation of Proterozoic carbonaceous compressions using BSE-SEM can help to rectify this.

2.6 Conclusions

The evolution of multicellularity endowed organisms with critical advantages and greater evolutionary potential, allowing greater size, greater complexity, circumvention of diffusion limits, and many other evolutionary benefits (Knoll, 2011). The discovery of simple multicellular forms in association with *Chuaria* vesicles from the Tonian Liulaobei Formation allows us to critically evaluate the various hypotheses about *Chuaria*. Available evidence favors the hypothesis that *Chuaria* was a simple multicellular organism (i.e., a colonial organism without cell differentiation), possibly a eukaryote with a multicellular vegetative stage in its life cycle. This raises an important question about its relationship with much smaller cell aggregates such as *Symplassosphaeridium* and *Synsphaeridium* that are often found in Tonian rocks (Tang et al., 2013; Tang et al., 2015). Although these fossils are characterized by simple multicellularity, they represent an evolutionary stage that underlies the greater diversity and complexity as manifested by the many multicellular organisms that came afterwards in the Cryogenian and Ediacaran Periods (Butterfield, 2007; Ye et al., 2015). More systematic investigation of *Chuaria* and other carbonaceous compressions using BSE-SEM holds promise to further illuminate the evolution of multicellularity in the Tonian Period.

2.7 Acknowledgements

This research was supported by the U.S. National Science Foundation (grant EAR-1528553), the National Natural Science Foundation of China (grants 41272011, 41602007), the Geological Society of America, Sigma Xi, the Chinese Ministry of Science and Technology (grant 2013CB835000), the Chinese Academy of Sciences (grant KZZD-EW-02, KZCX2-YW-153), the Science Foundation of Jiangsu Province of China (grant BK20161090), and the State Key Laboratory of Palaeobiology and Stratigraphy (grant 20162109). We thank Bin Wan, Jinlong Wang, Lei Chen, and Zhiji Ou for field assistance.

2.8 Figures and figure captions

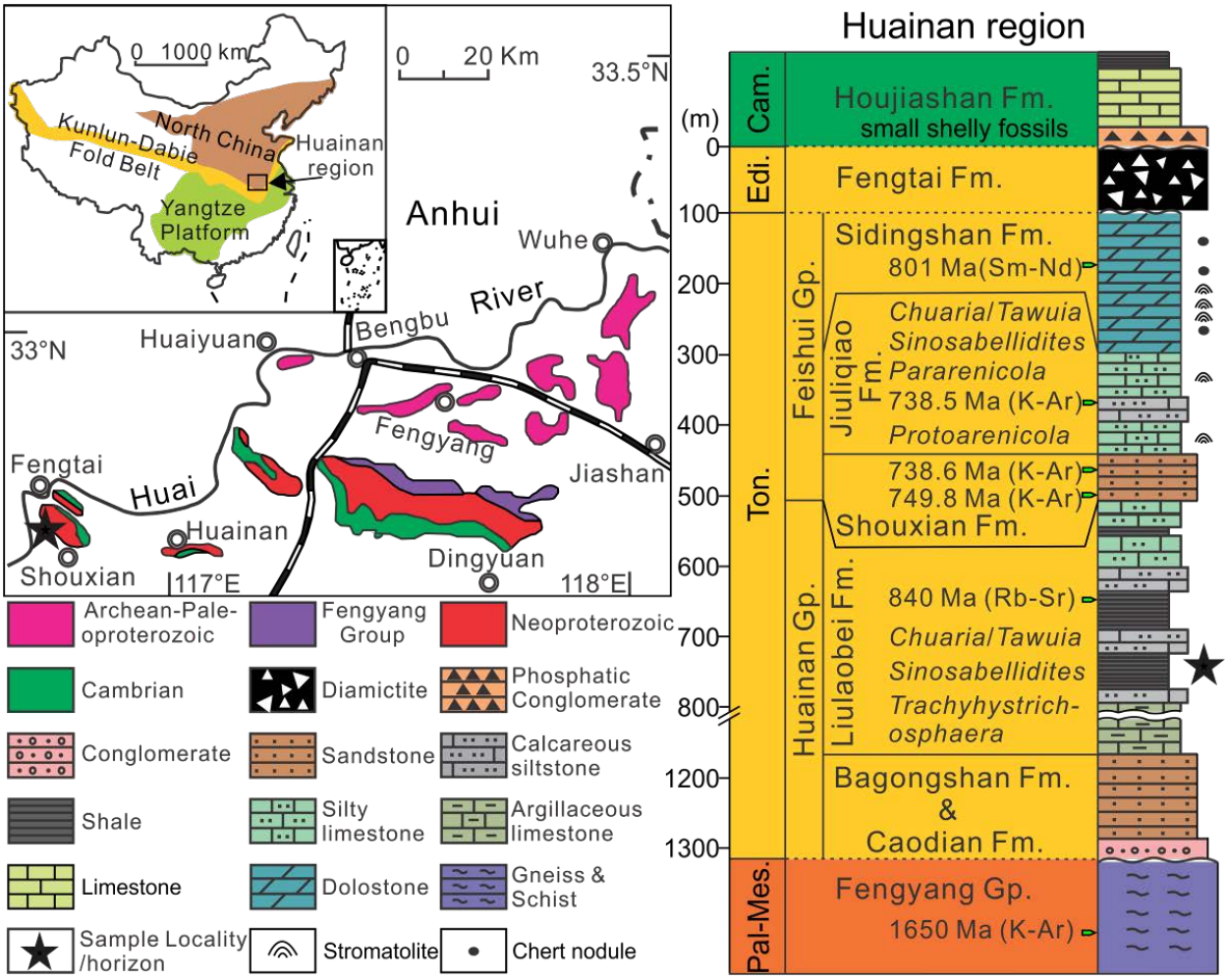

Fig. 2. 1. Geological map and stratigraphic column of Proterozoic sequence in Huainan region, North China (modified from Xiao et al., 2014b). Stars mark geographic locality and stratigraphic horizon from which *Chuaria* fossils were collected. Biostratigraphic, chemostratigraphic, and geochronological data suggest a Tonian age for the Huainan and Feishui groups (Dong et al., 2008; Tang et al., 2013; Xiao et al., 2014b), although Sm-Nd age from the upper Feishui Group does not agree with the Rb-Sr and K-Ar ages from the below due to differences in dating technique. Pal-Mes.—Paleoproterozoic-Mesoproterozoic; Ton.—Tonian (ca. 1000–720 Ma); Edi.—Ediacaran (635–541 Ma); Cam.—Cambrian; Fm.—Formation; Gp.—Group.

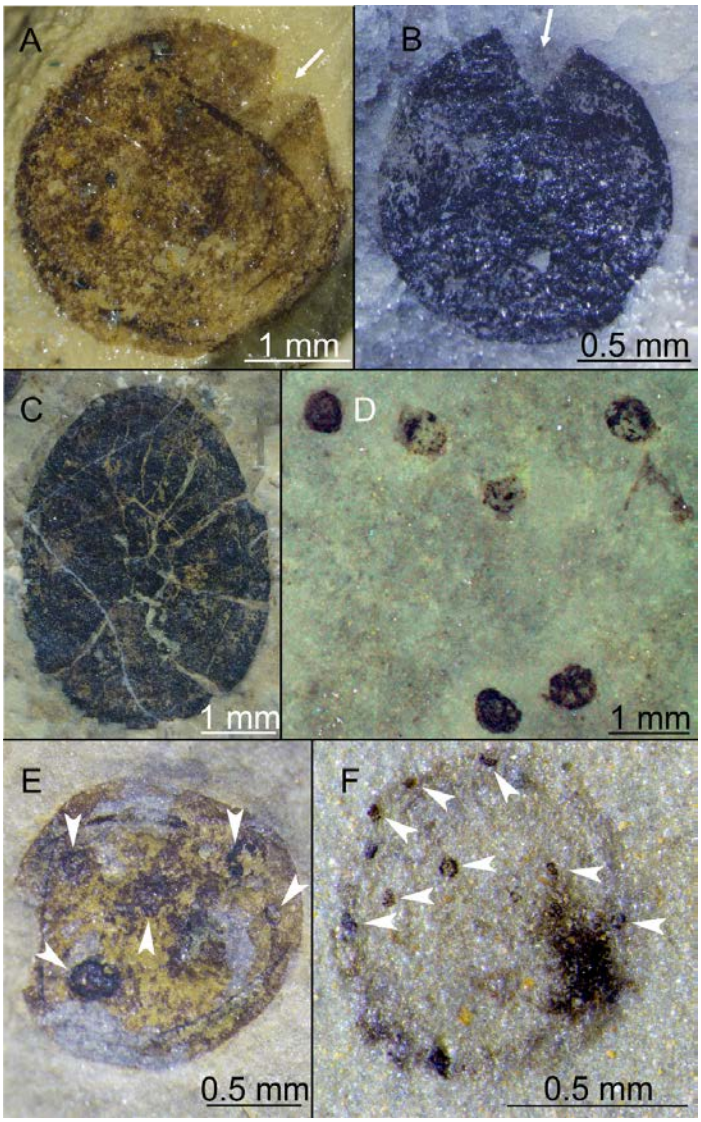

Fig. 2. 2. Reflected light microscopy (RLM) photographs of *Chuaria* and associated fossils from the Liulaobei Formation, North China. A, B: Specimen with concentric compressional folds (A) and V-shape rupture (A, B, arrows), VPIGM-4688 (Virginia Polytechnic Institute Geosciences Museum, Virginia, USA), LLB-T1-1-2 and VPIGM-4689, LLB-T9-9-1. C: Specimen with radial splits likely of taphonomic origin, VPIGM-4690, LLB-T2-4-5. D: Small specimens (<1 mm in diameter) on bedding surface, VPIGM-4691, LLB-T10-1-1. E–F: Loosely packed cells (arrowheads) enclosed within a common envelope with concentric compressional folds, VPIGM-4692, LLB-T8-16-3 and VPIGM-4693, LLB-T9-39-1, respectively.

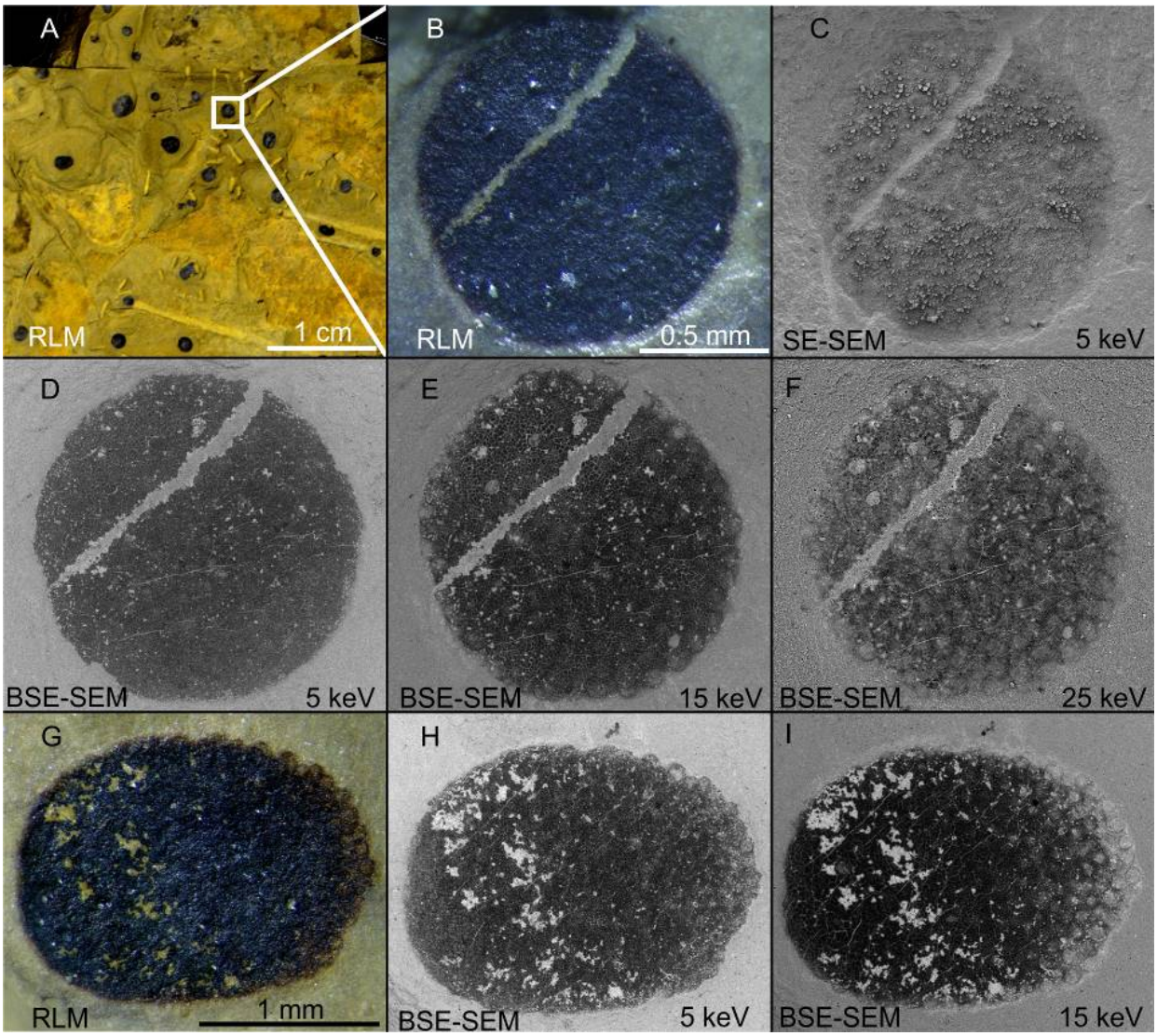

Fig. 2. 3. Reflected light microscopy (RLM), secondary-electron scanning electron microscopy (SE-SEM), and backscattered-electron SEM (BSE-SEM) photographs of tightly packed cell aggregates interpreted as *Chuaria* colonies. A: Slab with randomly distributed *Chuaria* and associated fossils, VPIGM-4694 (Virginia Polytechnic Institute Geosciences Museum, Virginia, USA), LLB-T2-31. B–F: Magnified view of one specimen shown in A, VPIGM-4694a, LLB-T2-31-3. G–I: VPIGM-4694, LLB-T1-18-1. Photographic modes are marked in lower left of each panel. D–F and H–I are series of variable-voltage BSE-SEM photographs, with accelerating voltages marked in lower right.

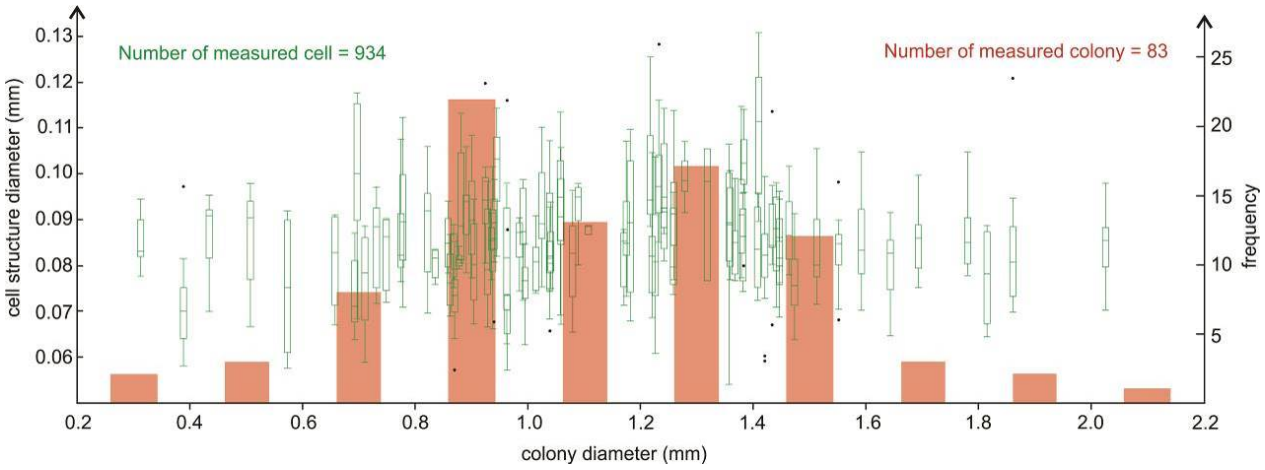

Fig. 2. 4. Histogram of colony size distribution and cross-plot of colony size vs. cell size of tightly packed *Chuaria* colonies. Each box-and-whisker plot shows the median, 25 and 75 percentiles, range, and outliers ($\geq 3^{rd}$ quartile + 1.5 * interquartile range or $\leq 1^{st}$ quartile – 1.5 * interquartile range; denoted by black dots) of cell diameters of a colony.

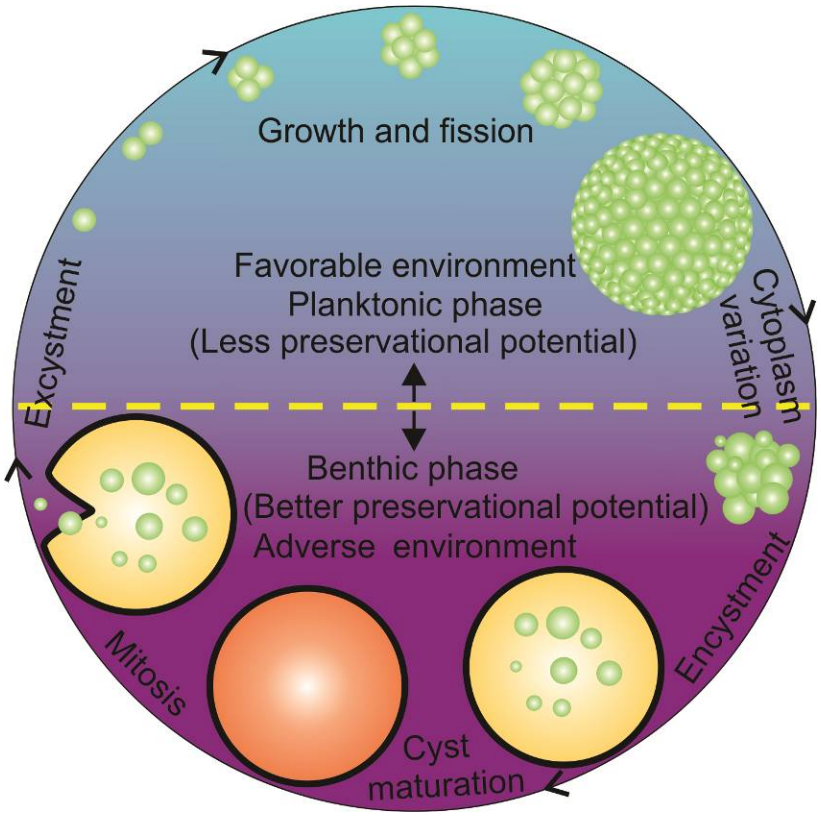

Fig. 2. 5. A possible life cycle of *Chuaria*.

2.9 References

Bišová, K., and Zachleder, V., 2014, Cell-cycle regulation in green algae dividing by multiple fission: Journal of Experimental Botany, v. 65, p. 2585–2602.

Bonner, J.T., 2000, First Signals: the Evolution of Multicellular Development. Princeton University Press, Princeton, 146 p.

Butterfield, N.J., 2000, *Bangiomorpha pubescens* n. gen., n. sp.: Implications for the evolution of sex, multicellularity, and the Mesoproterozoic/Neoproterozoic radiation of eukaryotes: Paleobiology, v. 26, p. 386–404.

Butterfield, N.J., 2007, Macroevolution and macroecology through deep time: Palaeontology, v. 50, p. 41–55.

Butterfield, N.J., 2009, Modes of pre-Ediacaran multicellularity: Precambrian Research, v. 173, p. 201–211.

Butterfield, N.J., Knoll, A.H., and Swett, K., 1994, Paleobiology of the Neoproterozoic Svanbergfjellet Formation, Spitsbergen: Fossils and Strata, v. 34, p. 1–84.

Coleman, A.W., 1983, The roles of resting spores and akinetes in chlorophyte survival. *In* Fryxell, G.A., eds., Survival strategies of the algae. Cambridge University Press, Cambridge, p. 1–22.

Cross, F.R., and Umen, J.G., 2015, The Chlamydomonas cell cycle: The Plant Journal, v. 82, p. 370–392.

Dong, L., Xiao, S., Shen, B., Yuan, X., Yan, X., and Peng, Y., 2008, Restudy of the worm-like carbonaceous compression fossils *Protoarenicola*, *Pararenicola*, and *Sinosabellidites* from early Neoproterozoic successions in North China: Palaeogeography, Palaeoclimatology, Palaeoecology, v. 258, p. 138–161.

Grosberg, R.K., and Strathmann, R.R., 2007, The evolution of multicellularity: a minor major transition?: Annual Review of Evolution, Ecology, and Systematics, v. 38, p. 621–654.

Guan, C., Zhou, C., Wang, W., Wan, B., Yuan, X., and Chen, Z., 2014, Fluctuation of shelf basin redox conditions in the early Ediacaran: Evidence from Lantian Formation black shales in South China: Precambrian Research, v. 245, p. 1–12.

Guilbaud, R., Poulton, S.W., Butterfield, N.J., Zhu, M., and Shields-Zhou, G.A., 2015, A global transition to ferruginous conditions in the early Neoproterozoic oceans: Nature Geoscince, v. 8, p. 466–470.

Herron, M.D., Rashidi, A., Shelton, D.E., and Driscoll, W.W., 2013, Cellular differentiation and individuality in the 'minor' multicellular taxa: Biological Reviews, v. 88, p. 844−861.

Hofmann, H.J., 1976, Precambrian Microflora, Belcher Islands, Canada: Significance and Systematics: Journal of Paleontology, v. 50, p. 1040–1073.

Johnston, D.T., Poulton, S.W., Dehler, C., Porter, S., Husson, J., Canfield, D.E., and Knoll, A.H., 2010, An emerging picture of Neoproterozoic ocean chemistry: Insights from the Chuar Group, Grand Canyon, USA: Earth and Planetary Science Letters, v. 290, p. 64–73.

Knoll, A.H., 2011, The multiple origins of complex multicellularity: Annual Review of Earth and Planetary Sciences, v. 39, p. 217–239.

Kumar, S., 2001, Mesoproterozoic megafossil *Chuaria–Tawuia* association may represent parts of a multicellular plant, Vindhyan Supergroup, Central India: Precambrian Research, v. 106, p. 187–11.

LoDuca, S.T., Caron, J.-B., Schiffbauer, J.D., Xiao, S., and Kramer, A., 2015, A reexamination of *Yuknessia* from the Cambrian of British Columbia and Utah: Journal of Paleontology, v. 89, p. 82–95.

Maynard Smith, J., and Szathmary, E., 1997, The Major Transitions in Evolution. Oxford University Press, Oxford, 346 p.

Muscente, A.D., and Xiao, S., 2015, Resolving three-dimensional and subsurficial features of carbonaceous compressions and shelly fossils using backscattered electron scanning electron microscopy (BSE-SEM): PALAIOS, v. 30, p. 462–481.

Orr, P.J., Kearns, S.L., and Briggs, D.E., 2002, Backscattered electron imaging of fossils exceptionally-preserved as organic compressions: PALAIOS, v. 110–117.

Pang, K., Tang, Q., Schiffbauer, J.D., Yao, J., Yuan, X., Wan, B., Chen, L., Ou, Z., and Xiao, S., 2013, The nature and origin of nucleus-like intracellular inclusions in Paleoproterozoic eukaryote microfossils: Geobiology, v. 11, p. 499–510.

Schiffbauer, J.D., Xiao, S., Sen Sharma, K., and Wang, G., 2012, The origin of intracellular structures in Ediacaran metazoan embryos: Geology, v. 40, p. 223–226.

Sharma, M., Mishra, S., Dutta, S., Banerjee, S., and Shukla, Y., 2009, On the affinity of *Chuaria-Tawuia* complex: A multidisciplinary study: Precambrian Research, v. 173, p. 123–136.

Steiner, M., 1997, *Chuaria circularis* Walcott 1899–"megasphaeromorph acritarch" or prokaryotic colony?: Acta Universitatis Carolinae Geologica, v. 40, p. 645–665.

Sun, W., 1987, Palaeontology and biostratigraphy of Late Precambrian macroscopic colonial algae: *Chuaria* Walcott and *Tawuia* Hofmann: Palaeontographica Abt. B, v. 203, p. 109–134.

Tang, Q., Pang, K., Xiao, S., Yuan, X., Ou, Z., and Wan, B., 2013, Organic-walled microfossils from the early Neoproterozoic Liulaobei Formation in the Huainan region of North China and their biostratigraphic significance: Precambrian Research, v. 236, p. 157–181.

Tang, Q., Pang, K., Yuan, X., Wan, B., and Xiao, S., 2015, Organic-walled microfossils from the Tonian Gouhou Formation, Huaibei region, North China Craton, and their biostratigraphic implications: Precambrian Research, v. 266, p. 296–318.

Vidal, G., and Ford, T.D., 1985, Microbiotas from the late Proterozoic Chuar Group (northern Arizona) and Uinta Mountain Group (Utah) and their chronostratigraphic implications: Precambrian Research, v. 28, p. 349–389.

Walcott, C.D., 1899, Pre-Cambrian fossiliferous formations: Bulletin of the Geological Society of America, v. 10, p. 199–244 (plates 122–128).

Xiao, S., Muscente, A.D., Chen, L., Zhou, C., Schiffbauer, J.D., Wood, A.D., Polys, N.F., and Yuan, X., 2014a, The Weng'an biota and the Ediacaran radiation of multicellular eukaryotes: National Science Review, v. 1, p. 498–520.

Xiao, S., Shen, B., Tang, Q., Kaufman, A.J., Yuan, X., Li, J., and Qian, M., 2014b, Biostratigraphic and chemostratigraphic constraints on the age of early Neoproterozoic carbonate successions in North China: Precambrian Research, v. 246, p. 208–225.

Ye, Q., Tong, J., Xiao, S., Zhu, S., An, Z., Tian, L., and Hu, J., 2015, The survival of benthic macroscopic phototrophs on a Neoproterozoic snowball Earth: Geology, v. 43, p. 507–510.

Yuan, X., Chen, Z., Xiao, S., Zhou, C., and Hua, H., 2011, An early Ediacaran assemblage of macroscopic and morphologically differentiated eukaryotes: Nature, v. 470, p. 390–393.

Yuan, X., Xiao, S., Li, J., Yin, L., and Cao, R., 2001, Pyritized chuarids with excystment structures from the late Neoproterozoic Lantian Formation in Anhui, South China: Precambrian Research, v. 107, p. 253–263.

CHAPTER 3

Organic-walled microfossils from the Tonian Gouhou Formation, Huaibei region, North China Craton, and their biostratigraphic implications

QING TANG[1], KE PANG[2], SHUHAI XIAO[1], XUNLAI YUAN[2,3], BIN WAN[2]

[1]*Department of Geosciences, Virginia Tech, Blacksburg, VA 24061, USA*

[2]*State Key Laboratory of Palaeobiology and Stratigraphy, Center for Excellence in Life and Paleoenvironment, Nanjing Institute of Geology and Palaeontology, Chinese Academy of Sciences, Nanjing, 210008*

[3]*University of Chinese Academy of Sciences, Beijing 100039, China*

3.1 Abstract

The Meso-(?) and Neoproterozoic Huaibei Group in the Huaibei region, North China Craton (NCC), is emerging as a target for paleontological and tectonic studies due to its thick unmetamorphosed sediments with well-preserved organic-walled fossils. However, the lack of accurate age constraints for this sedimentary sequence dramatically hampers our ability to take full advantage of rich geological and paleontological history recorded in the Huaibei Group. Particularly, the depositional age of the uppermost unit of the Huaibei Group, the Gouhou Formation, is a controversial issue. Although the age for the overlaying early Cambrian Houjiashan Formation is well constrained by trilobite and small shelly fossil biostratigraphy, the Precambrian-Cambrian boundary in the Huaibei region has been long debating due to the uncertainty of the sedimentary age for the Gouhou Formation which has been variously interpreted as Cambrian, Cryogenian–Ediacaran (ca. 720 Ma to ca. 541 Ma), and Tonian (1000

Ma to ca. 720 Ma). To reposition the Precambrian-Cambrian boundary in the Huaibei region and unveil the magnitude of underlying tectonic event, we carried out a biostratigraphic study of the Gouhou Formation. Our investigation using a low manipulation maceration technique revealed a diverse organic-walled microfossil assemblage. A total of 22 taxa have been revealed, including a new species—*Dictyosphaera tacita* n. sp. Importantly, the co-occurrence of *Trachyhystrichosphaera*, *Valeria*, and *Dictyosphaera* in the lower Gouhou Formation suggests a likely Tonian age. Given that recent detrital zircon dating have shown Cambrian ages from the Middle Gouhou Formation, integrated biostratigraphic and geochronological data indicate that the Precambrian-Cambrian boundary may be located on the disconformable contact between the lower and middle Gouhou Formation with an infra-Cambrian depositional gap of >200 myr, perhaps driven by a major tectonostratigraphic event.

3.2 Introduction

The North China Craton (NCC) is one of the oldest cratons and a major tectonic unit in China with crustal remnants as old as 3.8 Ga (Liu et al., 1992). Various tectonic-magmatic-thermal events shaped the Archean-Paleoproterozoic history of the NCC, which was stabilized at the Paleoproterozoic-Mesoproterozoic transition (Liu et al., 2011; Santosh et al., 2013). Thick Meso-Neoproterozoic sedimentary packages were deposited along the margins of the NCC, particularly in the Jixian area to the north, southern Liaoning to the northeast, Huainan and Huaibei regions to the southeast, and western Henan and southern Shanxi provinces to the southwest (Xiao et al., 2014a). In the Huainan and Huaibei regions (Fig. 3.1), more than 5 km of Meso-(?) and Neoproterozoic strata were laid down, including the Huainan and Feishui groups in the Huainan region and the Huaibei Group in the Huaibei region (Xiao et al., 2014a). These

strata not only record important sedimentary information relevant to the tectonic history of NCC (Liu et al., 2005; Peng et al., 2011a; Peng et al., 2011b; Wang et al., 2011; Yang et al., 2012), but also preserve valuable paleontological data documenting the early evolution of eukaryotes (Zheng, 1980; Wang et al., 1984a; Yin, 1985; Sun et al., 1986; Zang and Walter, 1992; Yin and Sun, 1994; Dong et al., 2008; Qian et al., 2009; Tang et al., 2013).

However, the exact depositional age of these strata in the Huainan and Huaibei regions has not been well constrained. Available U–Pb ages of detrital zircons and intrusive igneous rock broadly constrain much of the Huaibei Group between ~1069 Ma and ~890 Ma (Xiao et al., 2014a), or Meso-(?) and Neoproterozoic in age. However, the age of the uppermost unit of the Huaibei Group—the Gouhou Formation—is a matter of debate. Xing et al. (1996) and Zang and Walter (1992) suggest the Gouhou Formation is lower Cambrian, whereas Cao (2000) and Wang et al. (1984a) suggest that it is Cryogenian–Ediacaran in age. Recently, the Gouhou Formation is suggested to be Tonian in age (1000 to ~720 Ma) on the basis of chemostratigraphic correlations (Xiao et al., 2014a), but Cambrian detrital zircon ages have also been reported from the middle Gouhou Formation (He et al., 2017). Since the Gouhou Formation is overlain by the lower Cambrian Houjiashan Formation, a higher resolution of its depositional age would help to determine whether there is a significant depositional gap between these two formations; the magnitude of this depositional gap would help to confirm the global distribution of the Great Unconformity that pertinent to the Cambrian explosion out of the Laurentia (Peters and Gaines, 2012). To test the different age interpretations of the Gouhou Formation, we carried out a biostratigraphic investigation of this unit. Our study revealed a diverse assemblage of organic-walled microfossils, including a new species and the potential Tonian index fossil *Trachyhystrichosphaera aimika* from the lower Gouhou Formation, providing significant

biostratigraphic constraints for the Gouhou Formation. Our biostratigraphic study indicates that the Precambrian-Cambrian boundary in Huaibei region may be located within the Gouhou Formation with a depositional gap of >200 myr and represents a major tectonostratigraphic event.

3.3 Geological background

The Huainan and Huaibei regions are geographically located to the south and north of the Huai River, respectively. Geologically, they are located on the southeastern margin of the NCC (Fig. 3.1). Proterozoic stratigraphy of the Huainan and Huaibei regions has been described in Wang et al. (1984a) and Xiao et al. (2014a).

In the Huaibei region, the Huaibei Group consists of 13 lithostratigraphic formations and is characterized by siliciclastic rocks in the lower part, carbonates in the middle part, and carbonates intercalated with siliciclastic rocks in the upper part (Fig. 3.2; Cao et al., 1985). The uppermost unit of the Huaibei Group, the Gouhou Formation, is approximately 130 m thick at the Langan section which was sampled in this study (Fig. 3.2). The lower Gouhou Formation consists of yellowish green shale and grey thin- to medium-bedded siltstone with several sandstone interbeds. In addition, calcareous nodules of various sizes are common in the shales, and mud cracks are occasionally present in the calcareous siltstone. A conglomerate bed is identified at the base of the middle Gouhou Formation, which mainly consists of grey thin- to medium-bedded argillaceous limestone intercalated with reddish shales. The upper Gouhou Formation is mainly composed of greyish thin-bedded argillaceous limestone intercalated with dolostone in the lower part and light-grey medium- to thick-bedded dolostone with nodular cherts in the upper part. Previous researchers have reported *Chuaria circularis*, *Tawuia dalensis*,

cyanobacterium-like filaments, leiospheres, and acanthomorphic acritarchs from shales of the lower Gouhou Formation (Wang et al., 1984a; Zang and Walter, 1992; Qian et al., 2002).

Overlying the Huaibei Group is the lower Cambrian Houjiashan Formation, which is composed of yellowish thin-bedded dolomitic siltstone at the base and succeeded with a reddish weathering crust of thin-bedded limestone. Above the crust deposited with thick bioturbated limestone (Wang et al., 1984a). Trilobites from the Houjiashan Formation indicate a Tsanglanpu age (Zhang and Zhu, 1979), corresponding to Cambrian Stage 4, roughly 509–514 Ma (Peng et al., 2012).

There is a lithostratigraphic disconformity between the lower and middle Gouhou Formation and probably also between the Gouhou and Houjiashan formations at the Langan section in Huaibei region (Li et al., 2013). The transition from yellowish green shale of the lower Gouhou Formation to a distinct conglomerate layer succeeded with reddish shale of the middle Gouhou Formation indicate a significant transition of redox history. Similarly, the transition from light grey thick-bedded dolostone of the upper Gouhou Formation to yellowish siltstone and then reddish crust of thin-bedded limestone of the Houjiashan Formation may indicate another sharp environmental change. Regional mapping also shows that the Houjiashan Formation onlaps different units of the Huaibei Group, suggesting regional unconformity between them (Qian et al., 2001; Li et al., 2013). Thus, an age determination of the youngest unit in the Huaibei Group, the Gouhou Formation, would provide an estimate for the duration of these unconformities. Unfortunately, although U–Pb ages of detrital zircons and intrusive sills and dikes constrain much of the Huaibei Group between approximately 1069 Ma and 890 Ma (summarized in Xiao et al., 2014a), the depositional age of the Gouhou formations is not tightly constrained by any radiometric ages, and it has been previously interpreted as Cambrian (Xing et

al., 1985; Xing, 1989; Zang and Walter, 1992; Zheng et al., 1994; He et al., 2017), Cryogenian–Ediacaran (Wang et al., 1984b; Cao, 2000), or Tonian in age (Xiao et al., 2014a).

3.4 Materials and Methods

A total of 15 shale/mudstone samples, all of which were fossiliferous, were collected from the Gouhou Formation at the Langan section (33°59.563' N, 117°18.007'E) in Suzhou of northern Anhui Province (Fig. 3.1). The shale samples were processed by low-manipulation maceration techniques (Butterfield et al., 1994; Tang et al., 2013) in the palynological laboratory of Nanjing Institute of Geology and Palaeontology (NIGPAS). Organic-walled microfossils were manually removed from maceration residues and individually mounted on glass slides for light microscopy. Selected microfossils were also examined using scanning electron microscopy. All illustrated specimens are reposited in NIGPAS.

3.5 Summary of microfossils from the Gouhou Formation

The Gouhou Formation contains a rich assemblage of microfossils (Fig. 3.3), as well as common Proterozoic macrofossils such as *Chuaria circularis* Walcott, 1899 and *Tawuia dalensis* Hofmann *in* Hofmann and Aitken, 1979 (Fig. 4A, B; Hofmann and Aitken, 1979). The microfossil assemblage is dominated by leiospheric acritarchs and cyanobacterial filaments. Specimens of the smooth-walled sphaeromorph genus *Leiosphaeridia*, ranging from 32 μm to 196 μm in diameter (average = 117 μm; n = 148), are present in almost all samples (Fig. 3.4C–G). Their relatively simple morphology makes it difficult to infer their biological affinities, and some leiospheres may represent early life stages or taphonomically degraded variants of co-existing complex forms. Thus, we follow the practice of Butterfield et al. (1994) and Tang et al. (2013) to

identify the morphospecies of *Leiosphaeridia* on the basis of wall thickness and vesicle dimension. Namely, *Leiosphaeridia* specimens are assigned to *L. minutissima* (Naumova, 1949) Jankauskas *in* Jankauskas et al., 1989 (thin-walled, less than 70 μm in diameter); *L. tenuissima* Eisenack, 1958 (thin-walled, 70–200 μm in diameter); *L. crassa* (Naumova, 1949) Jankauskas *in* Jankauskas et al., 1989 (thick-walled, less than 70 μm in diameter); and *L. jacutica* (Timofeev, 1966) Mikhailova and Jankauskas *in* Jankauskas et al., 1989 (thick-walled, 70–800 μm in diameter).

Aggregates of spheroidal or ellipsoidal vesicles are also common in the Gouhou Formation, including *Eosynechococcus moorei* Hofmann, 1976, *Symplassosphaeridium* sp., *Synsphaeridium* sp., and *Fabiformis baffinensis* Hofmann *in* Hofmann and Jackson, 1994. The rod-shaped cells or bacilloids identified as *Eosynechococcus moorei* Hofmann, 1976 are 2.7–16.5 μm in length, 1.2–6.8 μm in width, and 1.2–4.0 in length/width ratio (n = 118). They can be clustered (Fig. 3.5A, B) or randomly dispersed (Fig. 3.5C). The genus *Eosynechococcus* was originally erected for small ellipsoidal microfossils by Hofmann (1976), and several species have been recognized subsequently based on the cell sizes and length/width ratios (Fig. 3.6; Hofmann, 1976; Knoll and Golubic, 1979; Knoll, 1982; McMenamin et al., 1983; Strother et al., 1983; Golovenoc and Belova, 1984; Jankauskas et al., 1989). However, the variable cell size and length/width ratio as observed in the same cluster may reflect intraspecific or ontogenetic variations. Thus, we identify the Gouhou bacilloidal fossils as *E. moorei*, the type species of *Eosynechococcus*. Vesicles of *Symplassosphaeridium* sp. are generally 12–36 μm in diameter (average = 29 μm; n = 507) and regularly arranged in compact globular aggregates 88–195 μm across (average = 143 μm; n = 42; Fig. 3.7). Like *Symplassosphaeridium* sp., *Synsphaeridium* sp. is also characterized by aggregates of spheroidal vesicles (Fig. 3.8A–C), but the cells of

Synsphaeridium are relatively larger (36–62 μm in diameter), fewer per cluster (3–15), and more irregularly arranged (74–182 μm in maximum cluster dimension; n = 7). Although *Symplassosphaeridium* and *Synsphaeridium* are morphotaxa with close morphological similarities and perhaps biological affinities, here we follow the practice of Jankauskas et al. (1989) and Hofmann and Jackson (1994) to differentiate them on the basis of cell size and number. An elongate aggregate (261 μm in length and 39 μm in width) consisting of hundreds of tightly arranged spheroidal vesicles (each about 7 μm in diameter; Fig. 3.8D) is identified as *Fabiformis baffinensis* Hofmann *in* Hofmann and Jackson, 1994.

In addition to the smooth-walled sphaeromorphs, several morphologically complex netromorph, sculptured sphaeromorphs, and acanthomorphs were also revealed from the Gouhou Formation, including *Navifusa majensis* Pyatiletov, 1980, *Dictyosphaera tacita* n. sp., *Valeria lophostriata* (Jankauskas, 1979) Jankauskas, 1982, *Squamosphaera colonialica* (Jankauskas, 1979) n. comb., and *Trachyhystrichosphaera aimika* Hermann *in* Timofeev et al., 1976. The smooth-walled tomaculate vesicles of *Navifusa majensis* are approximately 92–191 μm in length and 30–64 μm in width (n = 5; Fig. 9A–C, 9D?, 9E?). Their relatively small length/width ratios (between 2.2 and 3.1) and nearly cylindrical vesicles with closed round ends distinguish them from the spindle shaped vesicles of *Leiovalia* Eisenack, 1965, but fit the definition of *N. majensis*. *Navifusa* can be differentiated from other Proterozoic–Paleozoic netromorphic forms such as *Teophipolia* Kirjanow *in* Volkova, 1979, *Pololeptus* Yin *in* Yin and Sun, 1994, and *Torgia* Grigorieva and Kolosov *in* Jankauskas et al., 1989. For example, *Teophipolia* is characterized by a biological opening at one end of its circular or elongated vesicle (Volkova et al., 1979); *Pololeptus* vesicles are typically decorated with fine arranged transverse annulations (best seen in the equatorial region) and pitted textures in one or both polar regions (Tang et al., 2013); and

Torgia is characterized by ellipsoidal or highly elongate spindle-like vesicle with compact ends, sporadically distributed processes, and sometimes an organic outer membrane (Jankauskas et al., 1989; Kolosov, 2014). The herkomorph *Dictyosphaera tacita* n. sp. is characterized by interlocking polygonal sculptures on the interior surface of its vesicle wall (Fig. 3.10). The polygonal ornamentations typically consist of interlocking equilateral hexagons, 0.5–0.9 μm in width. Another common element in the Gouhou Formation is *Valeria lophostriata,* characterized by evenly spaced concentric striations on the interior surface of the vesicle, which is 106–216 μm in diameter (average = 167; n = 9; Fig. 3.11). *Squamosphaera colonialica* (Jankauskas, 1979) n. comb. is an acanthomorph with a single-walled spheroidal to tomaculate vesicle (Figs. 3.12 and 3.13), 80–489 μm in length (average = 189 μm; n = 127), 43–219 μm in width (average = 105 μm; n = 127), and 1.0–6.2 in length/width ratio (Figs. 3.14 and 3.15). Its processes are broadly or obtusely domical, in contact at base, apparently communicate with the vesicle cavity, 10–33 μm in basal width, 1–8 μm in length, and 0.07–0.38 in length/width ratio (Fig. 3.16). The processes are similar to those of *Culcitulisphaera revelata* (Riedman and Porter, 2015), but the latter are much smaller and more densely distributed. The acanthomorphic acritarch *Trachyhystrichosphaera aimika*, a potential Tonian index fossil (Butterfield et al., 1994; Tang et al., 2013), has also been found in the Gouhou Formation (Fig. 3.17). Specimens in our collection are 38–109 μm in vesicle diameter (average = 85 μm; n = 4), with sporadically distributed hollow cylindrical or conical processes (1–4 μm in basal width, average = 3 μm; n = 8).

Like many other Tonian microfossil assemblages, filamentous fossils, sometimes occurring in fragments of microbial mats, are very common in the Gouhou Formation. Some of these microbial mat fragments can be seen on bedding surfaces (Fig. 3.18A). The extracted microbial mat fragments, with a maximum dimension of 142–370 μm, mainly consist of the

genus *Siphonophycus* (Fig. 3.18B, C). *Siphonophycus* species are distinguished based on their filament diameter (Knoll et al., 1991; Butterfield et al., 1994). *Siphonophycus* species in the Gouhou Formation include: *S. septatum* (Schopf, 1968) Knoll, Swett, and Mark, 1991 (1–2 μm in filament diameter); *S. robustum* (Schopf, 1968) Knoll, Swett, and Mark, 1991 (2–4 μm); *S. typicum* (Hermann, 1974) Butterfield *in* Butterfield, Knoll, and Swett, 1994 (4–8 μm); *S. kestron* Schopf, 1968 (8–16 μm); and *S. solidum* (Golub, 1979) Butterfield *in* Butterfield, Knoll, and Swett, 1994 (16–32 μm). Some *Siphonophycus* filaments are coiled to form a loop structure up to 142 μm in maximum dimension (Fig. 3.19A). An unbranched form of uniserial filament characterized by a gradually swelling clavate end was recovered from the Gouhou Formation (Fig. 3.19B–D); the filaments are 140–308 μm in length (average = 203 μm; n = 3) and 30–33 μm in maximum width (average = 32 μm; n = 3). This form is placed in an unnamed taxon, but it could represent fragments of *Palaeovaucheria clavata* Hermann, 1981 or *Aimonema ramosa* Hermann *in* Hermann and Podkovyrov, 2010. Its gradually expanded termination can be distinguished from the abrupt transition from a spherical vesicle to a tubular appendage in *Clavitricoides rugosus* Mikhailova *in* Jankauskas et al., 1989, *Caudosphaera expansa* Herman and Timofeev *in* Jankauskas et al., 1989, and *Germinosphaera bispinosa* Mikhailova, 1986. Finally, bundled filaments identified as *Polytrichoides lineatus* (sometimes spelt as *Polythrichoides lineatus*) Hermann, 1974, are present in the Gouhou Formation (Fig. 3.19E, F). Those bundles, 171–528 μm in length and 6–112 μm in width (n = 10), consist of unbranched filaments. Some of these filaments show impressions of trichome cells about 10 μm in length and 5 μm in width (Fig. 3.19E).

3.6 Discussion

3.6.1 Biostratigraphic implications

The organic-walled microfossil assemblage from the Gouhou Formation is characterized by abundant smooth-walled sphaeromorphs and filaments with relatively low abundance of netromorph, sculptured sphaeromorphs, and acanthomorphs. Generally, this assemblage is distinct from Ediacaran acritarch assemblages which are characterized by diverse taxa of large acanthomorphs (Zhang et al., 1998; Grey, 2005; Vorob'eva et al., 2009b; Sergeev et al., 2011; Moczydlowska and Nagovitsin, 2012; Liu et al., 2014; Xiao et al., 2014b), but similar to the Tonian microfossil assemblages from the Liulaobei Formation in Huainan region and other Tonian strata worldwide summarized in Tang et al. (2013).

Several taxa in the lower Gouhou Formation have important biostratigraphic significance and are consistent with a Tonian age. The acanthomorphic acritarch *T. aimika* is a potential Tonian index fossil with nearly all of its occurrences restricted to the Tonian Period (Butterfield et al., 1994; Tang et al., 2013), except its presence in Lakhanda Group (Timofeev et al., 1976) that has been directly dated at 1025 ± 40 Ma using Pb–Pb isochron method (Semikhatov et al. (2000) and constrained to be >1005 ± 4 Ma by a U–Pb baddeleyite age of intruding gabbro sills (Rainbird et al. (1998). The concentrically striated acritarch *Valeria lophostriata* is also a widely distributed taxon that has been reported only from pre-Cryogenian strata so far (Hofmann, 1999). *Dictyosphaera tacita* n. sp. is a new form from the lower Gouhou Formation and its complete stratigraphic range remains undocumented, but the genus *Dictyosphaera* seems to have a long stratigraphic range extending to the Paleo-Mesoproterozoic (Xing and Liu, 1973; Xiao et al., 1997; Javaux et al., 2001; Pang et al., 2013; Agić et al., 2015). However, the occurrence of *Chuaria* and *Tawuia* in the lower Gouhou Formation (Fig. 3.3A, B; Wang et al., 1984a; Zang

and Walter, 1992) is consistent with a Tonian age; although *Chuaria circularis* is very common in Precambrian successions and *Tawuia dalensis* may range into Ediacaran (Tang et al., 2008), the *Chuaria-Tawuia* assemblage is most abundant in Tonian strata (Hofmann, 1994; Steiner, 1997). It is true that some Gouhou genera, such as *Valeria* and *Dictyosphaera*, *Chuaria*, and *Tawuia* can range into the Mesoproterozoic or even Paleoproterozoic, but their co-occurrence with *Trachyhystrichosphaera aimika* indicates a likely Tonian age for the lower Gouhou Formation.

Our study confirms most taxa previously reported from the Gouhou Formation, but we were unable to verify the presence of *Baltisphaeridium* and *Micrhystridium* in the Gouhou Formation (Wang et al., 1984a; Zang and Walter, 1992). The specimen identified as *Micrhystridium* sp. was poorly illustrated (Wang et al., 1984), and its taxonomic identification is questionable. We concur with Yin and Sun (1994) that specimens described as *Baltisphaeridium* spp. in Zang and Walter (1992) might be contaminations because their somewhat three-dimensional preservation is distinct from the flattened acritarchs in the Gouhou Formation.

Depositional age for the middle to upper Gouhou Formation is ambiguous and yet to be constrained. Our study shows there are only a few *Leiosphaeridia*, which has long stratigraphic range, recovered from the middle Gouhou Formation (Fig. 3.3) and no fossils found from the upper Gouhou Formation so far. Given the disconformity identified on the contact between the lower and middle Gouhou Formation and the early Cambrian detrital zircons from the middle Gouhou Formation (He et al., 2017), we retain the possibility that a significant depositional hiatus might happen on this disconformable contact.

In summary, biostratigraphic data from the lower Gouhou Formation—particularly the occurrence of *Trachyhystrichosphaera aimika* indicate a Tonian rather than Cryogenian–

Ediacaran (Wang et al., 1984a; Cao, 2000) or Cambrian age (Xing, 1989; Zang and Walter, 1992; Xing et al., 1996). Whether the entire Gouhou Formation is Tonian age or the middle and upper Gouhou Formation are much younger deposits (e.g., early Cambrian deposits) is dependent on further investigation of the middle to lower part of this unit, particularly the detrital zircon geochronological analysis.

3.6.2 Tectonic implications

A Tonian age for the lower Gouhou Formation is consistent with regional geological mapping that shows a significant unconformity on the Precambrian-Cambrian contact (Li et al., 2013). Our study further confirms that this contact is likely located at the boundary between the lower and middle Gouhou Formation with a missing of >200 million years. The magnitude of this unconformity implies a major tectonostratigraphic event. Future research should be directed to investigate whether the infra-Cambrian unconformity observed along the northern, southeastern, and southwestern margins of NCC is related to the same tectonostratigraphic event, whether this event was caused by the assembly and disassembly of the Rodinia supercontinent, and its impact on global geochemical cycles and the Cambrian radiation of animals (Peters and Gaines, 2012).

3.7 Conclusions

The organic-walled microfossil assemblage from the Gouhou Formation is mainly composed of sphaeromorphic acritarchs and cyanobacterium-like filaments, as well as several morphologically complex taxa. A total of 22 taxa have been recognized, including a new species—*Dictyosphaera tacita* n. sp. Particularly important is the occurrence of

Trachyhystrichosphaera aimika and *Valeria lophostriata* from the lower Gouhou Formation, which indicate that the lower Gouhou Formation is Tonian in age. Together, biostratigraphic data and lithostratigraphic correlation with other radiometrically dated Tonian successions imply a >200 myr unconformity (i.e., the Great Unconformity) between the Precambrian-Cambrian boundary in Huaibei region of North China, which might be located between the lower and middle Gouhou Formation in Huaibei region. The magnitude of this unconformity suggests that a major tectonostratigraphic event occurred in the southeastern margin of NCC between Tonian and early Cambrian periods.

3.8 Systematic Paleontology

Group Acritarcha Evitt, 1963

Genus *Dictyosphaera* Xing and Liu, 1973

Type species: *Dictyosphaera macroreticulata* Xing and Liu, 1973.

Dictyosphaera tacita n. sp.

Figure 3.10

2014 *Dictyosphaera* sp., Xiao et al., 2014a, p. 217, fig. 6A–B, I, J.

Holotype: The specimen illustrated in Fig. 3.10A is designed as the holotype; Nanjing Institute of Geology and Palaeontology, catalog # PB21865; slide 11-GH-10-6-8; England Finder coordinates U-62-4.

Type locality: Langan section near Langan of northern Anhui Province; 30 m above the base of the Gouhou Formation.

Material: Two specimens from shale sample 11-GH-10.

Diagnosis: Spheroidal to subspheroidal vesicle with interlocking hexagonal ridges (<1 μm in width) on interior vesicle surface. Exterior surface of vesicle wall apparently smooth.

Description: Single-layered spheroidal vesicle (101–119 μm in diameter; n = 2) ornamented with interlocking equilateral hexagons (0.5–0.9 μm in width) on interior vesicle surface. Hexagonal ridge approximately 0.3–0.5 μm wide, 0.07–0.1 μm thick, and 0.15–0.2 μm high (Fig. 3.10B_4).

Remarks: The genus *Dictyosphaera* with *D. macroreticulata* as its type species was erected by Xing and Liu (1973), and several additional species have been recognized subsequently, including *Dictyosphaera sinica* Xing and Liu, 1973 and *Dictyosphaera delicata* Hu and Fu, 1982. *D. macroreticulata* and *D. sinica* are both characterized by reticulate vesicle surface, it is not clear on the basis of published transmitted light micrographs whether the sculpture is on the interior or exterior surface of the vesicle wall (Xing and Liu, 1973). *Dictyosphaera delicata* and the morphologically similar but process-bearing acritarch *Shuiyousphaeridium macroreticulatum* from Paleo-Mesoproterozoic Ruyang Group and Gaoshanhe Formation in NCC are both characterized by interlocking polygonal platelets on the interior vesicle surface and corresponding polygonal ridges on the exterior vesicle surface (Hu and Fu, 1982; Xiao et al., 1997; Javaux et al., 2004; Yin et al., 2005; Schiffbauer and Xiao, 2009; Pang et al., 2013). Agić et al. (2015) have demonstrated that the polygonal platelets on the interior vesicle surface of *D. delicata* can be enhanced by taphonomic disintegration of a secondary vesicle wall, resulting in incisions following polygonal ridges and improving the

visibility of the platelets. They also argue that *D. delicata* and *D. macroreticulata* are synonymous, a taxonomic proposition that needs to be evaluated in the future by a critical re-examination and re-illustration of *D. macroreticulata*.

Regardless, *Dictyosphaera tacita* n. sp. is different from other species of *Dictyosphaera* in its apparently smooth exterior vesicle surface and the apparent presence of hexagonal only on interior vesicle surface. Furthermore, the hexagons on its vesicle wall are 0.5–0.9 μm in size, smaller than the polygonal structures in *D. macroreticulata* (2–6 μm in diameter), *D. sinica* (0.5–1.5 μm in diameter), and *D. delicata* (1–3 μm in width) (Xing and Liu, 1973; Yin et al., 2005). Its vesicle size is much larger than that of *D. macroreticulata* (10–20 μm in diameter) and *D. sinica* (15–45 μm in diameter).

Dictyosphaera tacita n. sp. can also be differentiated from *Dictyotidium* Eisenack, 1955 by the polygonal ridges on its interior vesicle surface, as opposed to the prominent polygonal walls or fences on the exterior vesicle surface of *Dictyotidium* (Eisenack, 1955). The Tonian species of *Dictyotidium*, *D. fullerene* Butterfield, 1994 from the Svanbergfjellet Formation of Svalbard, is additionally characterized by short protruding spines rising from the intersecting points of polygons and supporting a thin outer membrane (Butterfield et al., 1994); these features are not present in *D. tacita* n. sp.

Etymology: Species epithet derived from Latin *tacitus*, with reference to polygonal ornaments that are hidden on the interior surface of the vesicle wall.

Genus *Eosynechococcus* Hofmann, 1976

non 1980 *Eosynechococcus minutus* Nautiyal, p. 6, fig. 1S, T.

nec 1984 *Eosynechococcus major* Golovenoc and Belova, p. 28, pl. II, fig. 2.

nec 1984 *Eosynechococcus giganteus* Golovenoc and Belova, p. 28–29, pl. II, fig. 3.

nec 1984 *Eosynechococcus crassus* Golovenoc and Belova, p. 29, pl. II, fig. 4.

nec 1984 *Eosynechococcus elongatus* Golovenoc and Belova, p. 29, pl. II, fig. 5.

Type species: *Eosynechococcus moorei* Hofmann, 1976.

Remarks: The genus *Eosynechococcus* is characterized by small bacilloidal or ellipsoidal cells (typically with a length of <20 μm, a width of <10 μm, and a maximum length/width ratio of ~4) that are solitary, chained, or clustered, and sometimes show evidence of binary fission (Hofmann, 1976; Butterfield et al., 1994; Sergeev et al., 1995). *Archaeoellipsoides* Horodyski and Donaldson, 1980, also has ellipsoidal cells, but its cells are much larger, have a broader size range (~20–150 μm in length and 2–40 μm in width), and show no evidence of binary fission (Sergeev et al., 1995). Hence, *E. elongatus*, *E. major*, *E. crassus*, and *E. giganteus*—all of which were established by Golovenoc and Belova (1984) from the Mesoproterozoic Billyakh Group in northern Siberia—have been removed from *Eosynechococcus* to *Archaeoellipsoides* because of their large cell size and lack of binary division (Sergeev et al., 1995). Furthermore, *E. minutus* has ensheathed colonial coccoids (Nautiyal, 1980) and thus does not fit the genus diagnosis according to Schopf and Klein (1992). According to Sergeev et al. (1995), Siberian specimens described as *E. grandis* Hofmann, 1976 by Golovenoc and Belova (1984, 1985) should also be transferred to the genus *Archaeoellipsoides*, although their cell size do overlap with the type material of *E. grandis* from the Belcher Supergroup of Canada (Hofmann, 1976).

Eosynechococcus moorei Hofmann, 1976

Figure 3.5

1976 *Eosynechococcus moorei* Hofmann, p. 1057, pl. 2, figs. 1–7, 8(?).

1994 *Eosynechococcus moorei* Hofmann; Butterfield et al., p. 54, fig. 23J.

1995 *Eosynechococcus moorei* Knoll; Sergeev et al., p. 27, fig. 9.8, 9. 12, 9. 13.

Material: Hundreds of well-preserved cells occurring individually or in clusters in shale samples from 11-GH-8 to 11-GH-12.

Description: Ellipsoidal to rod-like cells with smooth cell walls. Cells preserved in clusters or scattered randomly. Cells in the same cluster can be variable in size. Overall, cell length is 3–17 μm, cell width 1–7 μm, and length/width ratio 1.2–4 among specimens in our collection. Transverse fission not observed.

Remarks: The form genus *Eosynechococcus* was erected by Hofmann (1976) with its type species *E. moorei* and two other species, *E. medius* and *E. grandis*; specimens illustrated in plate 2, figure 8 of Hofmann (1976) could be assigned to either *Eosynechococcus moorei* or *Sphaerophycus parvum* Schopf, 1968. Subsequently named species include *E. amadeus* by Knoll and Golubic (1979), *E. brevis* and *E. depressus* by Knoll (1982), *E. burzjanicus* by Jankauskas et al. (1989), and *E. isolatus* by McMenamin et al. (1983). These species were established based on their different but overlapping cell sizes and length/width ratios (Fig. 3.6). In our collection, however, ellipsoidal cells in the same cluster can have a wide range of cell size and length/width ratio (Fig. 3.6). It is possible that the difference in cell size and length/width ratio among established *Eosynechococcus* species may be due to ontogenetic variation. If so, *Eosynechococcus medius* (cells 5.5–7.5 μm in length and 3–4 μm in width, with an average length/width ratio 1.9), *E. grandis* (cells 11.5–19 μm in length and 5–7 μm in width, with an average length/width ratio 2.1), *E. amadeus* (cells 1.85–4.53 μm in length and 0.96–1.88 μm in

width, with an average length/width ratio 2.3), *E. burzjanicus* (cells 6–10 μm in length and 3–6 μm in width), and *E. isolatus* (cells 1.7–8.5 μm in length and 1.7–6.8 μm in width, with an average length/width ratio 1.5) may be junior synonyms of *E. moorei* (our collection showing cell length of 2.7–16.5 μm, cell width of 1.2–6.8 μm, and length/width ratio of 1.2–4.0). Alternatively, our collection from the Gouhou Formation may represent multiple species of *Eosynechococcus*. Given the observation that *Eosynechococcus* cells in a single cluster from the Gouhou Formation span the size range of several established species, we favor the former possibility and tentatively identify all specimens in our collection as *E. moorei*. More research is needed to determine whether *E. medius*, *E. grandis*, *E. amadeus*, *E. burzjanicus*, and *E. isolatus* are junior synonyms of *E. moorei*.

Eosynechococcus moorei is distinct from the much larger and often individually preserved cells of *E. major* (cells 24–50 μm in length and 10–20 μm in width, with an average length/width ratio 2.4), *E. giganteus* (cells 50–100 μm in length and 15–30 μm in width, with an average length/width ratio 3.6), *E. crassus* (cells 96 μm in length and 32–36 μm in width, with an average length/width ratio 2.8), and *E. elongatus* (cells 16–40 μm in length and 2–8 μm in width, with an average length/width ratio 6) (Golovenoc and Belova, 1984); indeed, Sergeev et al. (1995) has transferred *E. major*, *E. crassus*, and *E. elongatus* to the genus *Archaeoellipsoides* Horodyski and Donaldson, 1980, and has synonymized *E. giganteus* with *A. grandis* Horodyski and Donaldson, 1980 on the basis of their large vesicle size, similarity to nostocalean akinetes, and lack of transverse fission. Additionally, *Eosynechococcus moorei* can also be distinguished from *E. brevis* Knoll, 1982 (which is characterized by nearly spherical cells, although its cell size is similar to *E. moorei* from the Gouhou Formation), *E. depressus* Knoll, 1982 (which may has originally compressed or flattened cells, although its cell size is similar to *E. moorei* from the

Gouhou Formation), and *E. thuleensis* Strother, Knoll, and Barghoorn, 1983 (which has relatively larger vesicles and almost constant vesicle width).

Occurrences: Palaeoproterozoic Belcher Supergroup, Canada (Hofmann, 1976); Mesoproterozoic Billyakh Group, northern Siberia (Sergeev et al., 1995); Early Neoproterozoic Svanbergfjellet Formation, Spitsbergen (Butterfield et al., 1994); and many other Proterozoic strata.

Genus *Squamosphaera* n. gen.

Type species: *Squamosphaera colonialica* (Jankauskas, 1979) n. comb., emended.

Diagnosis: Medium-sized to large, single-walled, and spheroidal to tomaculate vesicles ornamented with a moderate number of broadly domical processes. Processes evenly distributed, in contact at base, and freely communicate with vesicle cavity.

Remarks: The genus *Squamosphaera* n. gen. is characterized by evenly distributed and broadly (obtusely) domical processes which are in contact at base and freely communicate with the interior cavity of single-walled spheroidal, ellipsoidal, or tomaculate vesicles. When compressed over each other, the processes are flattened to form an imbricate pattern resembling fish scales (Fig. 3.12B), but the broadly domical processes are discernable at the vesicle periphery where they are not imbricate on each other (Figs. 3.12 and 3.13). Several Ediacaran acritarchs—including *Bacatisphaera* Zhou, Brasier and Xue, 2001, *Bullatosphaera* Vorob'eva et al., 2009b, *Eotylotopalla* Yin, 1987, *Pustulisphaera* Zhang et al., 1998, *Symphysosphaera* Yin, 1992, and *Timanisphaera* Vorob'eva et al., 2009b—also have domical to hemispherical processes or superficially resemble *Squamosphaera*. *Bacatisphaera* is different from

Squamosphaera n. gen. by its homomorphic or heteromorphic processes that are hemispherical in shape and separate at base (Xiao et al., 2014b). *Bullatosphaera* can be differentiated from the new genus by its double-walled vesicle with spheroidal structures that are located between the two vesicle walls and do not communicate with vesicle interior (Vorob'eva et al., 2009b). *Eotylotopalla strobilata* (Faizullin, 1998) Sergeev et al., 2011 has generally smaller vesicles than *Squamosphaera*, and its processes are much smaller, more numerous, more densely distributed, and more variable in shape, ranging from hemispherical to somewhat elongate (Sergeev et al., 2011). Other *Eotylotopalla* species can be easily differentiated by their small to medium-sized vesicle and cylindrical, digitate, bulbous, and sometimes bifurcate processes (Yin, 1987; Zhang et al., 1998; Liu et al., 2014; Xiao et al., 2014b). *Pustulisphaera* supposedly has three vesicle walls, with the middle wall bearing regularly distributed hemispherical processes that are basally in contact with each other. Even when the inner and outer membranes of *Pustulisphaera* are not preserved due to taphonomic loss (Xiao et al., 2014b), *Pustulisphaera* can still be differentiated from *Squamosphaera* by its much larger vesicle (>500 μm in diameter) and proportionately much smaller hemispherical processes. *Symphysosphaera* is a coeloblastula-like fossil with a layer of small spheroidal cells that are either supported by a basal membrane defining a central cavity (Liu et al., 2014) or surrounded by an outer membrane (Yin, 1992). It does not have true processes, and in this sense it is similar to *Bullatosphaera* and can be easily differentiated from *Squamosphaera*. *Timanisphaera* differs from the current genus in its relatively larger spheroidal vesicles and sporadically distributed broadly conoidal or somewhat elongate processes. Therefore, the vesicle size and process morphology, size, and density distinguish *Squamosphaera* n. gen. from seemingly similar Ediacaran acritarchs (Fig. 3.16).

Several Proterozoic forms, including *Satka* Jankauskas, 1979, *Spumosina* Naumova, 1968, and *Culcitulisphaera* Riedman and Porter, 2015, are superficially similar to *Squamosphaera* n. gen. *Satka* has a spheroidal or elongate vesicle consisting of regularly arranged polygonal plates (Jankauskas et al., 1989; Hofmann and Jackson, 1994; Javaux et al., 2004), which can appear similar to imbricate processes when viewed under transmitted light microscopy. *Spumosina* is a synaplomorph with a spherical aggregate of cells, which when compressed may have a spongy appearance and may appear similar to spherical processes (Hofmann and Jackson, 1994). *Culcitulisphaera* differs from *Squamosphaera* n. gen. in its blister-like outpocktes that are only 1.3–2.7 μm in size (Riedman and Porter, 2015).

Etymology: Genus epithet from Latin *squama* (scale) and Greek *sphaira*, with reference to the fish scale-like pattern of compressed processes.

Squamosphaera colonialica (Jankauskas, 1979) n. comb., emended

Figures 3.12 and 3.13

1979 *Satka colonialica* Jankauskas, p. 53, fig. 1.4–1.6.

1985 *Satka colonialica* Jankauskas; Vidal and Ford, p. 369, fig. 6A–F.

1989 *Satka colonialica* Jankauskas; Jankauskas et al., p. 51, pl. IV, figs. 4, 7.

Holotype: Jankauskas 1979, fig. 1.4.

Material: 127 specimens from shales of the lower Gouhou Formation.

Emended diagnosis: A species of *Squamosphaera* with vesicle size around 80–500 μm in length and 40–200 μm in width, and domical process around 5–30 μm in basal width.

Description: Originally spheroidal to sausage-shaped vesicles with broadly or obtusely domical processes that are evenly distributed on vesicle surface and freely communicate with vesicle interior. Approximately 80–489 μm in vesicle length (average = 189 μm; n = 127), 43–219 μm in vesicle width (average = 105 μm; n = 127), and 1.0–6.2 in vesicle length/width ratio. Processes 10–33 μm (n = 161) in basal width, 1–8 μm (n = 161) in length, 0.07–0.38 (n = 161) in process length/width ratio, and 0.04–0.30 in process basal width/vesicle length ratio; some processes are very short and barely stand above vesicle surface (e.g., fig. 3.13A, B). Approximately 15–38 (n = 22) processes per circumferential view.

Remarks: Most specimens of *Squamosphaera colonialica* n. comb. are spheroidal to subspheroidal with a length/width ratio less than 2, but some specimens have tomaculate vesicles with a length/width ratio up to 6.2 (Fig. 3.14). Because there are transitional forms between the spheroidal and tomaculate specimens (Fig. 3.13A–C), and there are no obvious cut-offs in vesicle and process morphologies (Figs. 3.14 and 3.15), we thus place all specimens in the same species. Some tomaculate vesicles appear to develop one or more transverse constrictions (Fig. 3.13E, F), which may be an indication of division through transverse fission. Hence, the variable vesicle morphologies of *S. colonialica* n. comb. may represent different ontogenetic stages.

The type material of *S. colonialica* n. comb. from the Neoproterozoic Zigazino-Komarovsk Beds of the Urals, as well as material from the Neoproterozoic Kwagunt Formation in Arizona, was misplaced in the genus *Satka*, which is characterized by polygonal plates comprising the vesicle wall, which does not bear processes (Hofmann and Jackson, 1994; Javaux et al., 2004). Specimens from the Gouhou Formation are generally larger in vesicle size and process basal width than the type material (up to 150 μm in vesicle diameter and 4–8 μm in process basal width) reported by Jankauskas (1979). Hence an emendation is provided here to

accommodate the Gouhou material and to emphasize the domical shape of the processes. Vidal and Ford (1985) indicated that the domical processes could be impressions of cells that once existed within the vesicle interior. However, no such cells have been found in specimens from the Kwagunt Formation or elsewhere, even when the vesicles are preserved intact without an excystment structure. Supported by new SEM observations, we describe these structures as domical processes rather than circular impressions on the vesicle wall.

Squamosphaera colonialica n. comb. is somewhat similar to *Eotylotopalla*? *grandis* Tang et al., 2013, which could be synonymous with *Timanisphaera apophysa* Vorob'eva et al., 2009b. However, *S. colonialica* n. comb. has relatively smaller vesicles and more numerous and smaller processes. The processes of *T. apophysa* are much larger and somewhat more conical in comparison with the broadly domical processes of *S. colonialica* n. comb. One of the unnamed specimens from the lower Vychegda Formation (pl. 4, fig. 24 of Veis et al., 2006), which was later assigned to *T. apophysa* by Vorob'eva et al. (2009b), could also be identified as *S. colonialica* based on their similarity in vesicle size and process size, shape, and density.

Eotylotopalla strobilata (Faizullin, 1998) Sergeev et al., 2011 also has densely and evenly distributed hemispherical processes on the spheroidal vesicles, but its processes are much smaller, more elongate, and more densely distributed than those of *S. colonialica* n. comb. *Culcitulisphaera revelata* differs from *S. colonialica* n. comb. by its more densely distributed and much smaller circular outpockets (1.3–2.7 μm in diameter; Riedman and Porter, 2015). Synaplomorphs, such as *Synsphaeridium* and *Symplassosphaeridium*, can appear superficially similar to *S. colonialica* n. comb., but they are characterized by aggregates of cells rather than vesicles with domical processes (compare Fig. 3.8B_2 with Figs. 3.12B_3, C_2, and 3.13D_2).

Genus *Trachyhystrichosphaera* Timofeev and Hermann, 1976, emended Tang et al., 2013

Type species: *Trachyhystrichosphaera aimika* Hermann *in* Timofeev et al., 1976.

Trachyhystrichosphaera aimika Hermann *in* Timofeev et al., 1976, emended Butterfield et al., 1994

Figure 3.17

2000 *Trachyhystrichosphaera stricta* Hermann; Gnilovskaya et al., pl. 1, fig. 19.

2004 *Trachyhystrichosphaera aimika* Hermann; Veis et al., pl. 1, fig. 4.

2004 *Trachyhystrichosphaera stricta* Hermann; Veis et al., pl. 1, fig. 5.

2004 *Trachyhystrichosphaera vidalii* Hermann; Veis et al., pl. 7, fig. 7.

2007 *Prolatoforma aculeata* Mikhailova; Vorob'eva et al., pl. 1, fig. C.

2007 *Trachyhystrichosphaera aimika* Hermann; Vorob'eva et al., pl. 1, fig. B.

2009a *Trachyhystrichosphaera aimika* Hermann; Vorob'eva et al., fig. 4t.

2009b *Trachyhystrichosphaera aimika* Hermann; Vorob'eva et al., p. 183, fig. 8.11.

2013 *Trachyhystrichosphaera aimika* Hermann; Tang et al., p. 175, figs. 8–10; and synonyms therein.

2014 *Trachyhystrichosphaera aimika* Hermann; Xiao et al., 2014a, p. 217, fig. 6C.

Material: Four specimens isolated from shale sample 11-GH-10.

Description: Spheroidal to sub-spheroidal vesicle with irregularly and sparsely distributed, heteromorphic, and conical to tubular processes. Processes are hollow and freely communicate with vesicle cavity. A dark central body is present in some vesicles. Remnant of an

outer membrane is present in some specimens (Fig. 3.17B_2). Vesicle diameter is 38–109 μm (average = 85 μm; n = 4) and process basal width is 1–4 μm (average = 3.1 μm; n = 8).

Remarks: Butterfield et al. (1994) synonymized *T. stricta* and *T. vidalii* with *T. aimika,* and Tang et al. (2013) synonymized *P. aculeata* with *T. aimika*. Thus, only three species of *Trachyhystrichosphaera* are recognized: *T. polaris*, *T. botula*, and *T. aimika*. *Trachyhystrichosphaera polaris* is characterized by echinate structures loosely or closed packed in spheroidal vesicles (Butterfield et al., 1994). *T. botula* has a distinctive sausage-shaped vesicle with a length/width ratio of >2 (Tang et al., 2013). *Trachyhystrichosphaera* specimens from the Gouhou Formation have spheroidal vesicles with sporadically distributed, hollow, conical or tubular processes (Fig, 3.17), and they are most appropriately identified as *T. aimika*.

Trachyhystrichosphaera aimika has been proposed as a potential Tonian index fossil (Butterfield et al., 1994; Tang et al., 2013). There are a few questionable reports of *T. aimika* from younger strata, such as the occurrences of ?*T.* aff. *aimika* in the Ediacaran Ura Formation of East Siberia (Moczydłowska and Nagovitsin, 2012; Nagovitsin et al., 2004) and *T. aimika* in the lower Vychegda Formation in East European Platform (Vorob'eva et al., 2009b; Vorob'eva et al., 2009a). However, the taxonomic identification of the Ura Formation specimens has been questioned (Chumakov et al., 2013; Sergeev et al., 2011), and the lower Vychegda Formation may be Tonian in depositional age (Vorob’eva et al., 2009b). Thus, there are no reliable Ediacaran occurrences of *T. aimika*.

Occurrences: *Trachyhystrichosphaera aimika* is widely distributed in uppermost Mesoproterozoic and Tonian successions around the world (see summary in Tang et al., 2013).

Genus *Valeria* Jankauskas, 1982, emended Nagovitsin, 2009

Type species: *Valeria lophostriata* (Jankauskas, 1979) Jankauskas, 1982.

1995 *Thecatovalvia* Yan, p. 364, 369.

Valeria lophostriata (Jankauskas, 1979) Jankauskas, 1982

Figure 11

1993 *Thecatovalvia annulata* Yan *in* Yan and Liu, pl. II, fig. 3. (nomen nudum)

1993 *Valvimorpha annulata* Yan *in* Yan and Liu, pl. III, fig. 8. (nomen nudum)

1994 *Valeria lophostriata* Jankauskas; Hofmann and Jackson, p. 24, figs. 17.14–17.15, 19.4; and synonyms therein.

1995 *Thecatovalvia annulata* Yan, p. 364, 369, pl. II, fig. 15.

1995 *Valvimorpha annulata* Yan, p. 365, pl. I, fig. 17, pl. II, figs. 1, 2.

1995 *Valeria lophostriata* Jankauskas; Zang, p. 170, fig. 28I.

1997 *Valeria lophostriata* Jankauskas; Xiao et al., p. 206, figs. 3d, 3e.

1997 *Valeria lophostriata* Jankauskas; Samuelsson, p. 181–182, figs. 10B–C.

1999 *Valeria lophostriata* Jankauskas; Samuelsson et al., fig. 8e.

2009 Ovoidal acritarch; Peng et al., figs. 4G–I.

2014 *Valeria lophostriata* Jankauskas; Xiao et al., 2014a, p. 217, fig. 6D–H.

2015 *Valeria lophostriata* Jankauskas; Pang et al., figs. 3, 6C–E.

Material: Nine well-preserved specimens and numerous fragments isolated from samples 11-GH-8 and 11-GH-10.

Description: Flattened spheroids with evenly spaced concentric striations on the interior surface of vesicle wall. Vesicle diameter 106–216 μm (average = 167; n = 9). Striations about 0.5–1.0 μm in width and 0.2–0.4 μm in spacing.

Remarks: *Valeria lophostriata* is characterized by its distinctive parallel, concentric striations (Pang et al., 2015). Combined light-electron microscopic analysis shows the concentric striations appear to be present on the interior surface of the vesicle wall (Fig. 3.10B; Javaux et al., 2004; Pang et al., 2015). *Valvimorpha annulata* and *Thecatovalvia annulata* from the late Paleoproterozoic Chuanlinggou Formation in North China Craton are characterized by medially split half-vesicles ornamented with concentric striations about 1–2 μm in width. These two species are considered as junior synonyms of *Valeria lophostriata*. Additionally, ovoidal acritarchs with parallel ridges on the interior vesicle surface described in Peng et al. (2009) are also assigned to *V. lophostriata*.

Occurrences: *Valeria lophostriata* is known from Paleoproterozoic to Neoproterozoic at more than 30 localities throughout the world (Hofmann and Jackson, 1994; Hofmann, 1999; Javaux, 2011).

Incertae Sedis

Unnamed form

Figure 3.19B–D

Material: Three specimens revealed from shale sample 11-GH-10.

Description: Unbranched, club-shaped tubular fossil with a shagreen surface and a gradually expanded end. Preserved tubes 140–308 μm in length (average = 203 μm; n = 3), 30–

33 μm in maximum width at expanded apex (average = 32 μm; n = 3), and 15–24 μm in minimum width (average = 19 μm; n = 3). Septa absent.

Remarks: The specimens from the Gouhou Formation can be distinguished from superficially similar Proterozoic forms such as *Clavitrichoides rugosus* Mikhailova *in* Jankauskas et al., 1989, *Caudosphaera expansa* Herman and Timofeev *in* Jankauskas et al., 1989, and *Germinosphaera bispinosa* Mikhailova, 1986. These forms have been interpreted by Butterfield (2004, 2005) as organ elements of *Jacutianema solubila* Timofeev and Hermann, 1979 and *Cheilofilum hysteriopsis* Butterfield, 2005. They are characterized by a tubular filament attached to a spherical vesicle, with an abrupt transition between the filament and the vesicle. Thus, they are different from the gradually expanded termination of the tubular fossils from the Gouhou Formation. In addition, the tubular filaments of *Germinosphaera bispinosa* are very thin (only 2.5–3.5 μm wide according to Butterfield et al., 1994) whereas those of *Caudosphaera expansa* are relatively wide (80–300 μm in basal width, gradually narrowed to 20–100 μm distally, according to Jankauskas et al., 1989), although those of *Clavitrichoides rugosus* are comparable in diameter to the Gouhou specimens (Jankauskas et al., 1989).

Several other Proterozoic fossils resemble the Gouhou specimens in having a tubular morphology with a club-shaped or clavate termination. These include *Lakhandina prolata* Timofeev and Hermann, 1979, *Palaeovaucheria clavata* Hermann, 1981, *Proterocladus hermannae* Butterfield *in* Butterfield et al., 1994, and *Aimonema ramosa* Hermann *in* Hermann and Podkovyrov, 2010. Of these taxa, *Lakhandina prolata* from the Lakhanda Group of Siberia has a tomaculate shape, with a much broader width of 300–1000 μm and a length:width ratio of 3:1 to 5:1 (Jankauskas et al., 1989; German and Podkovyrov, 2011). Filaments of *Palaeovaucheria clavata* from the Lakhanda Group have a diameter comparable to that of the

Gouhou fossils, but they sometimes branch and occasionally bear transverse septa (Hermann, 1990; Hermann and Podkovyrov, 2006). Filaments of *Aimonema ramosa* from the Lakhanda Group also have a comparable diameter (mostly 30–50 μm), but they can form networks similar to trapping loops of modern nematophagus fungi (Hermann and Podkovyrov, 2010). *Proterocladus hermannae* from the Tonian Svanbergfjellet Formation in Svalbard can also have a clavate termination (e.g., fig. 7G of Butterfield et al., 1994), but its filaments are relatively thin (7–14 μm) compared to the Gouhou specimens. Therefore, considering the filament size and shape, it is possible that the Gouhou specimens could represent fragments of *Palaeovaucheria clavata* or *Aimonema ramose*, but this possibility is difficult to verify before the discovery of the complete suite of morphologies characteristic of these Siberian forms. Thus, the Gouhou specimens are at present placed in an unnamed taxon.

3.9 Acknowledgements

This work was supported by National Natural Science Foundation of China (41272011 and 41130209), Chinese Ministry of Science and Technology (2013CB835000), Chinese Academy of Sciences (KZZD-EW-02 and KZCX2-YW-153), U.S. National Science Foundation (EAR-1250800), and American Association of Stratigraphic Palynologists. We thank Zhiji Ou and Lei Chen for field work assistance, Fengbao Huang and Jinlong Wang for sample preparation, Yongqiang Mao for electron microscopy, Leiming Yin and Chuanming Zhou for taxonomic discussion, and Leigh Anne Riedman and an anonymous reviewer for constructive comments.

3.10 Figures and figure captions

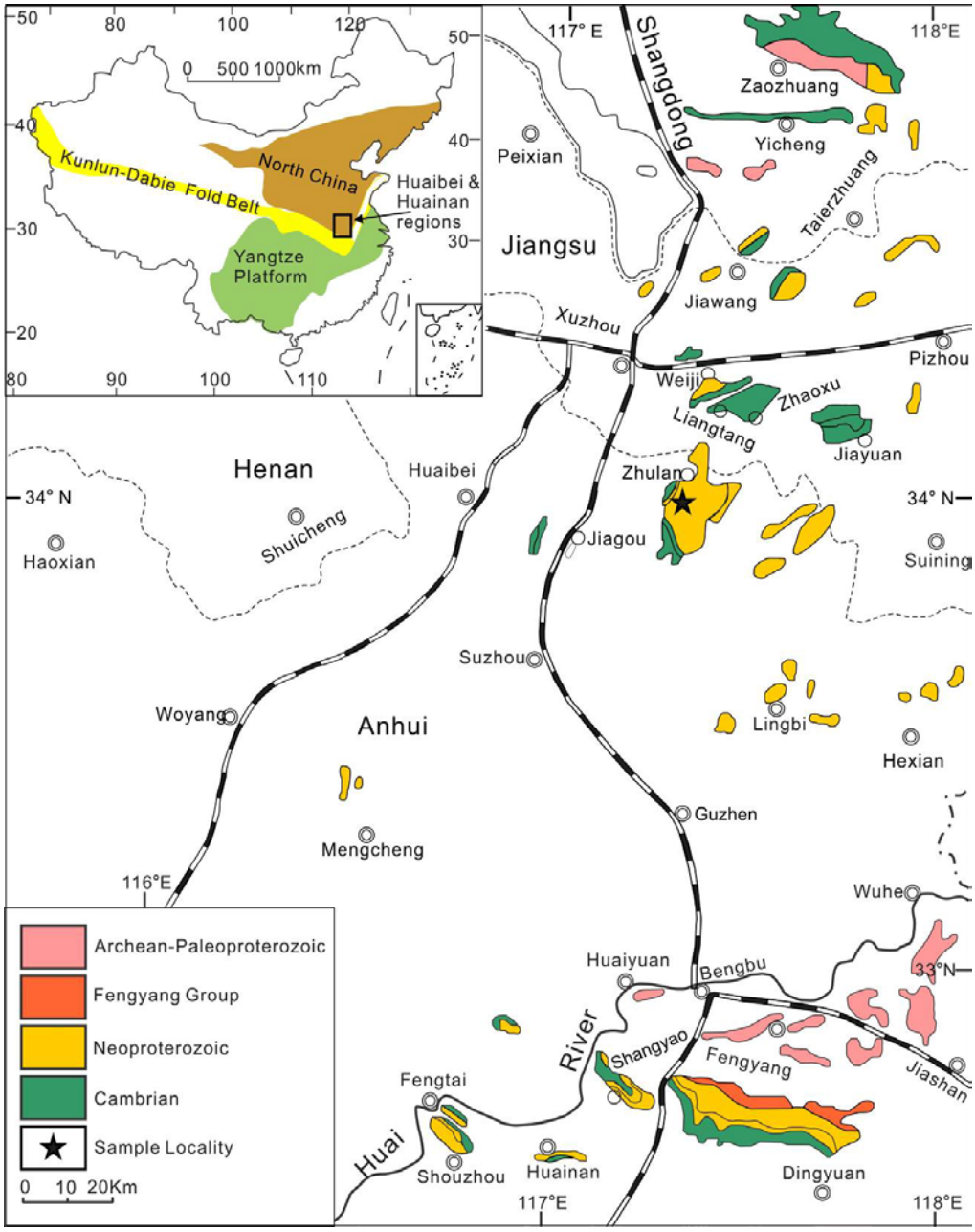

Fig. 3. 1. Geological map of the Huainan and Huaibei regions in North China, modified from Li et al. (2013). Huainan and Huaibei refer to regions to the south and north of the Huai River, respectively. Star denotes sample locality at the Langan section. White box in inset map shows the location of the Huainan and Huaibei regions in the North China Craton.

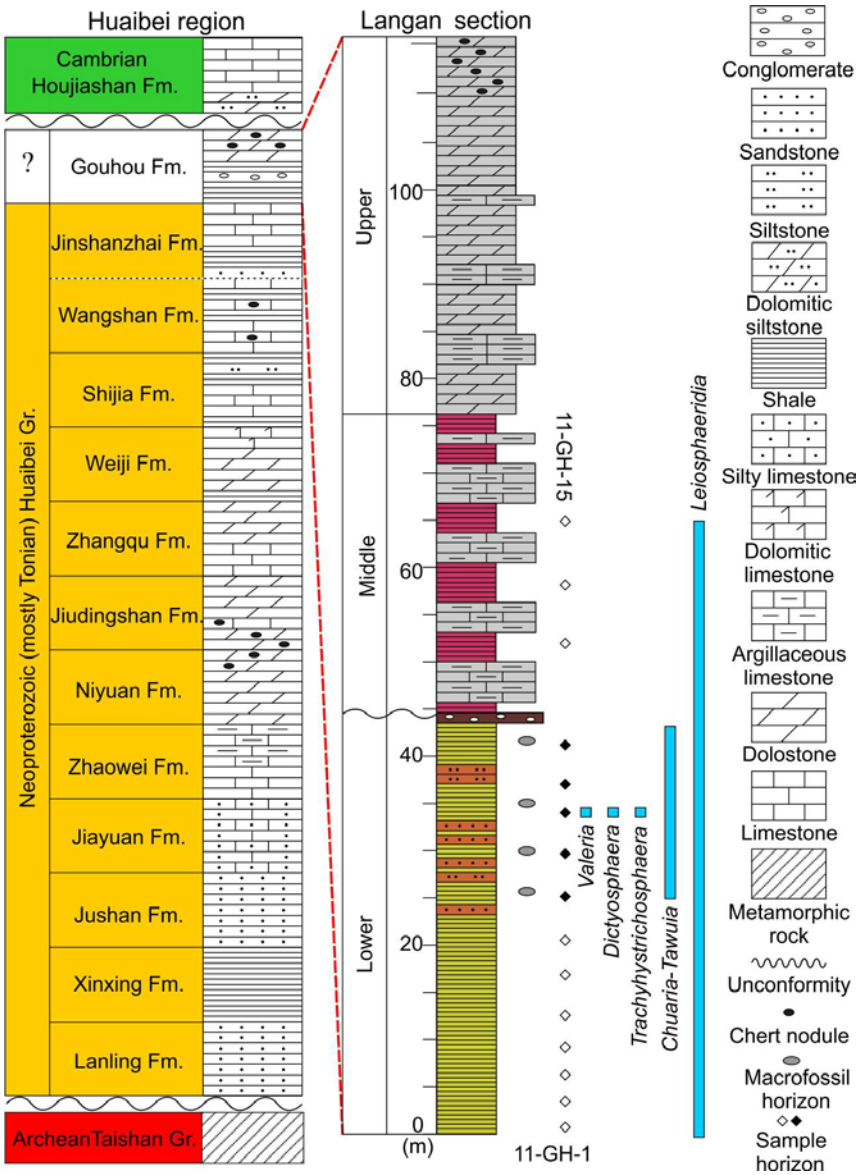

Fig. 3. 2. Generalized stratigraphic column of the Proterozoic succession in the Huaibei region, with an expansion of the Gouhou Formation as measured at the Langan section to show sampling horizons (empty and filled diamonds). All samples were productive, and five of them are richly productive (filled diamonds). Samples with the prefix of "11-GH-" were collected for HF maceration, and they are marked against the stratigraphic column. Samples with the prefix of "13-GH-T1-" are hand samples for macrofossil analysis, and they were collected approximately from the stratigraphic horizons of 11-GH-8 to 11-GH-12. Gr.: Group; Fm., Formation.

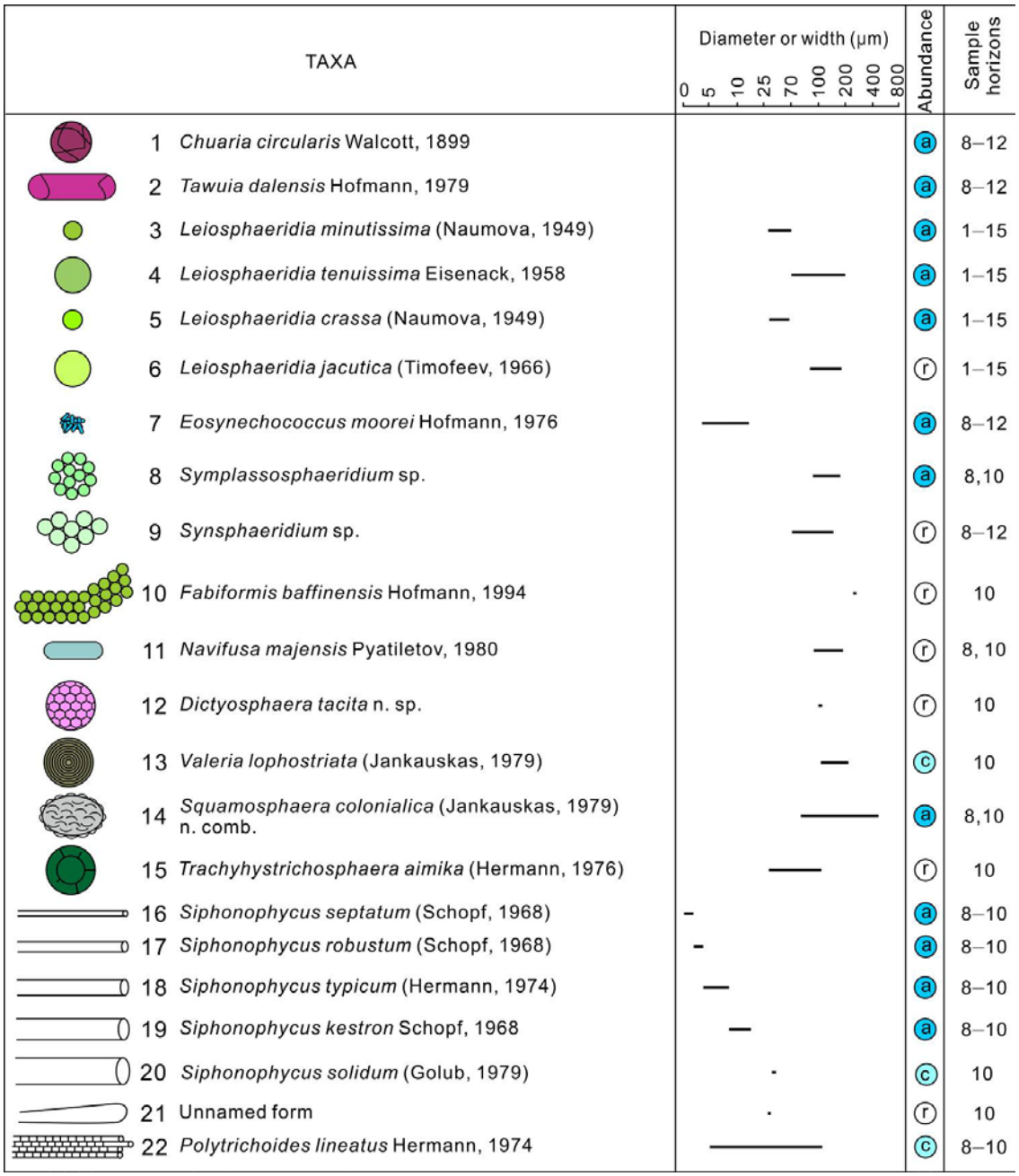

Fig. 3. 3. List of organic-walled microfossils, as well as millimeter-sized carbonaceous compressions such as *Chuaria circularis* and *Tawuia delensis*, from the Gouhou Formation. In the abundance column, circled letters “a”, “c”, and “r” denote abundant, common, and rare, respectively. In the column of “sample horizons”, numbers denote samples (with prefix “11-GH-” omitted) where fossil taxa have been found. See Fig. 2 for stratigraphic horizons of samples.

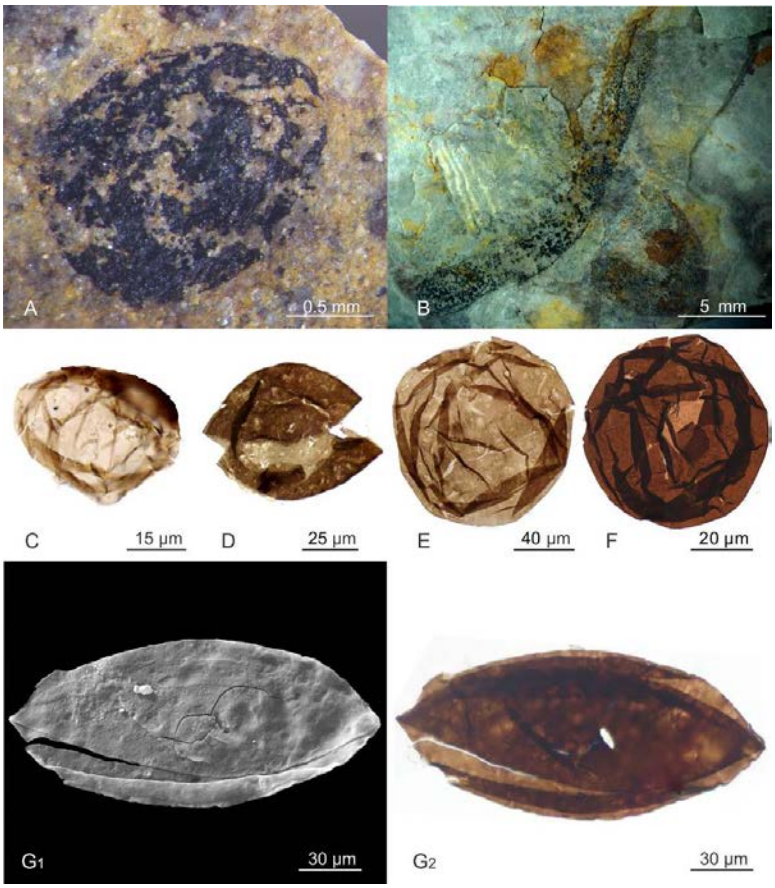

Fig. 3. 4. *Chuaria circularis*, *Tawuia dalensis*, and *Leiosphaeridia spp*. (A) *Chuaria circularis*, PB21840; 13-GH-T1-18-V1. (B*) Tawuia dalensis*, PB21841; 13-GH-T1-14-3. (C) *Leiosphaeridia minutissima*, PB21842; 11-GH-10-9-24 (N-13-1). (D) *Leiosphaeridia crassa*, PB21843; 11-GH-10-15-5b (C-56-2). (E) *Leiosphaeridia tenuissima*, PB21844; 11-GH-10-9-3 (E-64-4). (F and G) *Leiosphaeridia jacutica*, PB21845; 11-GH-10-S-3-15; and PB21846; 11-GH-10-S-5-14; respectively. (A–B) are reflected light micrographs and (G_1) is scanning electron microscopy (SEM) micrograph. All other fossil images in this and other figures are transmitted light micrographs unless otherwise noted. For each illustrated specimen in this and other figures, its NIGPAS museum catalog number (prefix PB), specimen or slide number (prefix 13-GH-T1- for hand specimens, prefix 11-GH-#-S- for SEM specimens, and prefix 11-GH- for slides), and, wherever appropriate, England finder coordinates (in parentheses) are given.

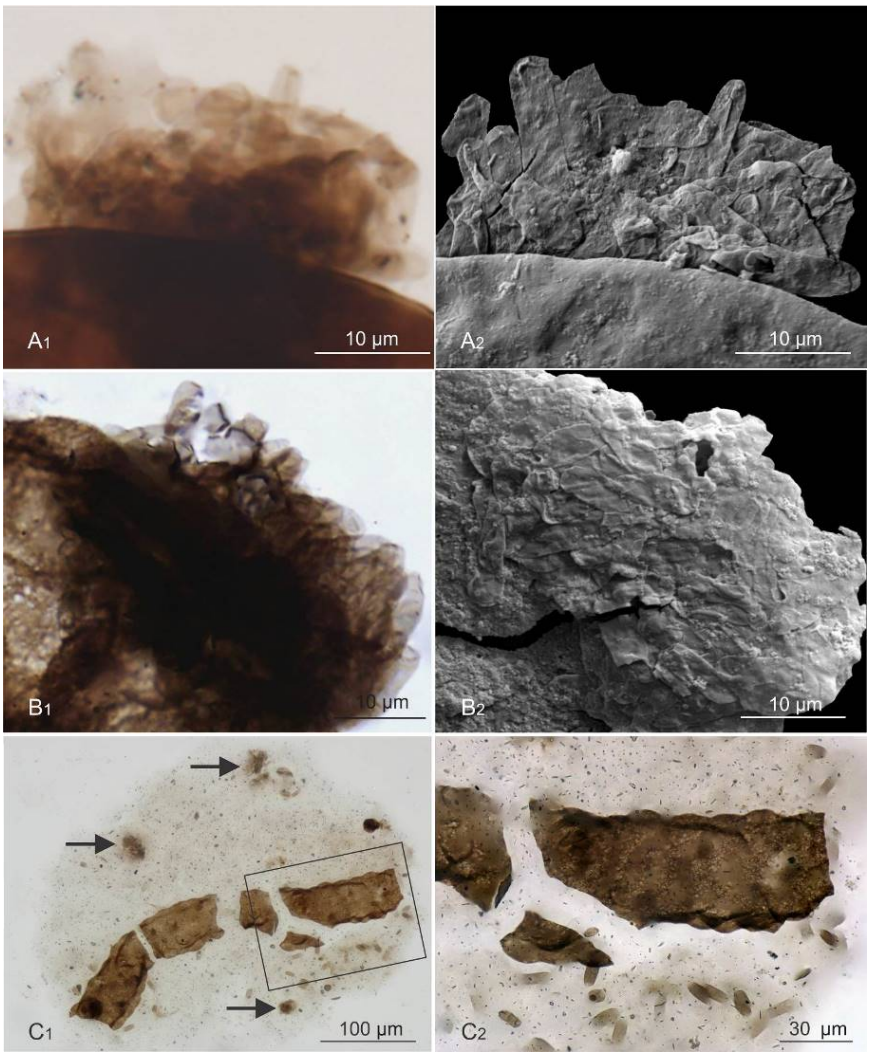

Fig. 3. 5. Clustered or dispersed bacilloids of *Eosynechococcus moorei*. (A) A cluster of *Eosynechococcus moorei* superimposed on a specimen of *Leiosphaeridia jacutica*, PB21847; 11-GH-10-S-5-15. (A_2) SEM micrograph. (B) A cluster of *Eosynechococcus moorei* superimposed on a specimen of *Squamosphaera colonialica* (Jankauskas, 1979) n. comb. PB21848; 11-GH-10-S-2-9. (B_2) SEM micrograph. (C) Clustered and dispersed bacilloids of *Eosynechococcus moorei* randomly distributed in an incompletely dissolved rock fragment, preserved along with a fragment of *Squamosphaera colonialica* (Jankauskas, 1979) n. comb. Arrows in C_1 denote clusters of *E. moorei*. PB21849; 11-GH-10-1-10 (S-20-3). (C_2) Magnification of box area in C_1, with arrows denoting dispersed cells of *E. moorei*.

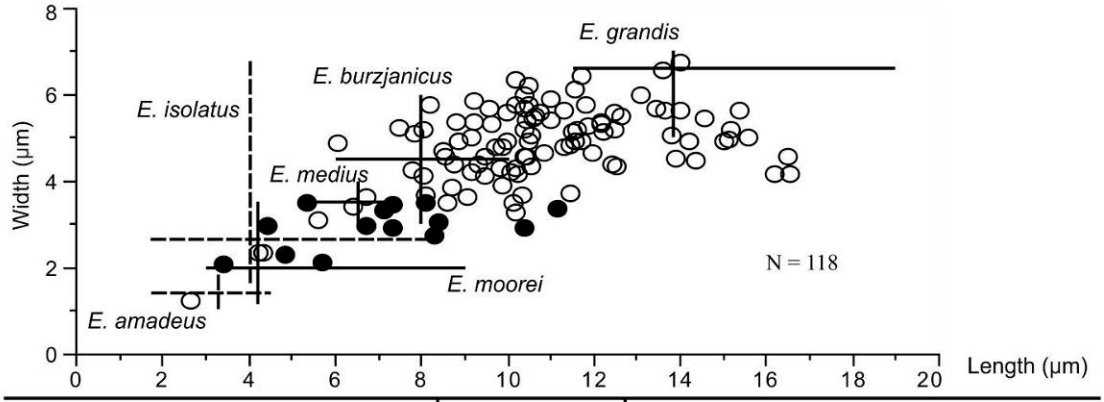

species name	length (μm)	width (μm)	average (μm)		average l/w ratio	measured specimen number	reference
			length	width			
E. amadeus	1.85–4.53	0.96–1.88	3.2	1.4	2.3	132	1
E. isolatus	1.7–8.5	1.7–6.8	4.07	2.7	1.5	91	2
E. moorei	3–9	1.2–3.5	4.2	2	2.1	21	3
E. medius	5.5–7.5	1.2–3.5	6.5	3.5	1.9	3	3
E. burzjanicus	No data	No data	6–10	3–6	No data	50	4
E. grandis	11.5–19	5–7	13.9	6.6	2.1	6	3
E. moorei	2.7–16.5	1.2–6.8	10.4	4.7	2.2	118	this study

Fig. 3. 6. Size distribution of *Eosynechococcus moorei* cells from the Gouhou Formation. Crosses denote the mean and range of previously published *Eosynechococcus* species. Numbers in the reference column denote sources of published data: 1 (Knoll and Golubic, 1979); 2 (McMenamin et al., 1983); 3 (Hofmann, 1976); 4 (Jankauskas et al., 1989). Empty and solid circles represent data from this study. Solid circles represent measurements from a single cluster illustrated in Fig. 5B, showing a wide range of cell size and L/W ratio in this cluster.

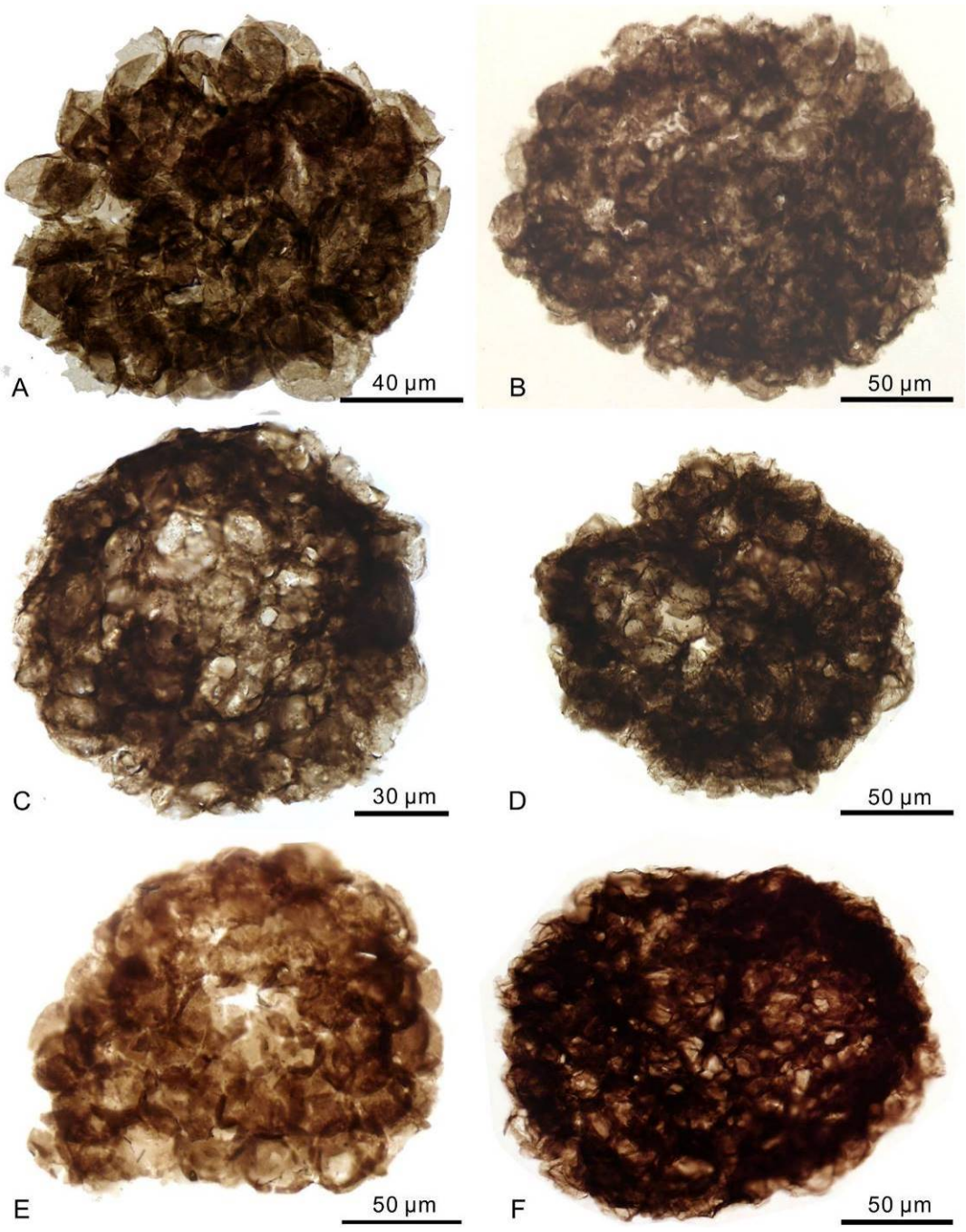

Fig. 3. 7. *Symplassosphaeridium* sp. (A) PB21850; 11-GH-10-2-2 (L-23-1). (B) PB21851; 11-GH-10-S-2-3. (C) PB21852; 11-GH-10-4-4 (C-59-1). (D) PB21853; 11-GH-10-5-19 (D-22-4). (E) PB21854; 11-GH-10-7-6 (Q-64-4). (F) PB21855; 11-GH-10-6-23 (W-25-2).

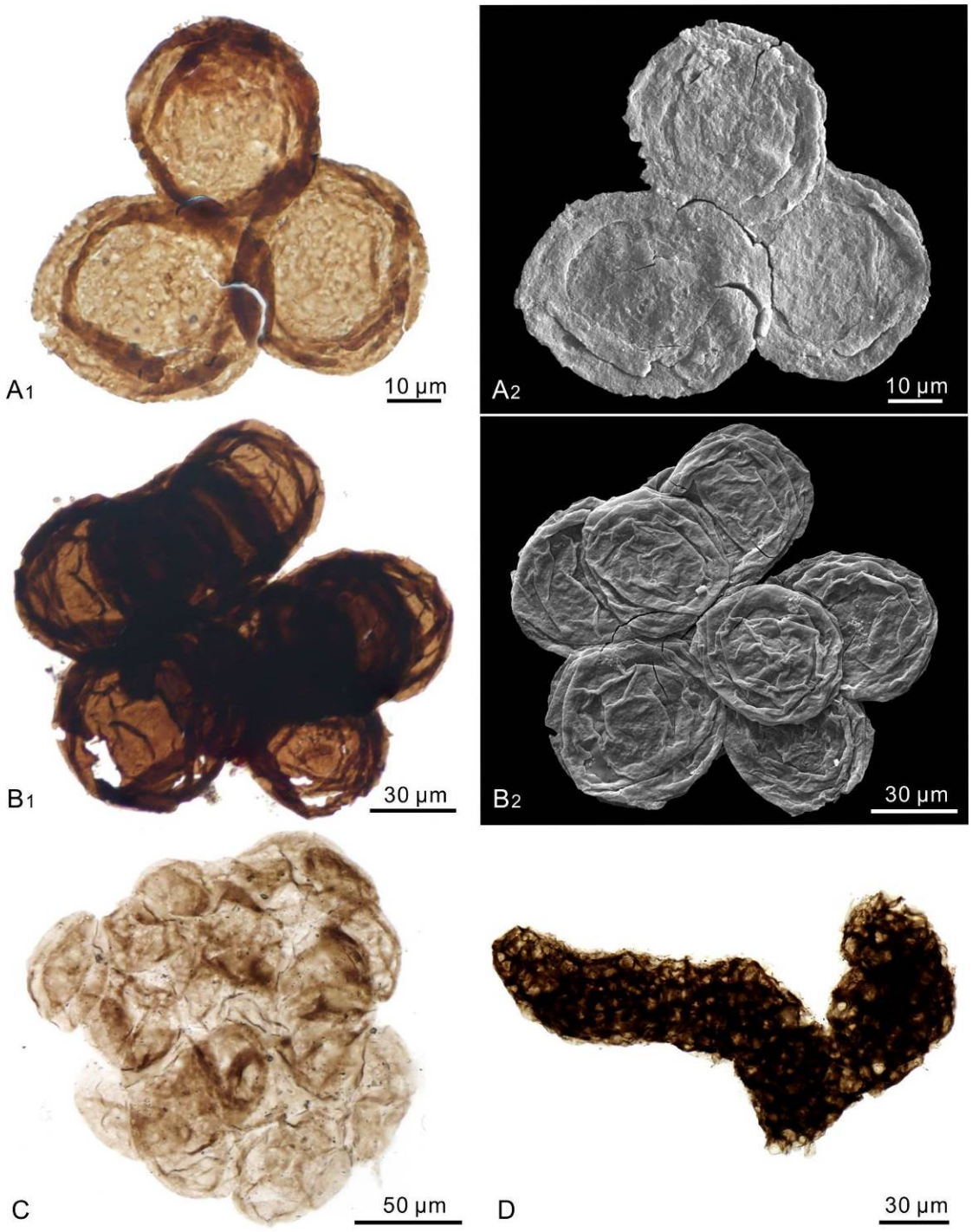

Fig. 3. 8. *Synsphaeridium* sp. (A–C) and *Fabiformis baffinensis* (D). (A) PB21856; 11-GH-10-S-3-18. (A_2) SEM micrograph. (B) PB21857; 11-GH-10-S-5-7. (B_2) SEM micrograph. (C) PB21858; 11-GH-10-10-13 (O-38-4). (D) PB21859; 11-GH-10-2-4 (U-42-2).

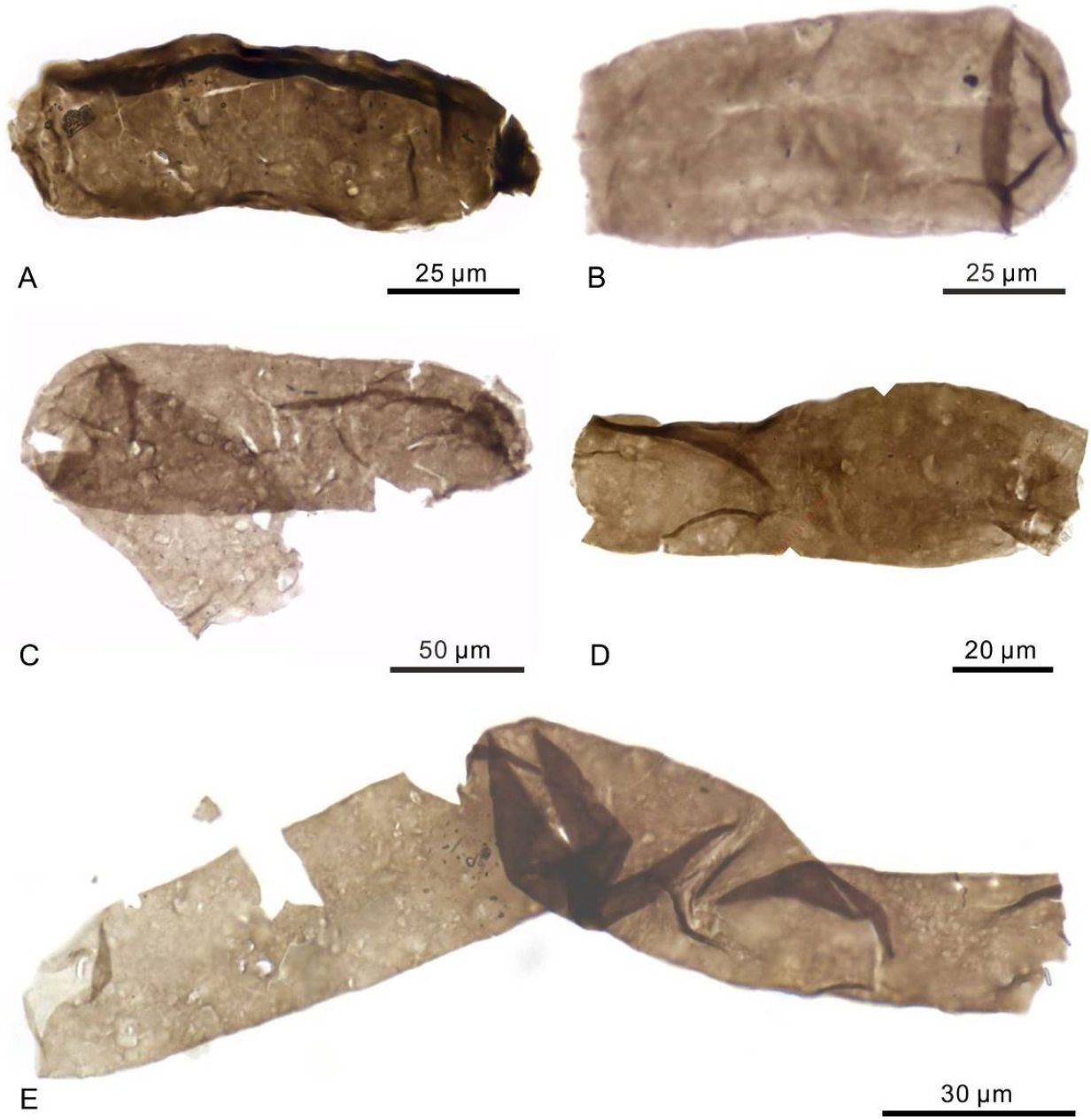

Fig. 3. 9. *Navifusa majensis* (A–C, D?, E?). (A) PB21860; 11-GH-8-3-1. (B) PB21861; 11-GH-8-3-10. (C) PB21862; 11-GH-8-3-7. (D) Because it is uncertain whether this specimen has a closed termination due to incomplete preservation, this specimen could be alternatively identified as *Siphonophycus solidum*. PB21863; 11-GH-8-3-8. (E) Because it is uncertain whether this specimen has a closed termination due to incomplete preservation, this specimen could be alternatively identified as *Siphonophycus solidum*. PB21864; 11-GH-10-17-8 (V-53-2).

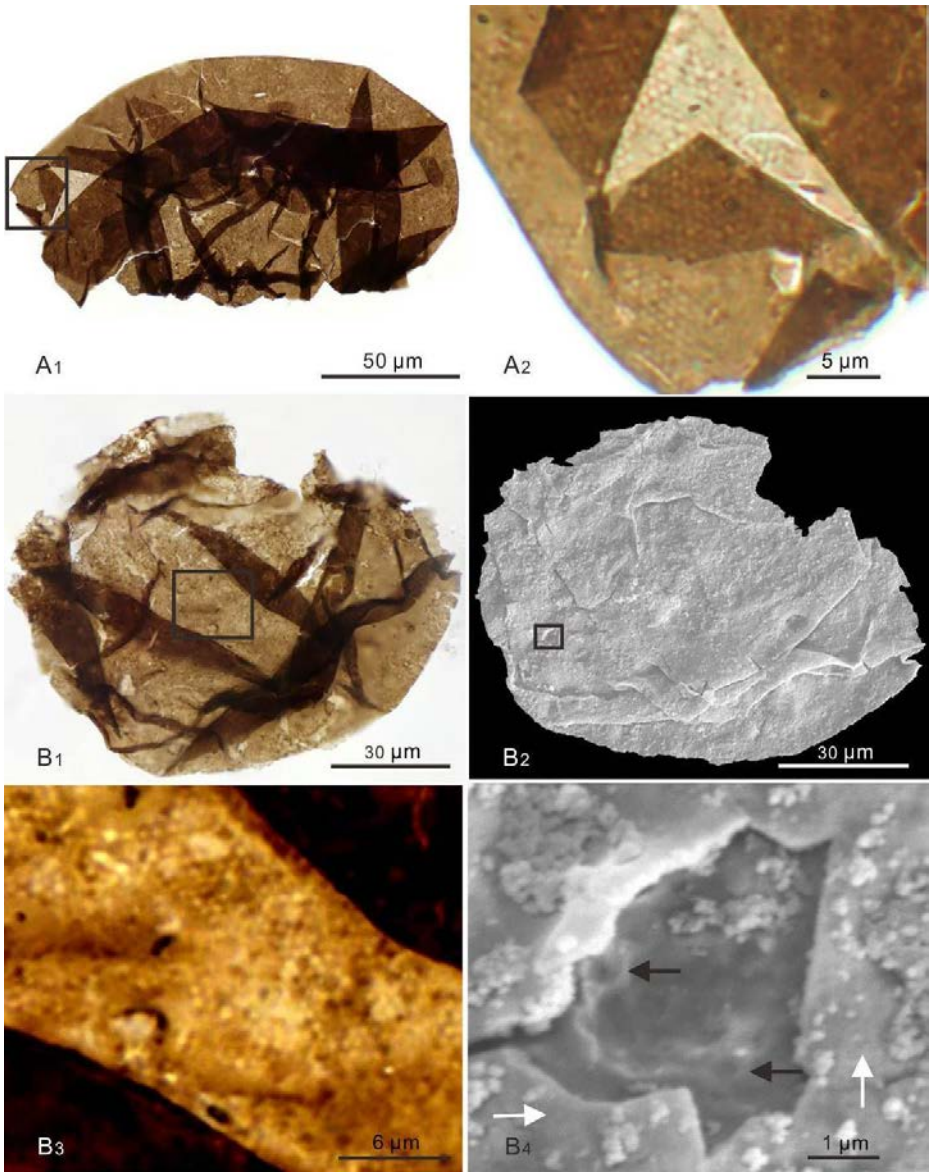

Fig. 3. 10. *Dictyosphaera tacita* n. sp. (A) Holotype, PB21865; 11-GH-10-6-8 (U-62-4). (A_2) Magnification of box area in A_1, showing polygonal structures on vesicle wall. (B) PB21866; 11-GH-10-S-3-3. (B_2) SEM micrograph. (B_3) Magnification of box area in B_1, showing polygonal structures on vesicle wall. (B_4) Magnification of box area in B_2. Black arrows denote possible polygonal structures (~0.5 µm in size) on interior vesicle surface, and white arrows denote apparently smooth exterior surface of vesicle wall. (A_1–A_2 and B_1–B_2) were also illustrated in Xiao et al. (2014a).

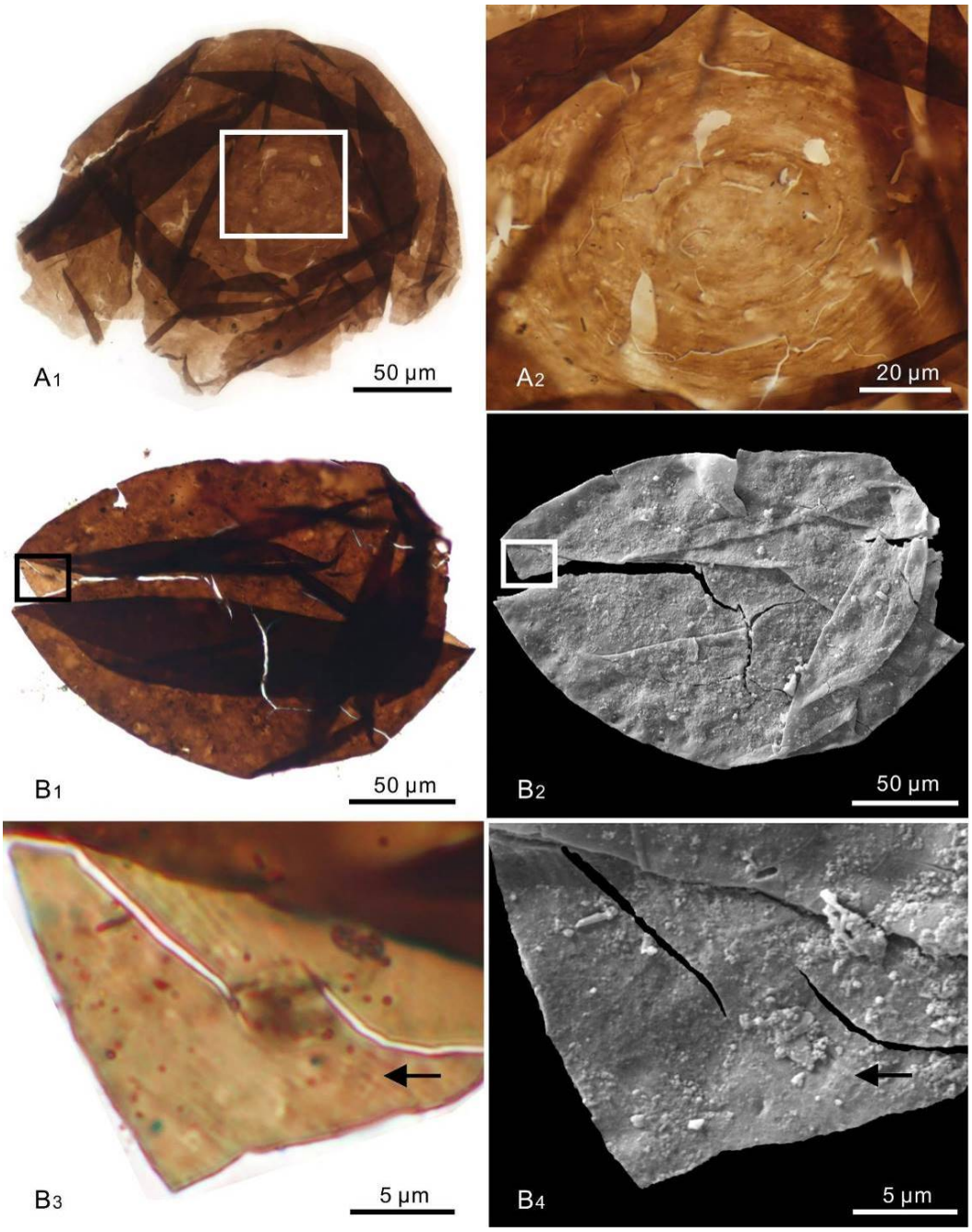

Fig. 3. 11. *Valeria lophostriata*. (A) PB21867; 11-GH-11-2-2 (O-5-3). (A_2) Magnification of box area in A_1, showing concentric striations on vesicle wall. (B) PB21868; 11-GH-10-S-5-5. (B_2) SEM micrograph. (B_3–B_4) Magnifications of box areas in B_1 and B_2, respectively, showing parallel, evenly spaced, concentric striations on interior surface of vesicle wall (arrows). (A_2) was also illustrated in Xiao et al. (2014a).

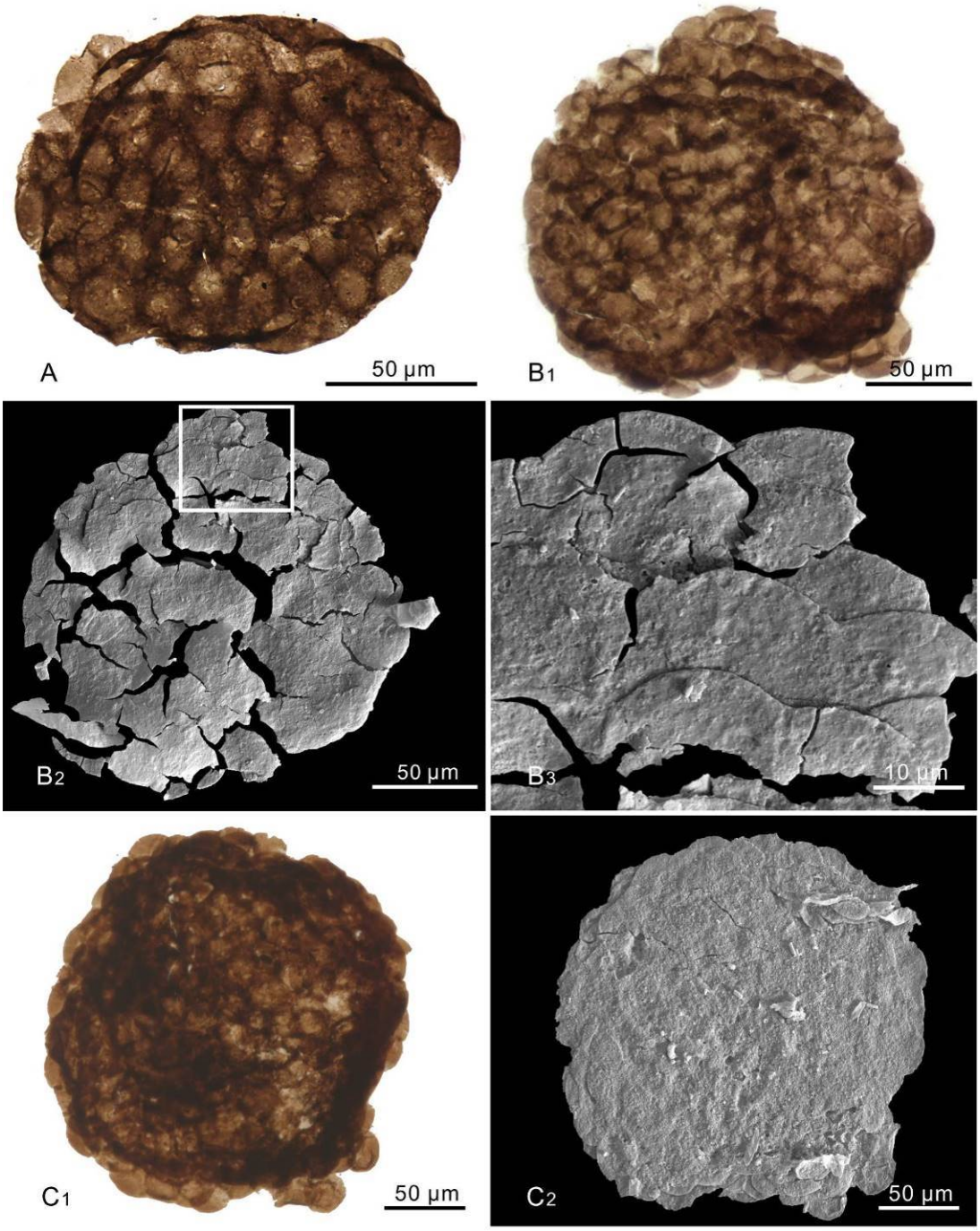

Fig. 3. 12. *Squamosphaera colonialica* (Jankauskas, 1979) n. comb., emended. (A) PB21869; 11-GH-10-2-5. (B) PB21870; 11-GH-10-S-2-1. (B_2) SEM micrograph. (B_3) Magnification of box area in B_2, showing obtusely domical processes compressed on vesicle wall. (C) PB21871; 11-GH-10-S-5-12. (C_2) SEM micrograph.

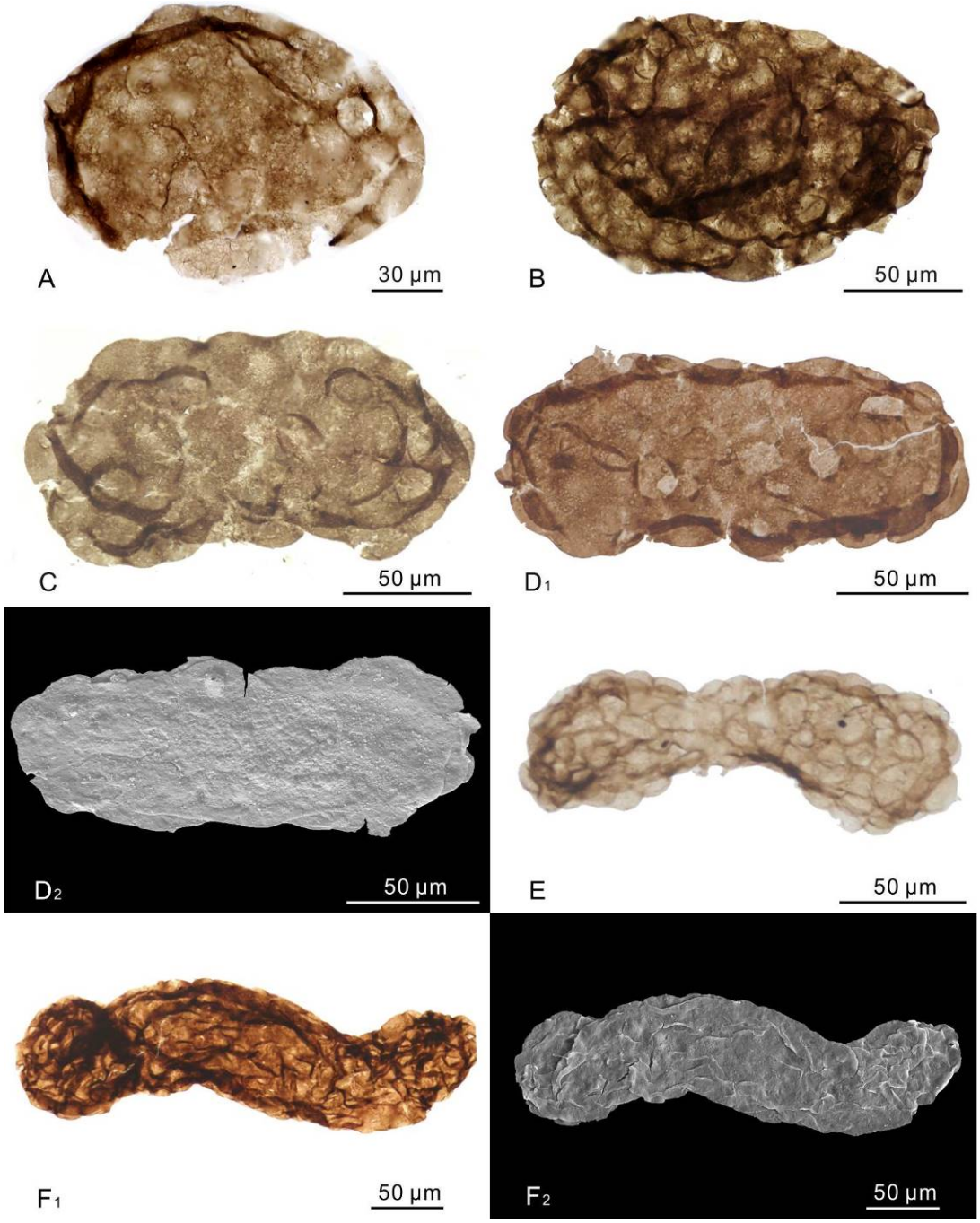

Fig. 3. 13. *Squamosphaera tholus* n. gen. and n. sp. (A) Specimen 11-GH-10-5-6. (B) Specimen 11-GH-10-19-3. (C) Specimen 11-GH-10-3-13. (D) Specimen 11-GH-10-S-5-16. (D_2) SEM micrograph. (E) Specimen 11-GH-10-S-5-21. (F) Specimen 11-GH-10-S-4-1. (F_2) SEM micrograph.

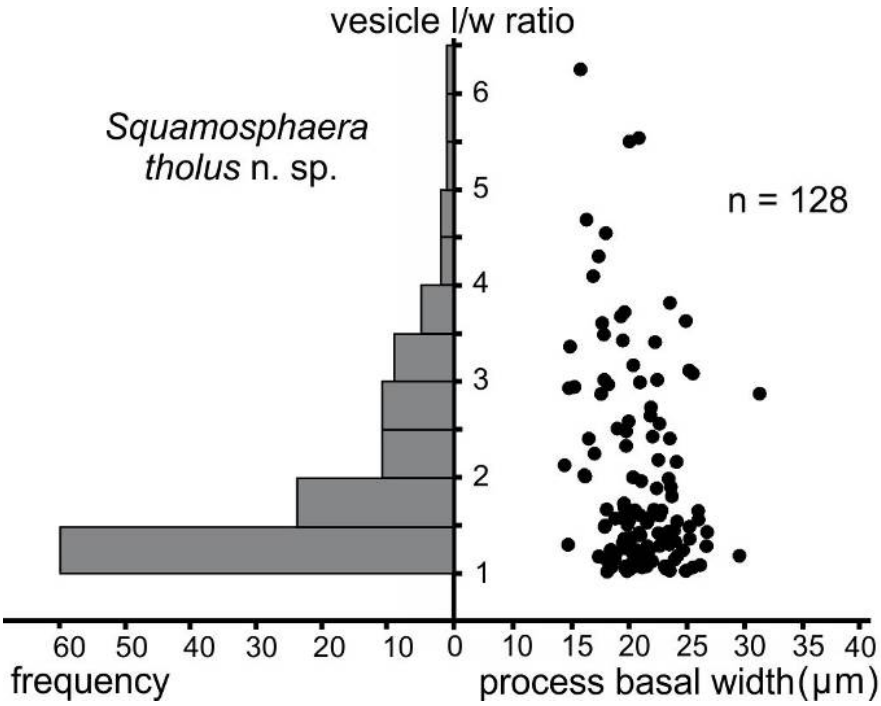

Fig. 3. 14. Cross-plot of process basal width vs. vesicle length/width ratio, and the frequency distribution of vesicle length/width ratios of *Squamosphaera colonialica* (Jankauskas, 1979) n. comb., emended.

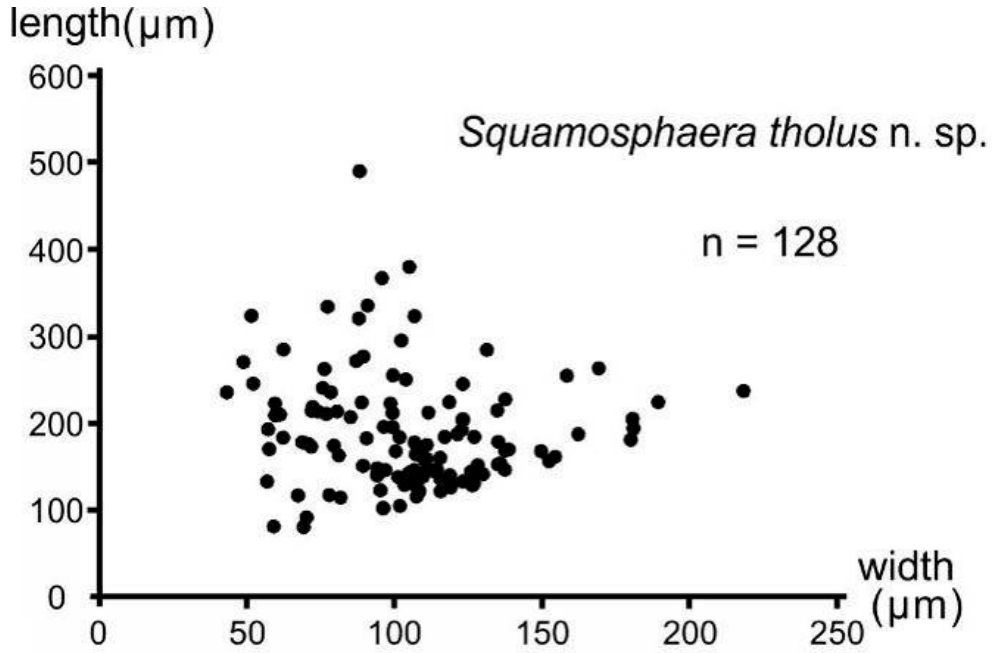

Fig. 3. 15. Cross-plot of vesicle width vs. length of *Squamosphaera colonialica* (Jankauskas, 1979) n. comb., emended.

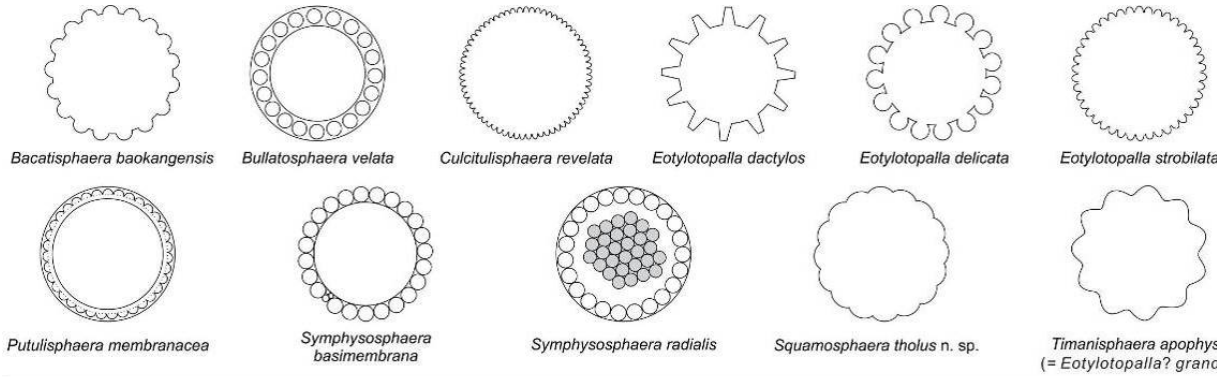

species name	vesicle shape	vesicle size (μm)	ornamentation				ornamentation size/diameter		reference
			type	morphology	density	contact at base	length (μm)	width at base (μm)	
B. baokangensis	spheroidal	150–600	process	hemispherical	moderate	No	10–30	20–50	1, 2, 3
B. velata	spheroidal	300–450	spheroid	spheroidal	dense	N/A	30–90		4
C. revelata	spheroidal	34.6–88.4	process	blister	dense	Yes	1.3–2.7		5
E. dactylos	spheroidal	35–200	process	cylindrical or digitate	moderate	No	6–30	5–22.5	1, 6, 7
E. delicata	spheroidal	28–100	process	bulbous	moderate	No	4.2–11	5–15	6, 7, 8, 9,10
E. strobilata	spheroidal	50–85	process	hemispherical	dense	Yes	2–8	2–8	4, 10, 11, 12
E.? grandis	spheroidal	~400	process	broadly conoidall	sparse	Yes	20–46	100–120	13
P. membranacea	spheroidal	>610	process	hemispherical	dense	Yes	15–22	25–32	7
S. basimembrana	spheroidal	87–155	spheroid	spheroidal	dense	N/A	12–24.5		6
S. radialis	spheroidal	60–130	spheroid	spheroidal	dense	N/A	8–20		14
S. tholus n. sp.	spheroidal to tomaculate	80–489 in length 43–219 in width	process	obtusely domical	moderate	Yes	1–8	10–33	this study
T. apophysa	spheroidal	265–450	process	broadly conoidal	moderate	Yes	50–90	70–110	15

Fig. 3. 16. Idealized sketches of *Squamosphaera* n. gen. and broadly similar taxa discussed in the text. Numbers in the reference column denote sources of information: 1 (Xiao et al., 2014b); 2 (Zhou et al., 2004); 3 (Liu and Yin, 2005); 4 (Vorob'eva et al., 2009b); 5 (Riedman and Porter, 2015); 6 (Liu et al., 2014); 7 (Zhang et al., 1998); 8 (Yin, 1987); 9 (Yin, 1999); 10 (Nagovitsin et al., 2004); 11 (Sergeev et al., 2011); 12 (Faizullin, 1998); 13 (Tang et al., 2013); 14 (Yin, 1992); 15 (Vorob'eva et al., 2009b).

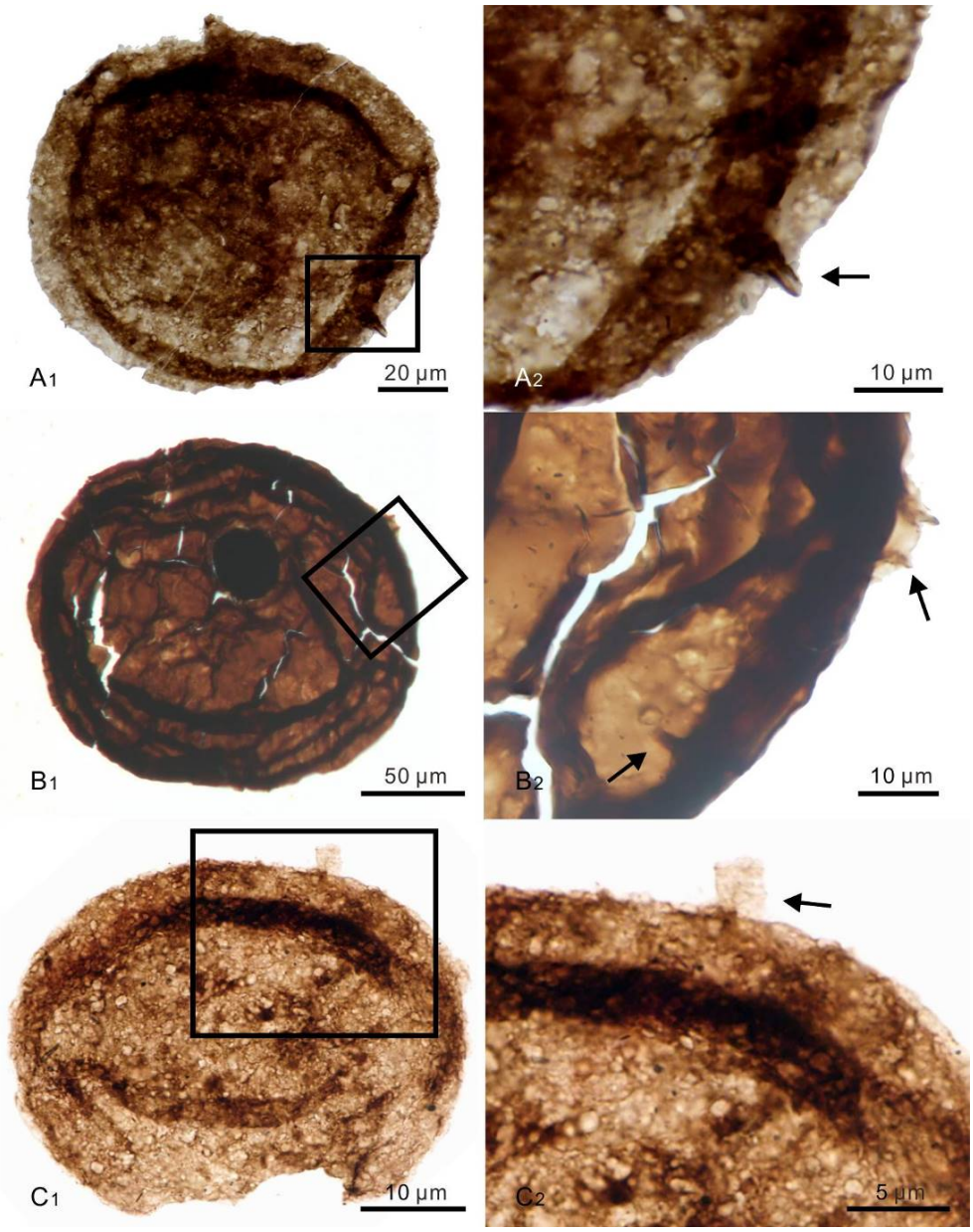

Fig. 3. 17. *Trachyhystrichosphaera aimika*. (A) PB21878; 11-GH-10-6-19 (T-28-4). (A_2) Magnification of box area in A_1, showing an apparently broken process (arrow). (B) PB21879; 11-GH-10-25-6 (G-17-2). Note dark central body. (B_2) Magnification of box area in B_1, showing tubular processes at arrows and remnant outer membrane at arrow to the right. (C) PB21880; 11-GH-10-S-3-1. Arrows denote processes. (C_2) SEM micrograph. (A_1) was also illustrated in Xiao et al. (2014a).

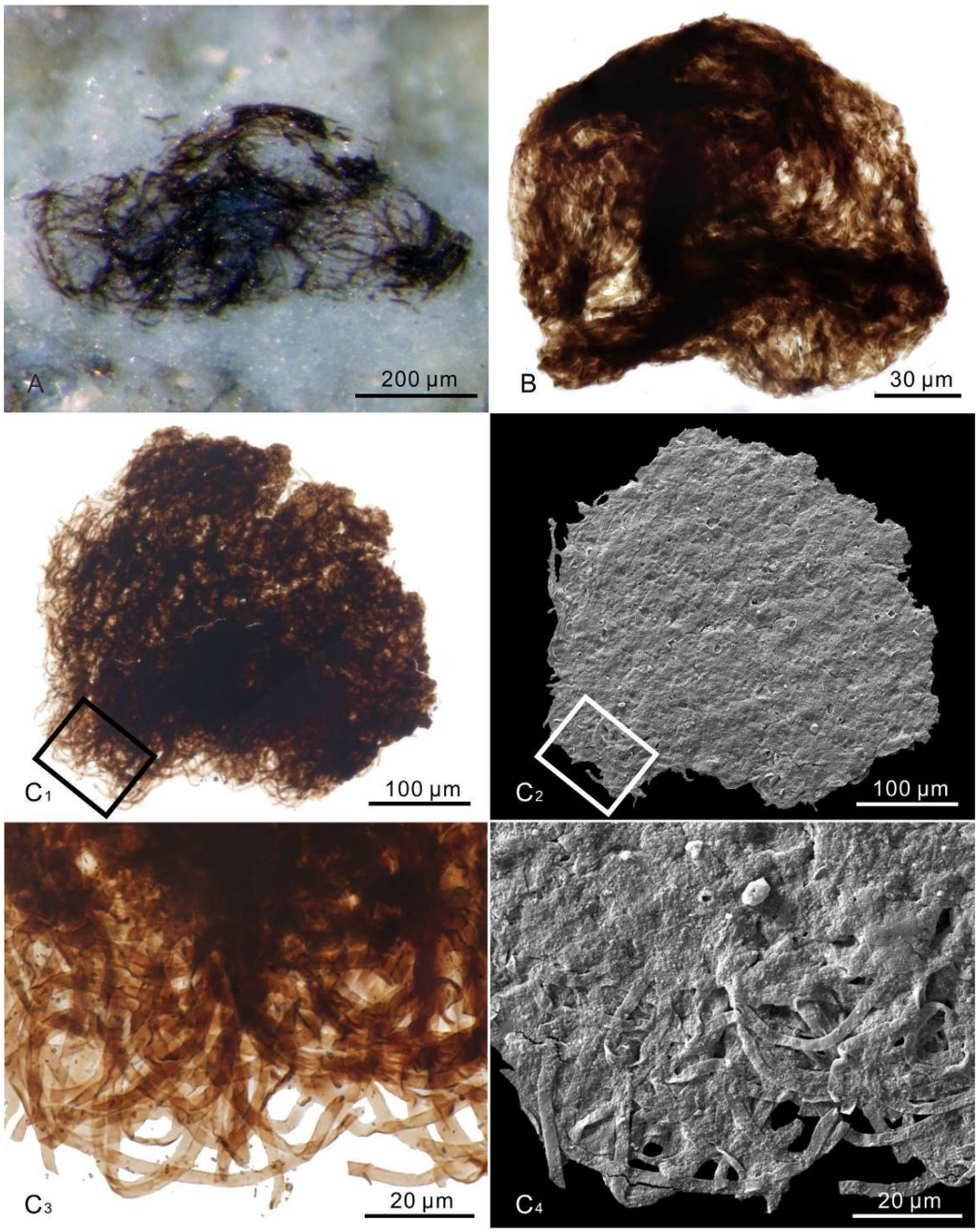

Fig. 3. 18. Fragments of microbial mats consisting of filamentous microfossils of *Siphonophycus* spp. (A) Bedding surface view of a hand sample, PB21881; 13-GH-T1-8-3. (B) *Siphonophycus septatum*, PB21882; 11-GH-10-8-26 (N-8-2). (C) *Siphonophycus robustum*, PB21883; 11-GH-10-S-5-8. (C_2) SEM micrograph. (C_3 and C_4) Magnifications of box areas in C_1 and C_2, respectively.

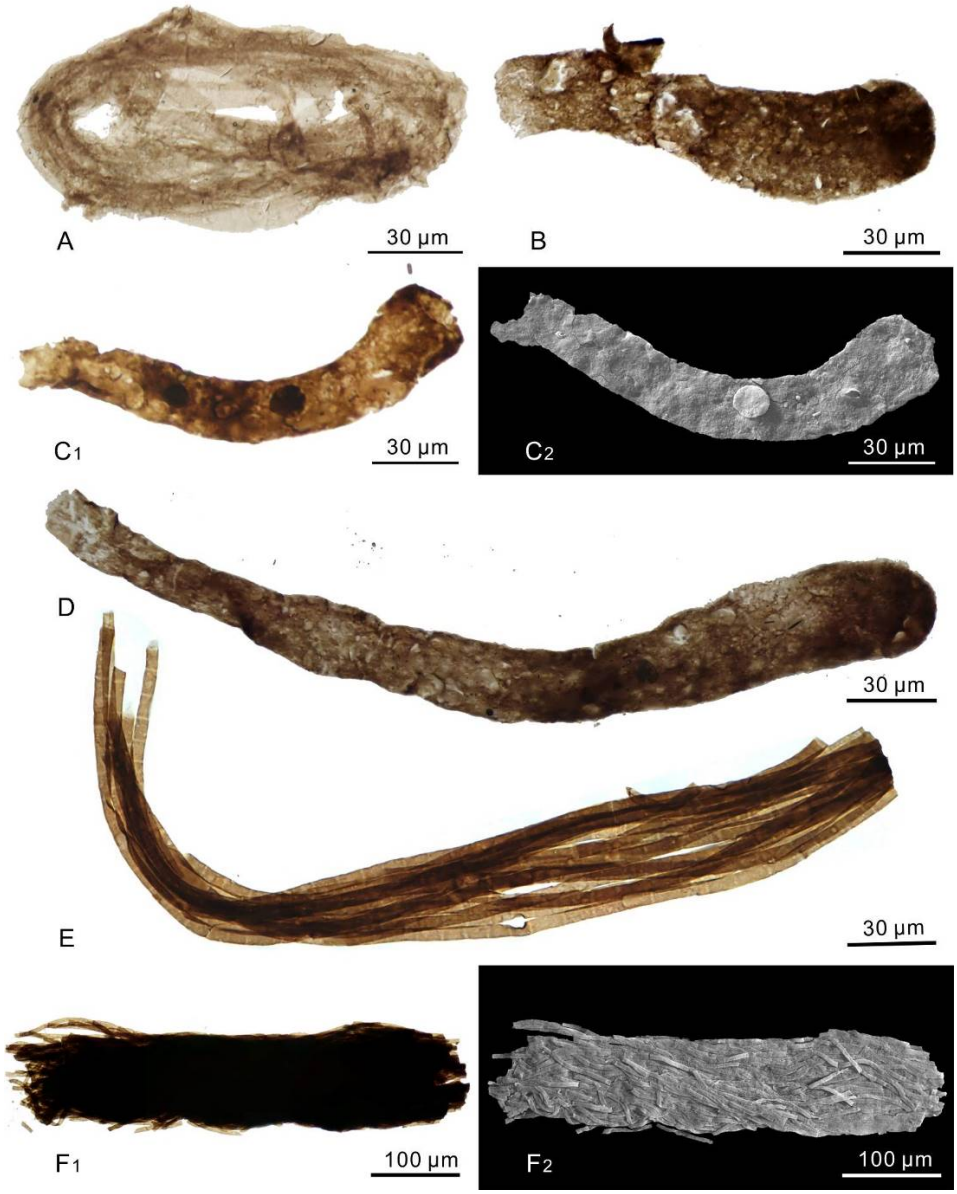

Fig. 3. 19. Filamentous microfossils of *Siphonophycus kestron* (A), unnamed form (B–D), and *Polytrichoides lineatus* (E–F). (A) PB21884; 11-GH-10-9-16 (J-31-2). Specimens similar to this have been illustrated as *Glomovertella eniseica* (Hermann *in* Timofeev et al., 1976), for example in pl. 9, fig. 3 of Hermann and Podkovyrov (2008). (B) PB21885; 11-GH-10-12-9 (K-47-1). (C) PB21886; 11-GH-10-S-3-17. (C_2) SEM micrograph. (D) PB21887; 11-GH-10-3-12 (K-25-4). (E) PB21888; 11-GH-10-1-1 (B-63-3). Note transverse marks, probably representing impression of trichome cells. (F) PB21889; 11-GH-10-S-3-7. (F_2) SEM micrograph.

3.11 References

Agić, H., Moczydłowska, M., and Yin, L, 2015, Affinity, life cycle, and intracellular complexity of organic-walled microfossils from the Mesoproterozoic of Shanxi, China: Journal of Paleontology, v. 89, p. 28–50.

Butterfield, N.J., Knoll, A.H., and Swett, K., 1994, Paleobiology of the Neoproterozoic Svanbergfjellet Formation, Spitsbergen: Fossils and Strata, v. 34, p. 1–84.

Cao, R., 2000, Discussion on some problems in the Mesoproterozoic and Neoproterozoic stratigraphical study in China: Journal of Stratigraphy, v. 24, p. 247–254.

Cao, R., Zhao, W., and Xiao, G., 1985, Late Precambrian stromatolites from north Anhui Province: Memoir Nanjing Institute of Geology and Palaeontology, Academia Sinica, v. 21, p. 1–54.

Dong, L., Xiao, S., Shen, B., Yuan, X., Yan, X., and Peng, Y., 2008, Restudy of the worm-like carbonaceous compression fossils *Protoarenicola*, *Pararenicola*, and *Sinosabellidites* from early Neoproterozoic successions in North China: Palaeogeography, Palaeoclimatology, Palaeoecology, v. 258, p. 138–161.

Eisenack, A., 1955, Chitinozoans, Hystrichospharen and other microfossils from the Beyrihia-Kalk: Senckenbergiana lethaea, v. 36, p. 157–188.

Eisenack, A., 1958, *Tasmanites* Newton 1875 und *Leiosphaeridia* n. gen. aus Gattungen der Hystrichosphaeridea: Palaeontographica Abteilung A, v. 110, p. 1–19.

Eisenack, A., 1965, Die Mikrofauna der Ostseekalke. 1. Chitinozoen, Hystrichosphären: Neues Jahrbuch fuer Geologie und Palaeontologie. Abhandlungen, v. 123, p. 149–159.

Evitt, W.R., 1963, A discussion and proposals concerning fossil dinoflagellates, hystrichospheres, and acritarchs: Proceedings of the National Academy of Sciences of the United States of America, v. 49, p. 158–164; 298–302.

Faizullin, M.S., 1998, New data on Baikalian microfossils of the Patom Upland: Russian Geology and Geophysics, v. 39, p. 328–337

Golovenoc, V.K., and Belova, M.Y., 1984, Riphean microbiota in cherts of the Billyakh Group on the Anabar Uplift: Paleontological Journal, v. 1984, p. 23–32.

Golub, I.N., 1979, A new group of problematic microstructures in Vendian deposits of the Orshanka Basin (Russian Platform). *In* Sokolov, S.B., eds., Paleontologiya Dokembriya i Rannego Kembriya. Leningrad, Nauka, p. 147–155.

Grey, K., 2005, Ediacaran palynology of Australia: Memoirs of the Association of Australasian Palaeontologists, v. 31, p. 1–439.

He, T., Zhou, Y., Vermeesch, P., Rittner, M., Miao, L., Zhu, M., Carter, A., Pogge von Strandmann, P.A.E., and Shields, G.A., 2017, Measuring the 'Great Unconformity' on the North China Craton using new detrital zircon age data: Geological Society, London, Special Publications, v. 448, p. 145–159.

Hermann, T.N., 1974, Findings of mass accumulations of trichomes in the Riphean. *In* Timofeev, B.V., eds., Proterozoic and Paleozoic microfossils of the USSR. Moscow, Nauka, p. 6–10.

Hofmann, H.J., 1976, Precambrian Microflora, Belcher Islands, Canada: Significance and Systematics: Journal of Paleontology, v. 50, p. 1040–1073.

Hofmann, H.J., 1994, Proterozoic carbonaceous compressions ("metaphytes" and "worms"). *In* Bengtson, S., eds., Early Life on Earth. Columbia University Press, New York, p. 342–357.

Hofmann, H.J., 1999, Global distribution of the Proterozoic sphaeromorph acritarch *Valeria lophostriata* (Jankauskas): Acta Micropalaeontologica Sinica, v. 16, p. 215–224.

Hofmann, H.J., and Aitken, J.D., 1979, Precambrian biota from the Little Dal Group, Mackenzie Mountains, northwestern Canada: Canadian Journal of Earth Sciences, v. 16, p. 150–166.

Hofmann, H.J., and Jackson, G.D., 1994, Shale-facies microfossils from the Proterozoic Bylot Supergroup, Baffin Island, Canada: Paleontological Society Memoir, v. 37, p. 1–35.

Horodyski, R.J., and Donaldson, J.A., 1980, Microfossils from the middle Proterozoic Dismal Lakes Group, Arctic Canada: Precambrian Research, v. 11, p. 125–159.

Hu, Y., and Fu, J., 1982, Micropalaeoflora from the Gaoshanhe Formation of Late Precambrian of Luonan, Shaanxi and its stratigraphic significance: Bulletin Xi'an Institute of Geology and Mineral Resources, Chinese Academy of Geological Sciences, v. No.4, p. 102–111.

Jankauskas, T.V., 1979, Lower Riphean microbiotas of the Southern Urals: Akademiya Nauk SSSR, Geology, v. 248, p. 190–193.

Jankauskas, T.V., 1982, Microfossils of the Riphean of the South Urals, eds., The Riphean Stratotype, Paleontology, Paleomagnitism. Akademia Nauk SSSR, Moscow, p. 84–120.

Jankauskas, T.V., Mikhailova, N.S., and Hermann, T.N., 1989, Precambrian Microfossils of the USSR. Nauka, Leningrad, 190 p.

Javaux, E., 2011, Early eukaryotes in Precambrian oceans. *In* Gargaud, M., Lopez-Garcia, P., and Martin, H., eds., Origins and Evolution of life: An Astrobiological Perspective. Cambrian University Press, New York, p. 414–449.

Javaux, E.J., Knoll, A.H., and Walter, M.R., 2001, Morphological and ecological complexity in early eukaryotic ecosystems: Nature, v. 412, p. 66–69.

Javaux, E.J., Knoll, A.H., and Walter, M.R., 2004, TEM evidence for eukaryotic diversity in mid-Proterozoic oceans: Geobiology, v. 2, p. 121–132.

Knoll, A.H., 1982, Microfossils from the late Precambrian Draken Conglomerate, NY Friesland, Svalbard: Journal of Paleontology, v. 56, p. 755–790.

Knoll, A.H., and Golubic, S., 1979, Anatomy and taphonomy of a Precambrian algal stromatolite: Precambrian Research, v. 10, p. 115–151.

Knoll, A.H., Swett, K., and Mark, J., 1991, Paleobiology of a Neoproterozoic tidal flat/lagoonal complex: The Draken Conglomerate Formation, Spitsbergen: Journal of Paleontology, v. 65, p. 531–570.

Kolosov, P.N., 2014, On some species of microfossils from the Torgin Formation of the Neoproterozoic of the Berezov Depression (Southern Siberian Platform): Paleontological Journal, v. 48, p. 330–338.

Li, J., Qian, M., and Jiang, Y., 2013, Overlapping of the lower Cambrian Houjiashan Formation over the pre-Cambrian sequences in the northern Jiangsu and Anhui provinces: Journal of Stratigraphy, v. 37, p. 232–241.

Liu, D.Y., Nutman, A.P., Compston, W., Wu, J.S., and Shen, Q.H., 1992, Remnants of ⩾3800 Ma crust in the Chinese part of the Sino-Korean craton: Geology, v. 20, p. 339–342.

Liu, P., Xiao, S., Yin, C., Chen, S., Zhou, C., and Li, M., 2014, Ediacaran acanthomorphic acritarchs and other microfossils from chert nodules of the upper Doushantuo Formation in the Yangtze Gorges area, South China: Paleontological Society Memoir, v. 72, p. 1–139.

Liu, P., and Yin, C., 2005, New data of phosphatized acritarchs from the Ediacaran Doushantuo Formation at Weng'an, Guizhou Province, southwest China: Acta Geologica Sinica, v. 79, p. 575–581.

Liu, S., Santosh, M., Wang, W., Bai, X., and Yang, P., 2011, Zircon U–Pb chronology of the Jianping Complex: Implications for the Precambrian crustal evolution history of the northern margin of North China Craton: Gondwana Research, v. 20, p. 48–63.

Liu, Y., Gao, L., Liu, X., Song, B., and Wang, Z., 2005, Zircon U-Pb age determination of early Neoproterozoic mafic magmatic event in the Xu-Huai region: Chinese Science Bulletin, v. 22, p. 2514–2521.

McMenamin, D.S., Kumar, S., and Awramik, S.M., 1983, Microbial fossils from the Kheinjua Formation, Middle Proterozoic Semri Group (Lower Vindhyan) Son Valley area, central India: Precambrian Research, v. 21, p. 247–271.

Moczydlowska, M., and Nagovitsin, K.F., 2012, Ediacaran radiation of organic-walled microbiota recorded in the Ura Formation, Patom Uplift, East Siberia Precambrian Research, v. 198/199, p. 1–24.

Nagovitsin, K., 2009, *Tappania*-bearing association of the Siberian platform: Biodiversity, stratigraphic position and geochronological constraints: Precambrian Research, v. 173, p. 137–145.

Nagovitsin, K.E., Faizullin, M.S., and Yakshin, M.S., 2004, New forms of Baikalian acanthomorphytes from the Ura Formation of the Patom Uplift, East Siberia: Geologiya e Geofisika, v. 45, p. 7–19.

Naumova, S.N., 1949, Spores from the Lower Cambrian: Izvestiya Akademii Nauk SSSR, Seriya Geologicheskaya, v. 1949 (4), p. 49–56.

Naumova, S.N., 1968, Zonal assemblages of Precambrian and Lower Cambrian plant microfossils of Eurasia and their stratigraphic significance Mezhdunarodnyy Geologicheskiy Kongress, XXIII Sessiya, Doklady Sovetskikh Geologov, p. 30–39.

Nautiyal, A.C., 1980, Cyanophycean algal remains and paleoecology of the Precambrian Gangolihat Dolomite Formation of the Kumaon Himalaya, India.: Indian Journal of Earth Sciences, v. 7, p. 1–11.

Pang, K., Tang, Q., Schiffbauer, J.D., Yao, J., Yuan, X., Wan, B., Chen, L., Ou, Z., and Xiao, S., 2013, The nature and origin of nucleus-like intracellular inclusions in Paleoproterozoic eukaryote microfossils: Geobiology, v. 11, p. 499–510.

Pang, K., Tang, Q., Yuan, X., Bin, W., and Xiao, S., 2015, Organic-walled microfossils from the Paleo-Mesoproterozoic Ruyang Group and a biomechanical analysis of the early eukaryotic fossil *Valeria*: Paleoworld, 24, 251–262.

Peng, P., Bleeker, W., Ernst, R.E., Söderlund, U., and McNicoll, V., 2011a, U–Pb baddeleyite ages, distribution and geochemistry of 925 Ma mafic dykes and 900 Ma sills in the North China craton: Evidence for a Neoproterozoic mantle plume: Lithos, v. 127, p. 210–221.

Peng, P., Zhai, M.-G., Li, Q., Wu, F., Hou, Q., Li, Z., Li, T., and Zhang, Y., 2011b, Neoproterozoic (~900Ma) Sariwon sills in North Korea: Geochronology, geochemistry and implications for the evolution of the south-eastern margin of the North China Craton: Gondwana Research, v. 20, p. 243–254.

Peng, S., Babcock, L.E., and Cooper, R.A., 2012, The Cambrian Period. *In* Gradstein, F.M., Ogg, J.G., Schmitz, M., and Ogg, G., eds., Geological Time Scale 2012. Elsevier, Oxford, p. 437–488.

Peng, Y., Bao, H., and Yuan, X., 2009, New morphological observations for Paleoproterozoic acritarchs from the Chuanlinggou Formation, North China: Precambrian Research, v. 168, p. 223–232.

Pyatiletov, V.G., 1980, Yudoma complex microfossils from southern Yakutia: Geologiya i Geofizika, v. 7, p. 8–20.

Qian, M., Jiang, Y., and Yi, M., 2009, Neoproterozoic millimetric-centimetric carbonaceous fossils from northern Anhui and Jiangsu, China: Acta Palaeontologica Sinica, v. 48, p. 73–88.

Qian, M., Yuan, X., Li, J., Yan, Y., and Wang, P., 2001, Comments on the Cambrian-Neoproterozoic boundary in Huaibei district, northern Anhui-Jiangsu: Journal of Stratigraphy, v. 25, p. 135–143.

Qian, M., Yuan, X., Yan, Y., and Ding, B., 2002, Neoproterozoic microfossils from northern Jiangsu and Anhui: Acta Micropalaeontologica Sinica, v. 19, p. 363–381.

Rainbird, R.H., Stern, R.A., Khudoley, A.K., Kropachev, A.P., Heaman, L.M., and Sukhorukov, V.I., 1998, U-Pb geochronology of Riphean sandstone and gabbro from Southeast Siberia and its bearing on the Laurentia-Siberia connection: Earth and Planetary Science Letters, v. 164, p. 409–420.

Riedman, L.A., and Porter, S., 2015, Organic-walled microfossils of the early to mid-Neoproterozoic Alinya Formation, Officer Basin, Australia: Journal of Paleontology, v. 90, p. 854–887.

Samuelsson, J., 1997, Biostratigraphy and paleobiology of early Neoproterozoic strata of the Kola Peninsula, northwest Russia: Norsk Geologisk Tidsskrift, v. 77, p. 165–192.

Samuelsson, J., Dawes, P.R., and Vidal, G., 1999, Organic-walled microfossils from the Proterozoic Thule Supergroup, Northwest Greenland: Precambrian Research, v. 96, p. 1–23.

Santosh, M., Liu, D., Shi, Y., and Liu, S.J., 2013, Paleoproterozoic accretionary orogenesis in the North China Craton: A SHRIMP zircon study: Precambrian Research, v. 227, p. 29–54.

Schiffbauer, J.D., and Xiao, S., 2009, Novel application of focused ion beam electron microscopy (FIB-EM) in the preparation and analysis of microfossil ultrastructures: PALAIOS, v. 24, p. 616–626.

Schopf, J.W., 1968, Microflora of the Bitter Springs Formation, Late Precambrian, central Australia: Journal of Paleontology, v. 42, p. 651–688.

Schopf, J.W., and Klein, C., 1992, The Proterozoic Biosphere: A Multidisciplinary Study. Cambridge University Press, Cambridge, 1348 p.

Semikhatov, M.A., Ovchinnikova, G.V., Gorokhov, I.M., Kuznetsov, A.B., Vasil’eva, I.M., Gorokhovskii, B.M., and Podkovyrov, V.N., 2000, Isotopic age of the Middle-Upper Riphean boundary: Pb–Pb geochronology of the Lakhanda Group carbonates, Eastern Siberia: Doklady Earth Sciences, v. 372, p. 625–629.

Sergeev, V.N., Knoll, A.H., and Grotzinger, J.P., 1995, Paleobiology of the Mesoproterozoic Billyakh Group, Anabar Uplift, Northern Siberia: Memoir (The Paleontological Society), v. 39, p. 1–37.

Sergeev, V.N., Knoll, A.H., and Vorob'Eva, N.G., 2011, Ediacaran microfossils from the Ura Formation, Baikal-Patom Uplift, Siberia: taxonomy and biostratigraphic significance: Journal of Paleontology, v. 85, p. 987–1011.

Steiner, M., 1997, *Chuaria circularis* Walcott 1899−"megasphaeromorph acritarch" or prokaryotic colony?: Acta Universitatis Carolinae Geologica, v. 40, p. 645–665.

Strother, P.K., Knoll, A.H., and Barghoorn, E.S., 1983, Micro-organisms from the late Precambrian Narssarssuk Formation, northwestern Greenland: Palaeontology, v. 26, p. 1–32.

Sun, W., Wang, G., and Zhou, B., 1986, Macroscopic worm-like body fossils from the Upper Precambrian (900–700Ma), Huainan district, Anhui, China and their stratigraphic and evolutionary significance: Precambrian Research, v. 31, p. 377–403.

Tang, F., Yin, C., Liu, P., Gao, L., and Zhang, W., 2008, A new diverse macrofossil Lagerstätte from the uppermost Ediacaran of southwestern China: Acta Geologica Sinica, v. 82, p. 1095–1103.

Tang, Q., Pang, K., Xiao, S., Yuan, X., Ou, Z., and Wan, B., 2013, Organic-walled microfossils from the early Neoproterozoic Liulaobei Formation in the Huainan region of North China and their biostratigraphic significance: Precambrian Research, v. 236, p. 157–181.

Timofeev, B.V., 1966, Mircropaleophytological Investigations of Ancient Formations. Nauka, Moscow, 237 p.

Timofeev, B.V., and Herman, T.N., 1979, Precambrian microbiota of the Lakhanda Formation. *In* Sokolov, B.S., eds., Paleontology of the Precambrian and Early Cambrian. Nauka, Leningrad, p. 137–147.

Timofeev, B.V., Hermann, T.N., and Mikhailova, N.S., 1976, Microphytofossils of the Precambrian, Cambrian and Ordovician. Nauka, Leningrad, 106 p.

Vidal, G., and Ford, T.D., 1985, Microbiotas from the late Proterozoic Chuar Group (northern Arizona) and Uinta Mountain Group (Utah) and their chronostratigraphic implications: Precambrian Research, v. 28, p. 349–389.

Volkova, N.A., Kirjanov, V.V., Piscun, L.V., Pashkyavichene, L.T., and Jankauskas, T.V., 1979, Plant microfossils. *In* Keller, B.M. and Rozanov, A.Y., eds., Upper Precambrian and Cambrian paleontology of the East European Platform. Nauka, Moscow, p. 4–38 (37–46 in English translation published in 1983).

Vorob'eva, N.G., Sergeev, V.N., and Knoll, A.H., 2009a, Neoproterozoic microfossils from the margin of the East European Platform and the search for a biostratigraphic model of lower Ediacaran rocks: Precambrian Research, v. 173, p. 163–169.

Vorob'eva, N.G., Sergeev, V.N., and Knoll, A.H., 2009b, Neoproterozoic microfossils from the northeastern margin of the East European Platform: Journal of Paleontology, v. 83, p. 161–196.

Walcott, C.D., 1899, Pre-Cambrian fossiliferous formations: Bulletin of the Geological Society of America, v. 10, p. 199–244 (plates 122–128).

Wang, G., Zhang, S., Li, S., Yan, Y., Dou, S., and Fang, D., 1984a, Research on the Upper Precambrian of Northern Jiangsu and Anhui Provinces. Anhui Press of Science and Technology, Hefei, Anhui, 209 p.

Wang, G., Zhou., B., and Xiao., L., 1984b, Late Precambrian macrofossils from Huainan, Anhui and their significance: Journal of Stratigraphy, v. 84, p. 271–278.

Wang, Q., Yan, D., and Xu, W., 2011, Neoproterozoic basic magmatism in the southeast margin of North China Craton: evidence from whole-rock geochemistry, U-Pb and Hf isotopic

study of zircons from diabase swarms in the Xuzhou-Huaibei area: Science in China (Series D), v. 41, p. 796–815.

Xiao, S., Knoll, A.H., Kaufman, A.J., Yin, L., and Zhang, Y., 1997, Neoproterozoic fossils in Mesoproterozoic rocks? Chemostratigraphic resolution of a biostratigraphic conundrum from the North China Platform: Precambrian Research, v. 84, p. 197–220.

Xiao, S., Shen, B., Tang, Q., Kaufman, A.J., Yuan, X., Li, J., and Qian, M., 2014a, Biostratigraphic and chemostratigraphic constraints on the age of early Neoproterozoic carbonate successions in North China: Precambrian Research, v. 246, p. 208–225.

Xiao, S., Zhou, C., Liu, P., Wang, D., and Yuan, X., 2014b, Phosphatized acanthomorphic acritarchs and related microfossils from the Ediacaran Doushantuo Formation at Weng'an (South China) and their implications for biostratigraphic correlation: Journal of Paleontology, v. 88, p. 1–67.

Xing, Y., 1989, The Upper Precambrian of China, Volume 3 of "The Stratigraphy of China". Geological Publishing House, Beijing, 314 p.

Xing, Y., Duan, C., Liang, Y., and Cao, R., 1985, Late Precambrian Palaeontology of China. Geological Publishing House, Beijing, 243 p.

Xing, Y., Gao, Z., Wang, Z., Gao, L., and Yin, C., 1996, Chinese Stratigraphy Catalog-Neoproterozoic. Geological Publishing House, Beijing, 117 p.

Xing, Y., and Liu, G., 1973, Sinian micropaleoflora in the Yan-Liao area and its geological significance: Acta Geologica Sinica, v. 1973, p. 1–31.

Yan, Y., 1995, Shale facies microfloras from Lower Changcheng System in Kuancheng, Hebei and comparison with those of neighboring areas: Acta Micropalaeontologica Sinica, v. 12, p. 349–373.

Yan, Y., and Liu, Z., 1993, Significance of eucaryotic organisms in the microfossil flora of the Changcheng System: Acta Micropalaeontologica Sinica, v. 10, p. 167–180.

Yang, D., Xu, W., Xu, Y., Wang, Q., Pei, F., and Wang, F., 2012, U-Pb ages and Hf isotope data from detrital zircons in the Neoproterozoic sandstones of northern Jiangsu and southern Liaoning Provinces, China: Implications for the late Precambrian evolution of the southeastern North China Craton: Precambrian Research, v. 216–219, p. 162–176.

Yin, C., 1985, Micropaleoflora from the late Precambrian in Huainan region of Anhui Province and its stratigraphic significance: Professional Papers of Stratigraphy and Palaeontology, Chinese Academy of Geological Sciences, v. 12, p. 97–119.

Yin, C., 1992, A new algal fossil from Early Cambrian in Qingzhen county, Guizhou Province, China: Acta Botanica Sinica, v. 34, p. 456–460.

Yin, C., 1999, Microfossils from the Upper Sinian (Late Neoproterozoic) Doushantuo Formation in Changyang, western Hubei, China: Continental Dynamics, v. 4, p. 1–18.

Yin, L., 1987, Microbiotas of latest Precambrian sequences in China. *In* Nanjing Institute of Geology and Palaeontology Academica Sinica, eds., Stratigraphy and Palaeontology of Systemic Boundaries in China: Precambrian–Cambrian Boundary (1). Nanjing University Press, Nanjing, p. 415–494.

Yin, L., and Sun, W., 1994, Microbiota from Neoproterozoic Liulaobei Formation in the Huainan region, Northern Anhui, China: Precambrian Research, v. 65, p. 95–114.

Yin, L., Yuan, X., Meng, F., and Hu, J., 2005, Protists of the Upper Mesoproterozoic Ruyang Group in Shanxi Province, China: Precambrian Research, v. 141, p. 49–66.

Zang, W., and Walter, M.R., 1992, Late Proterozoic and Early Cambrian microfossils and biostratigraphy, northern Anhui and Jiangsu, central-eastern China: Precambrian Research, v. 57, p. 243–323.

Zhang, W., and Zhu, Z., 1979, Notes on some trilobites from Lower Cambrian Houjiashan Formation in southern and southwestern parts of North China: Acta Palaeontologica Sinica, v. 18, p. 513–526.

Zhang, Y., Yin, L., Xiao, S., and Knoll, A.H., 1998, Permineralized fossils from the terminal Proterozoic Doushantuo Formation, South China: Journal of Paleontology, v. 72 (supplement to No. 4), p. 1–52.

Zheng, W., 1980, A new occurrence of fossil group *Chuaria* from the Sinian System in north Anhui and its geological meaning: Bulletin of the Tianjin Institute of Geology and Mineral Resources, v. 1, p. 49–69.

Zheng, W., Mu, Y., Zheng, X., Wang, J., and Xin, L., 1994, Discovery of carbonaceous megafossils from Upper Precambrian Shijia Formation, north Anhui and its biostratigraphic significance: Acta Palaeontologica Sinica, v. 33, p. 455–471.

Zhou, C., Brasier, M.D., and Xue, Y., 2001, Three-dimensional phosphatic preservation of giant acritarchs from the terminal Proterozoic Doushantuo Formation in Guizhou and Hubei provinces, South China: Palaeontology, v. 44, p. 1157–1178.

Zhou, C., Yuan, X., Xiao, S., Chen, Z., and Xue, Y., 2004, Phosphatized fossil assemblage from the Doushantuo Fromation in Baokang, Hubei Province: Acta Micropalaeontologica Sinica, v. 21, p. 349–366.

CHAPTER 4

A problematic animal fossil from the early Cambrian Hetang Formation, South China

Qing Tang[1], Jie Hu[2], Guwei Xie[3,4], Xunlai Yuan[5,6], Bin Wan[5], Chuanming Zhou[7], Xu Dong[8], Guohua Cao[8], Shuhai Xiao[1]

[1]*Department of Geosciences, Virginia Tech, Blacksburg, VA 24061, USA*

[2]*CNPC International (Chad) Co. Ltd., N'djamena, Chad*

[3]*Institute of Exploration, Development and Research of PetroChina Company Limited Changqing Oilfield Branch, Xi'an 710018, China*

[4]*National Engineering Laboratory for Exploration and Development of Low-permeability Oil & Gas Fields, Xi'an 710018, China*

[5]*State Key Laboratory of Palaeobiology and Stratigraphy, Center for Excellence in Life and Paleoenvironment, Nanjing Institute of Geology and Palaeontology, Chinese Academy of Sciences, Nanjing, 210008, China*

[6]*University of Chinese Academy of Sciences, Beijing 100039, China*

[7]*CAS Key Laboratory of Economic Stratigraphy and Palaeogeography, Nanjing Institute of Geology and Palaeontology, Chinese Academy of Sciences, Nanjing 210008, China*

[8]*Virginia Tech–Wake Forest University School of Biomedical Engineering and Sciences, Virginia Tech, Blacksburg, VA 24061*

4.1 Abstract

The lower-middle Hetang Formation (Cambrian Stage 2–3) deposited in slope-basinal facies in South China is well-known for its preservation of the earliest articulated sponge fossils, providing an important taphonomic window into the Cambrian Explosion. However, metazoan

fossils other than sponges are poorly documented from this stratigraphic interval, resulting in an incomplete picture of the Hetang biota and limiting its contribution to the understanding of the early evolution of animals. Here we describe a new animal taxon, *Cambrowania ovata* new genus new species, from the middle Hetang Formation in the Lantian area of southern Anhui Province, South China. Specimens are preserved as carbonaceous compressions, although some are secondarily mineralized. A comprehensive analysis using reflected light microscopy, scanning electron microscopy, energy dispersive X-ray spectroscopy, and micro-CT reveals that the new species is characterized by a fusoidal to ovoidal truss-like structure consisting of rafter-like crossbars, some of which may have been internally hollow. Some specimens show evidence of medial split, suggesting that they may represent the carapace of bivalved arthropods, although their phylogenetic affinity remains problematic. Along with other problematic metazoan fossils such as hyolithids and sphenothallids, *Cambrowania ovata* adds to the diversity of the sponge-dominated Hetang biota.

4.2 Introduction

The Cambrian Explosion marks the most important biodiversification event in Earth history (Erwin and Valentine, 2013). All major animal body plans appeared in the fossil record during this biodiversification event, setting the stage for the evolution of modern animal phyla (Knoll and Carroll, 1999; Erwin et al., 2011). Recently, our understanding of the Cambrian Explosion has been significantly improved, in a large part due to systematic studies of various exceptionally preserved fossil assemblages or Konservat-Lagerstätten from the early−middle Cambrian Period, including the Sirius Passet, Chengjiang, Guanshan, Emu Bay Shale, Kaili, and Burgess Shale biotas (Holmes et al., 2018). One of the early Cambrian Lagerstätten that has yet

to be brought under the spotlight is the Hetang biota, which occurs in black shales of the lower-middle Hetang Formation in southern Anhui Province of South China. The Hetang biota is dominated by sponge fossils and contains some of the earliest articulated sponges, particularly abundant in a unit of highly organic-rich and combustible mudstone (known locally as the stone coal unit) in the lower Hetang Formation (Hu et al., 2002; Yuan et al., 2002; Chen et al., 2004; Wu et al., 2005; Xiao et al., 2005; Botting et al., 2012; Botting et al., 2014). However, other metazoan fossils in the Hetang Formation are either poorly illustrated or largely ignored in previous studies (Yuan et al., 2002; Chen et al., 2004). To more fully document the diversity of the Hetang biota, here we describe a new group of problematic animal fossils from black shale/mudstone of the middle Hetang Formation (Cambrian Stage 2−3) in Lantian area of South China. The fossils, described under a new taxon, *Cambrowania ovata* new genus new species, may represent the carapace of bivalved arthropods although their phylogenetic affinity remains problematic.

4.3 Geological setting

The Hetang Formation is mainly distributed in southern Anhui and neighboring northern Jiangxi and western Zhejiang provinces. It can be traced with relative ease in these areas, although its stratigraphic thickness may vary in places (Xue and Yu, 1979). In this study, we focus on the Lantian area of southern Anhui Province where the Hetang Formation overlies siliceous rock of the largely terminal Ediacaran Piyuancun Formation and underlies the early Cambrian limestone of Dachenling Formation (Fig. 4.1). Regionally, the Hetang Formation is ~318 m in maximum thickness. It can be divided into four lithostratigraphic units. The basal unit is a ~68 m thick siliceous-carbonaceous mudstone rich in phosphorite nodules at the base.

Overlying this basal unit are, in ascending stratigraphic order, the lower unit of ~30 m thick stone coal (combustible organic-rich mudstone), the middle unit of ~110 m thick siliceous-carbonaceous mudstone and shale, and the upper unit of ~110 m thick carbonaceous shale with carbonate nodules. It should be noted that there are variations in the literature with regard to the lithostratigraphic boundary between the Piyuancun and Hetang formations: (1) some authors place the boundary just above the phosphorite bed at the base of the basal unit in the uppermost Piyuancun Formation (Yue and He, 1989; He and Yu, 1992; Yue and Zhao, 1993; Xiao et al., 2005); (2) Xiang et al. (2017) place the boundary at about 150 m below the stone coal unit; (3) in regional geological survey reports (Bureau of Geology and Mineral Resources of Anhui Province, 1987) and in more recent literature (Steiner et al., 2007; Dong et al., 2012), the Piyuancun-Hetang boundary is placed at the base of the phosphorite bed. In this paper we follow the latter stratigraphic treatment, in which the Ediacaran-Cambrian boundary is at or near the Piyuancun-Hetang boundary (contra Xiang et al., 2017) because the Piyuancun Formation contains typical terminal Ediacaran fossils whereas the phosphorite bed contains basal Cambrian small shelly fossils (Dong et al., 2012). Sedimentological and geochemical data suggest that the Hetang Formation was mainly deposited in ferruginous slope-basinal environment (Zhou and Jiang, 2009; Yuan et al., 2014; Xiang et al., 2017).

The Hetang Formation contains abundant fossils that are biostratigraphically informative. Regionally, phosphorite in the basal unit contains small shelly fossils such as *Anabarites trisulcatus*, *Protohertzina anabarica*, and *Kaiyangites novilis* (Yue and He, 1989; He and Yu, 1992; Yue and Zhao, 1993; Steiner et al., 2004). Together, these fossils are characteristic of the basal Cambrian *Anabarites trisulcatus–Protohertzina anabarica* Assemblage Zone (Yao et al., 2005; Steiner et al., 2007). In other words, the basal unit is likely Cambrian Stage 1. Stone coal

in the lower unit contains abundant articulated sponge fossils (Xiao et al., 2005). Regional litho- and biostratigraphic correlation on the basis of small shelly fossils, acritarchs, and trilobites of the Hetang Formation in southern Anhui and western Zhejiang provinces indicates the lower unit or the stone coal unit is Cambrian Stage 2 (Xiao et al., 2005). Carbonate nodules in the upper unit in western Zhejiang Province yields trilobites such as *Hunanocephalus*, *Hupeidiscus*, and *Hsuaspis* (Li et al., 1990; He and Yu, 1992), which are indicative of Cambrian Stage 3 (Peng et al., 2012). Therefore, the carbonaceous mudstone and shale of the middle unit of the Hetang Formation, from which the fossils reported in this paper were collected, can be constrained between Cambrian Stage 2 and Stage 3.

4.4 Materials and methods

Totally 436 specimens of *Cambrowania ovata* new genus new species were recovered from mudstone/shales of the middle Hetang Formation (Fig. 4.1). The majority of the specimens are preserved as carbonaceous compressions, although some are secondarily mineralized. All specimens were initially examined with reflected light microscopy (RLM) using an Olympus SZX7 stereomicroscope connected with an Infinity 1 camera. Well-preserved specimens were subsequently examined using backscattered electron scanning electron microscopy (BSE-SEM), secondary electron scanning electron microscopy (SE-SEM), and energy dispersive X-ray spectroscopy (EDS) on a FEI Quanta 600FEG environmental SEM coupled with a Bruker EDX with a silicon drifted detector (Muscente and Xiao, 2015). The operating voltage in BSE-SEM, SE-SEM, and EDS modes was 5−20 kV in high-vacuum condition. Selected specimens with mineralized structures were scanned using an Xradia micro-CT to visualize internal structures. The X-ray source for the micro-CT scanning was operated at 90 kV in voltage and 88 μA in

current with a flat area detector. The detector has a resolution of 2048 × 2048 pixels; each pixel size is 0.05 mm × 0.05 mm. The scanned sample was placed in the middle of X-ray source and the detector. The source-object and source-detector distances were 25 mm and 155 mm, respectively. Under such geometric setting, the generated micro-CT images have a matrix size of 2048 × 2048 with the voxel size of 4.40 μm × 4.40 μm. All illustrated specimens are reposited at Virginia Polytechnic Institute Geosciences Museum (catalog numbers with the prefix VPIGM-, Blacksburg, Virginia, USA).

4.5 Systematic paleontology

Pylum, Class, Order, Family incertae sedis

Genus *Cambrowania* new genus

Type species.—Cambrowania ovata n. gen. n. sp.; by present designation; by monotypy.

Diagnosis.—As for type species.

Occurrence.—Specimens were recovered from shale and mudstone of the middle Hetang Formation (Stage 2–3, lower Cambrian) in the Lantian area, South China.

Etymology.—Genus name derived from Cambrian and Wan (Anhui Province), referring to the stratigraphic and geographic occurrence of the type species.

Remarks.—Cambrowania n. gen. is distinguished from other known fossils of the early Cambrian Period by its spheroidal truss-like body-plan with rafter-like crossbars that are cylindrical and internally hollow.

Cambrowania ovata new species

Figures 4.2−4.5

Holotype.—VPIGM-4729 in Fig. 4.2a, reposited at Virginia Polytechnic Institute Geosciences Museum.

Paratype.—VPIGM-4742 in Fig. 4.4c, reposited at Virginia Polytechnic Institute Geosciences Museum.

Diagnosis.—Spheroidal, ovoidal, or fusoidal truss-like fossils consisting of rafter-like crossbars or blades. The crossbars are nearly straight or slightly curved, singularly or doubly arranged, originally cylindrical and internally hollow, and interlaced to form a network-like truss. Some specimens show evidence of medial split.

Occurrence.—Shale/mudstone of the middle Hetang Formation in Lantian area, South China.

Morphological description.—Fossils are preserved as discoidal (Fig. 4.2a, d), sub-polygonal (Fig. 4.2e), elliptical (Fig. 4.2f), and fusiform (Fig. 4.2g) carbonaceous compressions that are 1.7 to 10.7 mm in maximum dimension. Main structures of the fossil include marginal bars defining the outline of the fossil and interior crossbars contained within the fossil (Fig. 4.2b). Interior

crossbars can terminate at but never reach beyond the margin of the fossil. Multiple interior crossbars can terminally converge at a convergent point at fossil margin to form a cluster of radiating crossbars (Fig. 4.2a, b, e). Double crossbars consist of two crossbars that are sub-parallel and sometimes terminally convergent (Fig. 4.2a, b). Crossbars are 15–94 μm in width and 1–6 mm in length, with broader ones forming blades (Fig. 4.2c, d). Crossbars of different widths can be present in the same specimen (Fig. 4.2a). Most crossbars are straight (Fig. 4.2a, e), although some are curved (Fig. 4.2c, d) and even twisted (Fig. 4.2a, e). When the marginal bars are straight, the fossils typically have a polygonal outline (Fig. 4.2e).

A few specimens in our collection (4 out of 436 specimens) preserve a medial split (Fig. 4.3a−d) that is reminiscent of the ventral margin of the carapace of bivalved arthropods (e.g., fig. 20 in Hou and Bergström, 1997). This split results in a V-shaped cleft, with two hemispherical halves connected on one side and gaping on the other. Importantly, the gaping margin of the hemispherical halves is also defined by marginal crossbars, and no crossbars reach beyond the margin (Fig. 4.3a, b), suggesting that the medial split is likely a biological rather than a taphonomic structure. The gaping angle is 14° to 67°, and butterflied configuration (i.e., gaping angle of 180°; Briggs et al., 2015) is not seen. Those specimens that do not show a V-shaped cleft usually appear to have slightly offset margins (e.g., Figs. 4.2e and 4.3e−h). It is possible that specimens with V-shaped clefts (e.g., Fig. 4.3a−d) and those with slightly offset margins represent taphonomic variants (e.g., lateral vs. anterior-posterior compression of bivalved arthropod carapace with gaping margins).

Taphonomic description.—The crossbars are mostly preserved as two dimensional carbonaceous compressions, with a few exceptions where they are secondarily mineralized in three dimensions.

Abundant pyrite framboids and their molds are present in the crossbars (Fig. 4.4a, b), indicating organic degradation through sulfate reduction. The carbonaceous nature of the crossbars is confirmed in EDS point analysis and elemental maps. EDS point analyses show high C and O peaks and low S, Al, and Si peaks (Fig. 4.4c−f), indicating the crossbars mainly consists of organic material. EDS elemental maps confirm the enrichment of C in the crossbars relative to the matrix (Fig. 4.4g).

One secondarily mineralized fusoidal specimen has been analyzed in detail (Fig. 4.5). This specimen is partially covered with a thin barite layer, which is confirmed by BSE-SEM images and elemental maps (Fig. 4.5b, i). In cross-sections perpendicular to the bedding plane, it can be seen that the barite layer is 10−16 μm in thickness (Fig. 4.5c, d). A cluster of convergent crossbars occurs at one end of the fusoidal specimen (Fig. 4.5e, f). It is possible that another cluster occurs at the opposite end, but the crossbars are exfoliated and only vague imprints are visible. The crossbars are three-dimensionally replicated by barite, and this is clearly seen in a large crossbar running between the two apices of the fusoidal fossil (Fig. 4.5a). In transverse cross-sections, the baritized crossbars are internally hollow with centripetally growing barite crystals and slightly compressed with a maximum diameter of 180−208 μm (Fig. 4.5c, d, g, h).

Etymology.—Species epithet derived from Latin *ovatus*, referring to the fusoidal to ovoidal shape of this species.

Materials.—436 specimens from shale/mudstone of the middle Hetang Formation.

Remarks.—Cambrowania ovata n. gen. n. sp. is morphologically similar to the problematic fossil *Chuaria circularis* (Tang et al., 2017) and the carapaces of arthropods *Iosuperstes collisionis* (Briggs et al., 2015). However, neither of these species have rafter-like crossbars that are interlaced to form a network-like truss, which is the main character of *Cambrowania ovata*.

4.6 Discussion

Morphological reconstruction.—The morphological variation of *Cambrowania ovata* is partly due to taphonomic alteration. For example, the elongate fusiform specimens may represent curled hemispherical halves (compare Fig. 4.2f, g with the right half of Fig. 4.3b). As discussed above, specimens with a V-shaped cleft (Fig. 4.3a−d) and those with offset margins (Fig. 4.3e−h) may also represent different taphonomic variations. Given that none of the *Cambrowania ovata* specimens in our collection presents a butterflied configuration (Briggs et al., 2015), it is possible that *Cambrowania ovata* had a bivalved carapace with only limited gaping (Fig. 4.6a). Alternatively, *Cambrowania ovata* may be a spheroidal vesicle (Fig. 4.6b), with the V-shaped cleft being an excystment structure similar to medial split excystment structures in *Chuaria* (Yuan et al., 2001; Tang et al., 2017). Given that a spherical vesicle is unlikely to form a polygonal compression (e.g., Fig. 4.2e), we tentatively favor the former reconstruction. In addition, the crossbars or blades may represent either thickened ribs on the organic test or folded vesicle wall of *Cambrowania ovata*. Given that some crossbars are preserved as compressed hollow cylinders, we prefer the former interpretation. Regardless, much of the test or vesicle wall is not preserved, probably due to its limited thickness (and hence greater susceptibility to degradation) relative to the thickened ribs or folds.

Biological interpretation.—As discussed above, the similarities between *Cambrowania ovata* and organic vesicles of algal fossils such as *Chuaria* may be superficial. Indeed, we are unaware of any algae, fossil or extant, that have hollow cylindrical crossbars similar to those in *Cambrowania ovata*. Thus, the following discussion is focused on the possible animal affinities of *Cambrowania ovata*.

Considering that the clustered crossbars are superficially similar to hexactine-based sponge spicules such as pentactines (e.g., those in *Sanshapentella dapingi*, Xiao et al., 2005), it is tempting to consider *Cambrowania ovata* as a spheroidal sponge. This interpretation is also consistent with the hollow nature of the cylindrical crossbars, which would represent spicules that consisted mainly of organic material. Given that axial filaments of sponge spicules tend to be degraded soon after the death of the organisms, fossil sponge spicules are usually preserved as a cylinder with an enlarged axial canal (Botting and Muir, 2013), which could account for the hollow nature of the crossbars in *Cambrowania ovata*. Although extant sponge spicules are usually biomineralized (either siliceous or calcareous), some basal groups of demosponges can develop organic skeletons (de Cook and Bergquist, 2002; Hill et al., 2013). In addition, many fossil sponges also have developed weakly biomineralized or even organic skeletons, e.g., the demosponge *Vauxia* (Ehrlich et al., 2013) and some protomonaxoinids, such as piraniids and chancelloriids (Botting and Muir, 2018). Thus, the largely organic composition of the crossbars does not exclude a sponge interpretation for *Cambrowania ovata*. However, the lack of an osculum and any ostia in *Cambrowania ovata* is incompatible with the sponge interpretation. The sponge interpretation could be also falsified by the V-shaped cleft, which indicates that *Cambrowania ovata* had cohesive but flexible walls.

The V-shaped cleft suggests a tentative comparison between *Cambrowania ovata* and bivalved arthropods. As discussed above, the V-shaped cleft is likely a biological feature, because no interior crossbars reach beyond the margin of the cleft. Thus, specimens with a V-shaped cleft may represent carapaces of bivalved arthropods, but these bivalved carapaces probably had limited gaping, given the lack of any butterflied specimens in our collection. The strongly irregular traces of organic matter (yellow arrows in Fig. 4.2a, e) could be crumples or wrinkles on the flexible carapace due to taphonomic compaction, which are common in high-relieved carapaces of arthropods (Fu and Zhang, 2011; Briggs et al., 2015). However, the straight and gently curved crossbars of *Cambrowania ovata* likely represent thickened ribs that are structural components of the organism, particularly if their hollow and cylindrical nature, as shown in baritized specimens (Fig. 4.5), is confirmed in the future.

The crossbars of *Cambrowania ovata* may represent ornaments (e.g., thickened ribs or ridges) of bivalved carapaces. Many Paleozoic bivalved arthropods have various ornaments on their carapaces, such as reticulate ornaments on the carapace of *Tuzoia* (Vannier et al., 2007), striated ornaments on the carapace of *Isoxys* (Fu et al., 2009), and pits on the carapace of *Iosuperstes* (Briggs et al., 2015). It is acknowledged that these ornaments are morphologically distinct from the crossbars of *Cambrowania ovata* (hence the establishment of a new taxon), but in principle, thickened ribs or ridges are not unimaginable as carapace ornaments. Indeed, some extant crustaceans can develop reticulate ornaments on their carapaces, with cylindrical ridges somewhat similar to the crossbars of *Cambrowania ovata*. *Polycope reticulata* Müller, 1894, for example, develops reticulate sculptures with cylindrical ridges forming primary polygonal ornamentation on its carapace (Vannier et al., 2007). Thus, we tentatively interpret

Cambrowania ovata as a bivalved arthropod with a thin and narrowly gaping carapace ornamented with thickened ribs or ridges (Fig. 4.6a).

4.7 Conclusion

The early Cambrian Hetang Formation contains abundant articulated sponge fossils, but it also yields other animal fossils. This paper describes one of these animal fossils, *Cambrowania ovata* new genus new species, mostly preserved as carbonaceous compressions in the middle Hetang Formation. As preserved, *Cambrowania ovata* is characterized by a subcircular structure with a network of crossbars and some with a V-shaped cleft. It is reconstructed as either a spherical vesicle or more likely a carapace with limited gaping, ornamented with thickened ribs or ridges on the vesicle or carapace. *Cambrowania ovata* is tentatively interpreted as an arthropod with a bivalved carapace. It adds to the taxonomic diversity of the Hetang biota that is otherwise dominated by benthic sponges.

4.8 Acknowledgments

This research was supported by National Science Foundation (EAR 1528553), NASA Exobiology and Evolutionary Biology (NNX15AL27G), National Natural Science Foundation of China (41502010), Geological Society of America, Paleontological Society, and Society for Sedimentary Geology. We thank J.P. Botting and D.E.G. Briggs for discussion, Jinlong Wang for field assistance.

4.9 Figures and figure captions

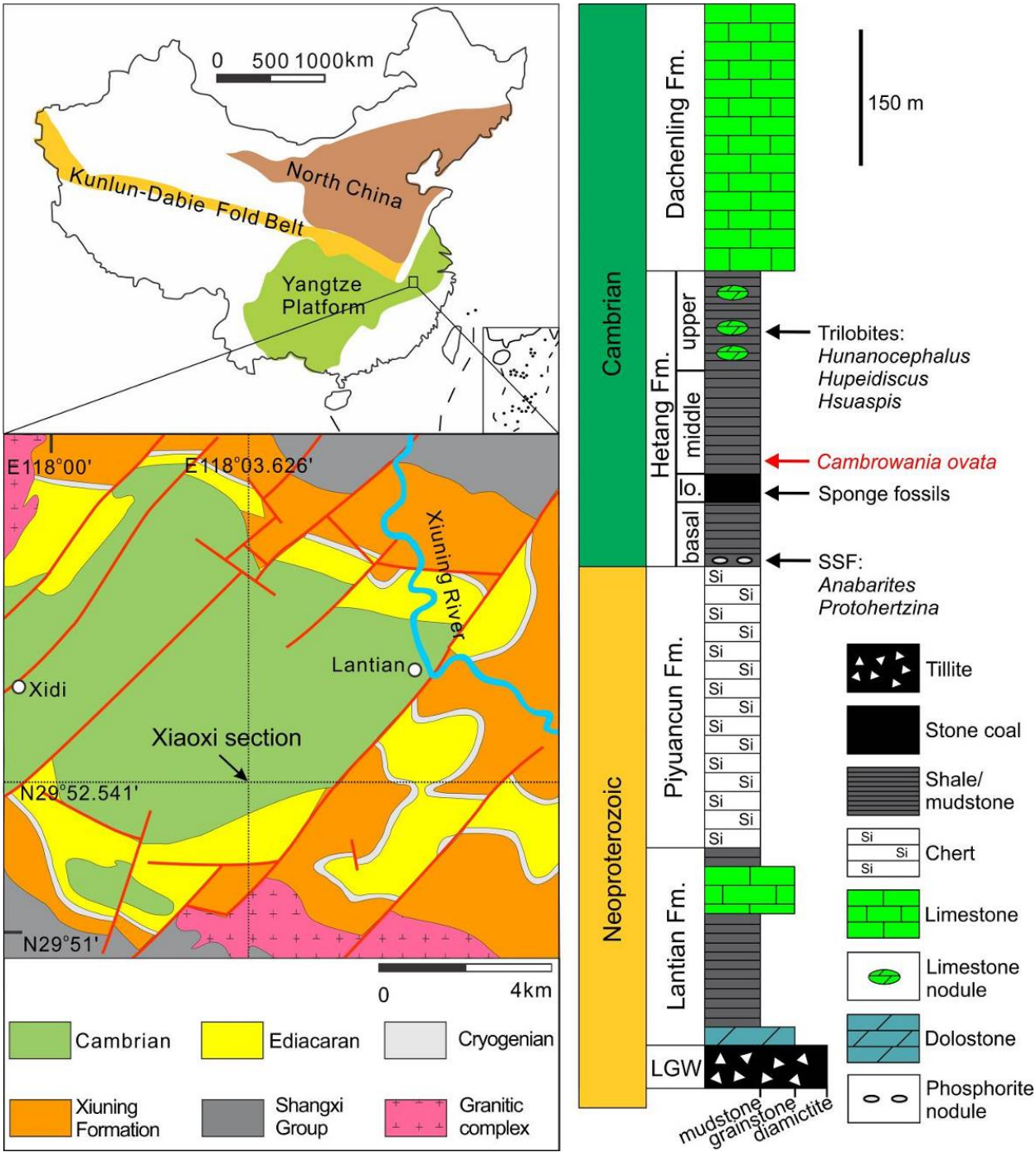

Fig. 4. 1. Geological map and stratigraphic column of the Neoproterozoic–early Cambrian succession in the Lantian area of southern Anhui Province in South China. lo. = lower, LGW = Leigongwu Formation, Fm. = Formation, SSF = small shelly fossils.

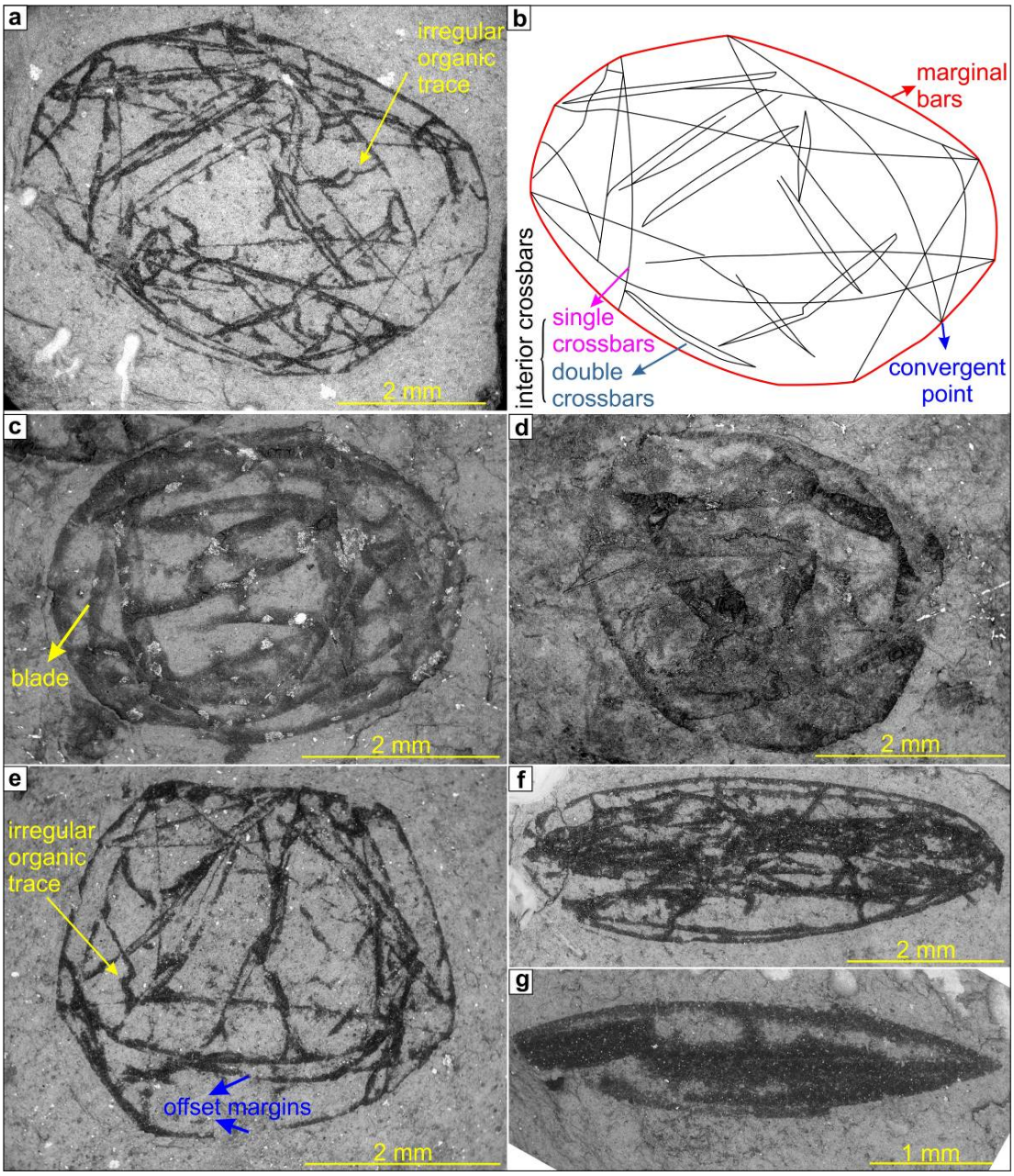

Fig. 4. 2. *Cambrowania ovata* new genus new species from the middle Hetang Formation. (a) Holotype, VPIGM-4729. (b) Schematic sketch of specimen in (a), highlighting the marginal crossbars, interior crossbars (e.g., single crossbars and double crossbars), and convergent point. (c−g) VPIGM-4730, VPIGM-4731, VPIGM-472, VPIGM-4733, and VPIGM-4734, respectively. All fossil images in this and other figures are backscattered electron scanning electron microscopy (BSE-SEM) photographs unless otherwise noted.

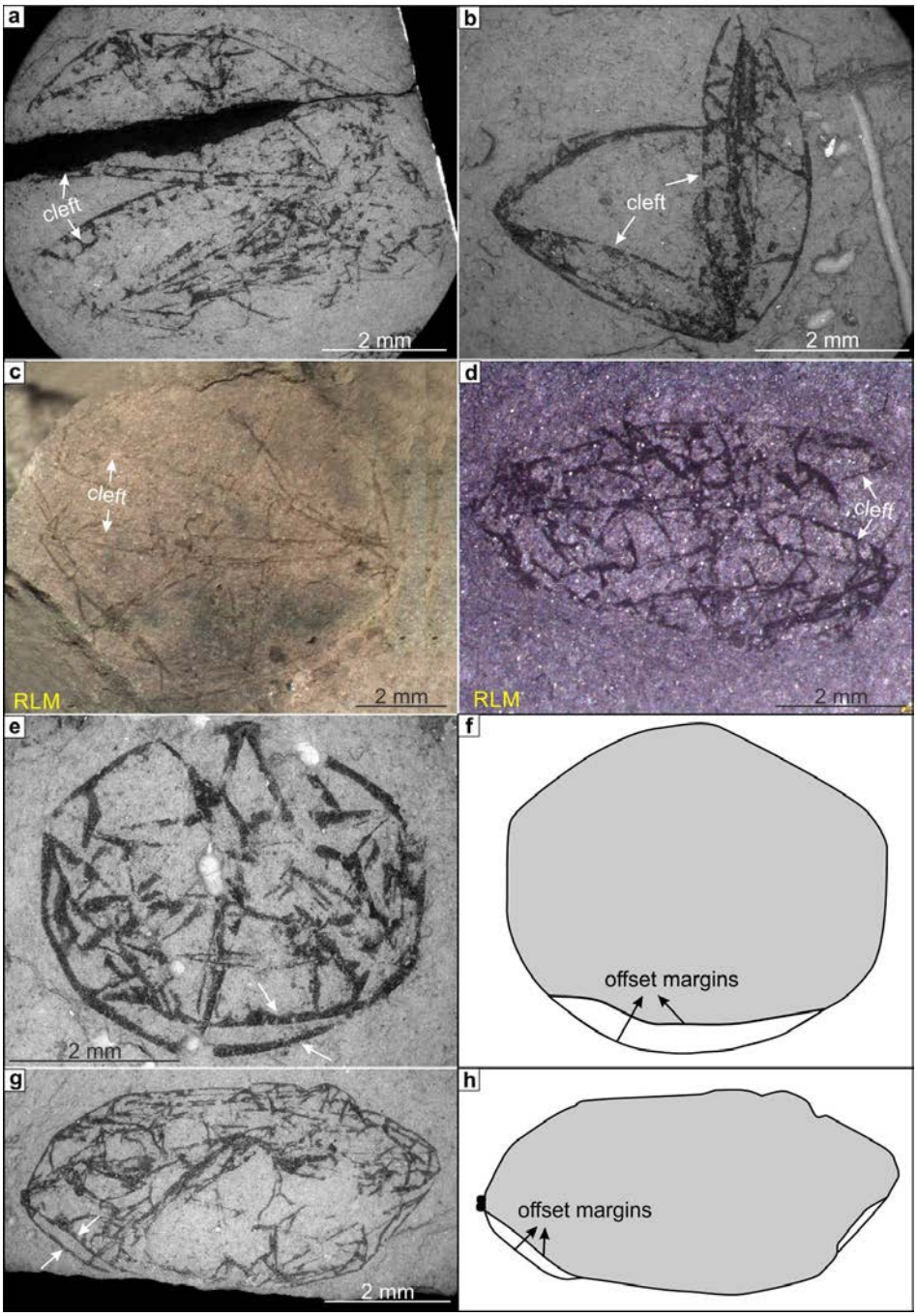

Fig. 4. 3. *Cambrowania ovata* with V-shaped clefts or offset margins that are interpreted as evidence for a gaping carapace. (a−e, g) VPIGM-4735, VPIGM-4736, VPIGM-4737, VPIGM-4738, VPIGM-4739, and VPIGM-4740, respectively. (f, h) Schematic sketches of specimens in (e) and (g), respectively. Arrows denote V-shaped clefts or offset margins. RLM = reflected light microscopy photograph.

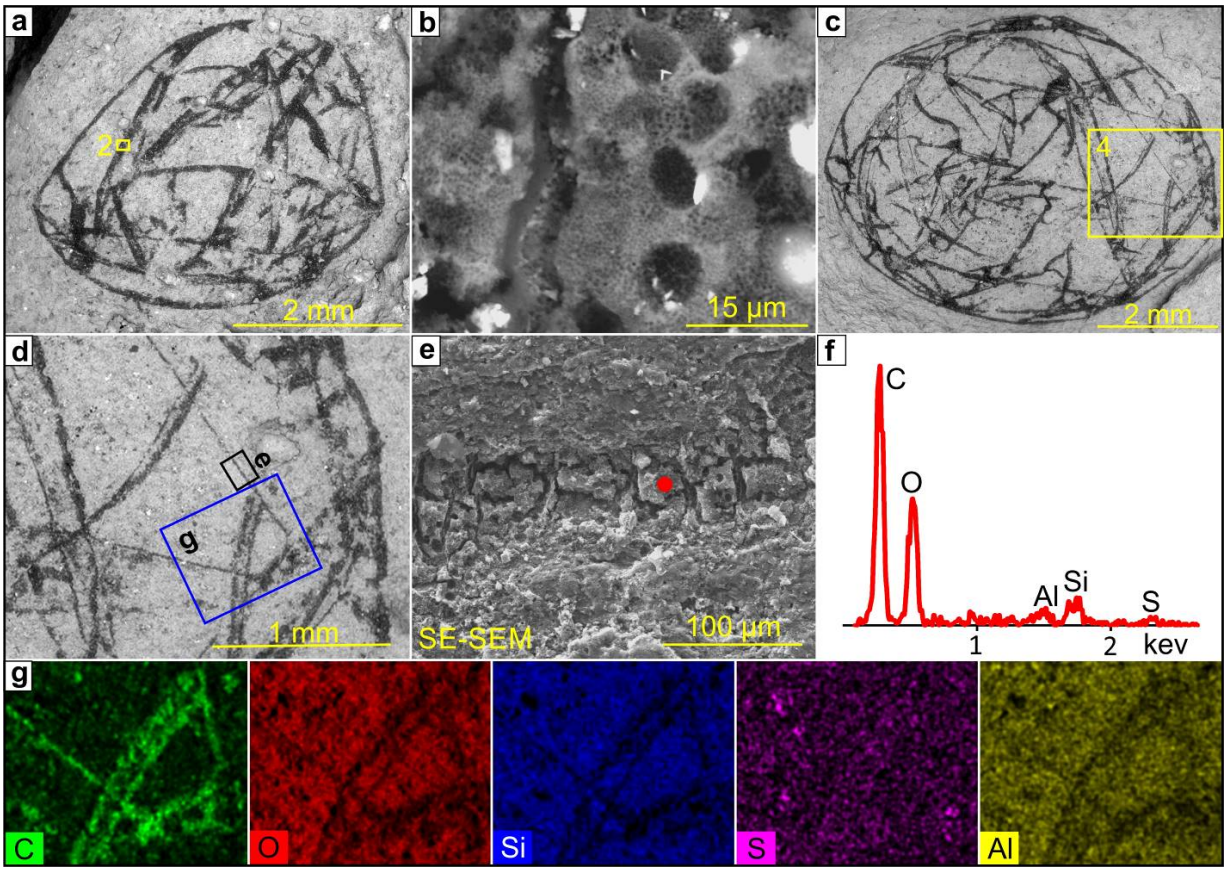

Fig. 4. 4. Taphonomy of *Cambrowania ovata*, with evidence for carbonaceous compression. (a) VPIGM-4741. (b) Close-up view of rectangle in (a), showing molds of pyrite framboids. (c) Paratype, VPIGM-4742. (d) Close-up view of rectangle in (c), showing crossbars of different widths. (e) Close-up view of black rectangle in (d). (f) Energy dispersive X-ray spectroscopy (EDS) point analysis at location marked by red circle in (e). (g) EDS elemental maps of blue rectangle in (d). Elements labeled in lower left. SE-SEM = secondary electron scanning electron microscopy photograph.

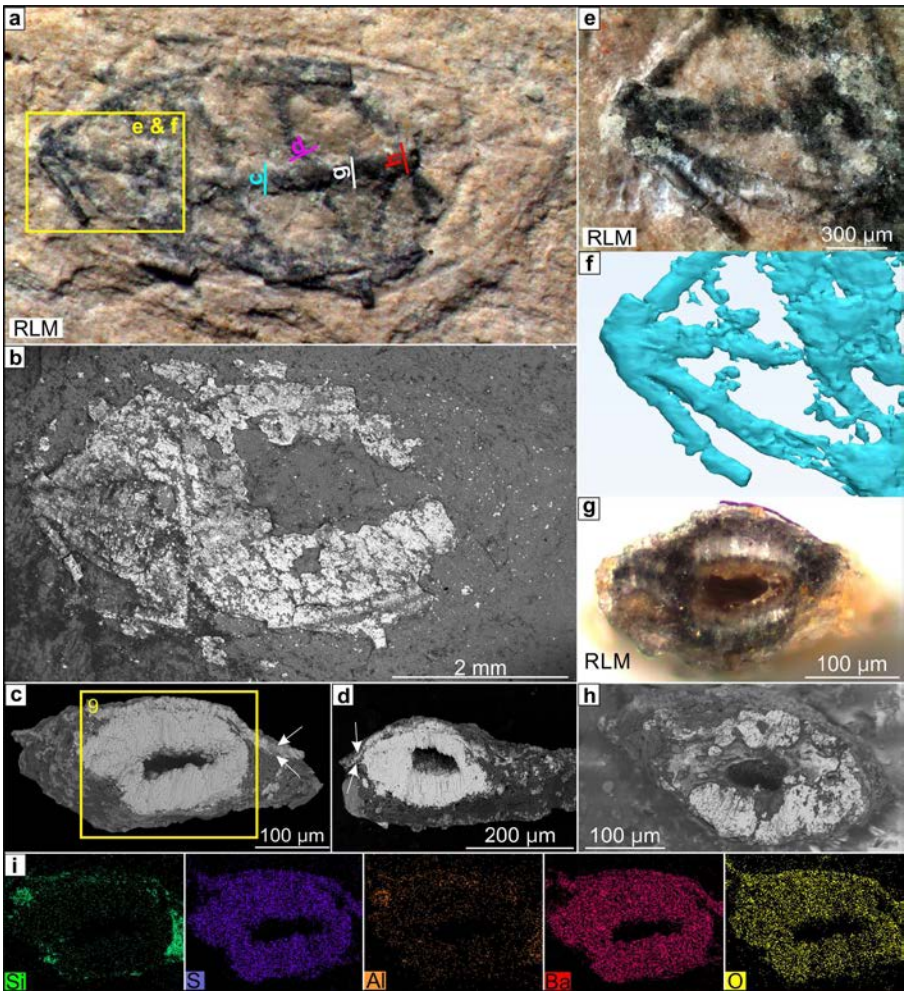

Fig. 4. 5. Taphonomy of *Cambrowania ovata*, with evidence for secondary baritization. (a–b) VPIGM-4743, RLM and BSE-SEM photographs, respectively, of the same baritized specimen. Bright area in (b) shows where barite is present. Note that the central part of the specimen [area marked as c, d, g, h in (a)] was removed after RLM (a) and before BSE-SEM (b), hence a window of no barite in (b). (c–d, g–h) Cross-sectional view of crossbars removed from marked and labeled positions in (a), showing baritized crossbars and a thin layer of barite [bracketed by white arrows in (c) and (d)] that covers the entire fossil. (e) Close-up view of yellow rectangle in (a); (f) Micro-CT reconstruction of radiating crossbars shown in (e). (i) EDS elemental maps of rectangle in (c), with elements marked in lower left. RLM = reflected light microscopy photograph.

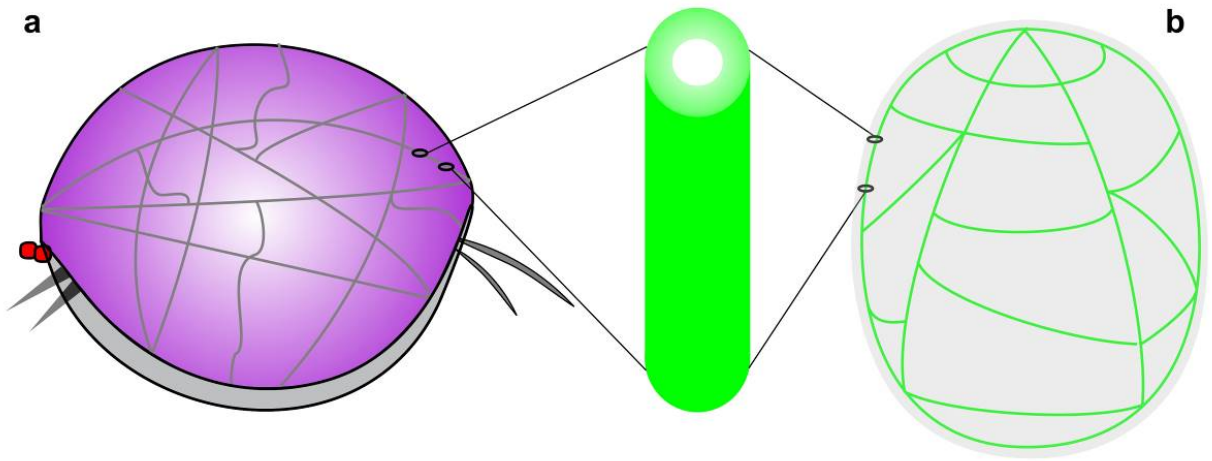

Fig. 4. 6. Morphological reconstructions of *Cambrowania ovata*. (a) Reconstructed as a bivalved arthropod with a narrowly gaping carapace ornamented with thickened ribs or ridges. Eyes and appendages are hypothetical. This is our favored reconstruction. (b) Reconstructed as a spheroidal organism with cylindrical and hollow crossbars as well as medial splits (not shown).

4.10 References

Botting, J.P., and Muir, L.A., 2013, Spicule structure and affinities of the Late Ordovician hexactinellid-like sponge *Cyathophycus loydelli* from the Llanfawr Mudstones Lagerstätte, Wales: Lethaia, v. 46, p. 454−469.

Botting, J.P., and Muir, L.A., 2018, Early sponge evolution: A review and phylogenetic framework: Palaeoworld, v. 27, p. 1−29.

Botting, J.P., Muir, L.A., Xiao, S., Li, X., and Lin, J.-P., 2012, Evidence for spicule homology in calcareous and siliceous sponges: biminerallic spicules in *Lenica* sp. from the Early Cambrian of South China: Lethaia, v. 45, p. 463–475.

Botting, J.P., Yuan, X., and Lin, J.P., 2014, Tetraradial symmetry in early poriferans: Chinese Science Bulletin, v. 59, p. 639−644.

Briggs, D.E.G., Liu, H.P., McKay, R.M., and Witzke, B.J., 2015, Bivalved arthropods from the Middle Ordovician Winneshiek Lagerstätte, Iowa, USA: Journal of Paleontology, v. 89, p. 991–1006.

Bureau of Geology and Mineral Resources of Anhui Province, 1987, Regional Geology of Anhui Province. Chinese Ministry of Geology and Mineral Resources, Geological Memoirs, series 1, number 5. Geological Publishing House, Beijing, 721 p.

Chen, Z., Hu, J., Zhou, C., Xiao, S., and Yuan, X., 2004, Sponge fossil assemblage from the Early Cambrian Hetang Formation in southern Anhui: Chinese Science Bulletin, v. 49, p. 1625−1628.

de Cook, S.C., and Bergquist, P.R., 2002, Family Irciniidae Gray, 1867. *In* Hooper, J.N.A., Van Soest, R.W.M., and Willenz, P., eds., Systema Porifera: A Guide to the Classification of Sponges. Springer US, Boston, MA, p. 1022–1027.

Dong, L., Song, W., Xiao, S., Yuan, X., Chen, Z., and Zhou, C., 2012, Micro- and macrofossils from the Piyuancun Formation and their implications for the Ediacaran-Cambrian boundary in southern Anhui: Journal of Stratigraphy, v. 36, p. 600−610.

Ehrlich, H., Rigby, J.K., Botting, J.P., Tsurkan, M.V., Werner, C., Schwille, P., Petrášek, Z., Pisera, A., Simon, P., Sivkov, V.N., Vyalikh, D.V., Molodtsov, S.L., Kurek, D., Kammer, M., Hunoldt, S., Born, R., Stawski, D., Steinhof, A., Bazhenov, V.V., and Geisler, T., 2013, Discovery of 505-million-year old chitin in the basal demosponge *Vauxia gracilenta*: Science Reports, v. 3, p. 3497.

Erwin, D.H., Laflamme, M., Tweedt, S.M., Sperling, E.A., Pisani, D., and Peterson, K.J., 2011, The Cambrian conundrum: Early divergence and later ecological success in the early history of animals: Science, v. 334, p. 1091–1097.

Erwin, D.H., and Valentine, J.W., 2013, The Cambrian Explosion: The Construction of Animal Biodiversity. Roberts and Company Publishers, Greenwood Village, 416 p.

Fu, D., and Zhang, X., 2011, A New Arthropod *Jugatacaris agilis* n. gen. n. sp. from the Early Cambrian Chengjiang Biota, South China: Journal of Paleontology, v. 85, p. 567–586.

Fu, D., Zhang, X., and Shu, D., 2009, Soft anatomy of the Early Cambrian arthropod *Isoxys curvirostratus* from the Chenjiang biota of South China with a discussion on the origination of great appendages: Acta Palaeontologica Polonica, v. 56, p. 843–852.

He, S., and Yu, G., 1992, The small shelly fossils from the Palaeocambrian Meishucunian Stage in western Zhejiang: Zhejiang Geology, v. 8, p. 1−7.

Hill, M.S., Hill, A.L., Lopez, J., Peterson, K.J., Pomponi, S., Diaz, M.C., Thacker, R.W., Adamska, M., Boury-Esnault, N., Cárdenas, P., Chaves-Fonnegra, A., Danka, E., De Laine, B.-O., Formica, D., Hajdu, E., Lobo-Hajdu, G., Klontz, S., Morrow, C.C., Patel, J.,

Picton, B., Pisani, D., Pohlmann, D., Redmond, N.E., Reed, J., Richey, S., Riesgo, A., Rubin, E., Russell, Z., Rützler, K., Sperling, E.A., di Stefano, M., Tarver, J.E., and Collins, A.G., 2013, Reconstruction of family-level phylogenetic relationships within Demospongiae (Porifera) using nuclear encoded housekeeping genes: PLoS ONE, v. 8, p. e50437.

Holmes, J.D., García-Bellido, D.C., and Lee, M.S.Y., 2018, Comparisons between Cambrian Lagerstätten assemblages using multivariate, parsimony and Bayesian methods: Gondwana Research, v. 55, p. 30–41.

Hou, X., and Bergström, J., 1997, Arthropods of the Lower Cambrian Chengjiang fauna, southwest China: Fossils and Strata, v. 45, p. 1−116.

Hu, J., Chen, Z., Xue, Y., and al., e., 2002, Sponge spicules in early Cambrian Hetang Formation, Xiuning, southern Anhui: Acta Micropalaeontologica Sinica, v. 19, p. 53−62.

Knoll, A.H., and Carroll, S.B., 1999, Early animal evolution: Emerging views from comparative biology and geology: Science, v. 284, p. 2129−2137.

Li, C., He, J., and Ye, H., 1990, Discovery of Early Cambrian trilobites in Guichi of Anhui Province: Journal of Stratigraphy, v. 14, p. 159−160.

Muller, E.B., 1894, Fauna und Flora des Golfes von Neapel und den angrenzenden Meers-Abschnitte: Herausgegeben von der Zoologischen Station zu Neapel, v. 21, p. 1−104.

Muscente, A.D., and Xiao, S., 2015, Resolving three-dimentional and subsurficial features of carbonaceous compressions and shelly fossils using backscattered electron scanning electron microscopy (BSE-SEM): PALAIOS, v. 30, p. 462−481.

Peng, S., Babcock, L.E., and Cooper, R.A., 2012, The Cambrian Period. *In* Gradstein, F.M., Ogg, J.G., Schmitz, M., and Ogg, G., eds., Geological Time Scale 2012. Oxford, Elsevier, p. 437−488.

Schröder, H.C., Wang, X., Tremel, W., Ushijima, H., and Müller, W.E.G., 2008, Biofabrication of biosilica-glass by living organisms: Nature Product Reports, v. 25, p. 455−474.

Steiner, M., Li, G., Qian, Y., and Zhu, M., 2004, Lower Cambrian Small Shelly Fossils of northern Sichuan and southern Shaanxi (China), and their biostratigraphic importance: Geobios, v. 37, p. 259−275.

Steiner, M., Li, G., Qian, Y., Zhu, M., and Erdtmann, B.-D., 2007, Neoproterozoic to early Cambrian small shelly fossil assemblages and a revised biostratigraphic correlation of the Yangtze Platform (China): Palaeogeography, Palaeoclimatology, Palaeoecology, v. 254, p. 67−99.

Tang, Q., Pang, K., Yuan, X., and Xiao, S., 2017, Electron microscopy reveals evidence for simple multicellularity in the Proterozoic fossil *Chuaria*: Geology, v. 45, p. 75–78.

Vannier, J., Caron, J.-B., Yuan, J., Briggs, D.E.G., Collins, D., Zhao, Y., and Zhu, M., 2007, *Tuzoia*: Morphology and lifestyle of a large bivalved arthropod of the Cambrian seas: Journal of Paleontology, v. 81, p. 445–471.

Wu, W., Yang, A.-H., Janussen, D., Steiner, M., and Zhu, M.-Y., 2005, Hexactinellid sponges from the early Cambrian black shale of south Anhui, China: Journal of Paleontology, v. 79, p. 1403−1051.

Xiang, L., Schoepfer, S.D., Shen, S., Cao, C., and Zhang, H., 2017, Evolution of oceanic molybdenum and uranium reservoir size around the Ediacaran–Cambrian transition:

Evidence from western Zhejiang, South China: Earth and Planetary Science Letters, v. 464, p. 84–94.

Xiao, S., Hu, J., Yuan, X., Parsley, R.L., and Cao, R., 2005, Articulated sponges from the Lower Cambrian Hetang Formation in southern Anhui, South China: their age and implications for the early evolution of sponges: Palaeogeography, Palaeoclimatology, Palaeoecology, v. 220, p. 89−117.

Xue, Y., and Yu, C., 1979, Lithological characteristics and sedimentary environments of the Lower Cambrian Hetang Formation in western Zhejiang and northern Jiangxi: Journal of Stratigraphy, v. 3, p. 283−293.

Yao, J., Xiao, S., Yin, L., Li, G., and Yuan, X., 2005, Basal Cambrian microfossils from the Yurtus and Xishanblaq formations (Tarim, north-west China): Systematic revision and biostratigraphic correlation of *Micrhystridium*-like acritarchs from China: Palaeontology, v. 48, p. 687−708.

Yuan, X., Xiao, S., Li, J., Yin, L., and Cao, R., 2001, Pyritized chuarids with excystment structures from the late Neoproterozoic Lantian Formation in Anhui, South China: Precambrian Research, v. 107, p. 253−263.

Yuan, X., Xiao, S., Parsley, R.L., Zhou, C., Chen, Z., and Hu, J., 2002, Towering sponges in an Early Cambrian Lagerstätte: Disparity between nonbilaterian and bilaterian epifaunal tierers at the Neoproterozoic-Cambrian transition: Geology, v. 30, p. 363−366.

Yuan, Y., Cai, C., Wang, T., Xiang, L., Jia, L., and Chen, Y., 2014, Redox condition during Ediacaran–Cambrian transition in the Lower Yangtze deep water basin, South China: constraints from iron speciation and $\delta^{13}C_{org}$ in the Diben section, Zhejiang: Chinese Science Bulletin, v. 59, p. 3638−3649.

Yue, Z., and He, S., 1989, Early Cambrian conodonts and bradoriids from Zhejiang: Acta Micropalaeontologica Sinica, v. 6, p. 289−300.

Yue, Z., and Zhao, J., 1993, Meishucunian (Early Cambrian) rod-like fossils from western Zhejiang: Acta Micropalaeontologica Sinica, v. 10, p. 89−97.

Zhou, C., and Jiang, S., 2009, Palaeoceanographic redox environments for the lower Cambrian Hetang Formation in South China: Evidence from pyrite framboids, redox sensitive trace elements, and sponge biota occurrence: Palaeogeography, Palaeoclimatology, Palaeoecology, v. 271, p. 279−286.

CHAPTER 5

Spiculogenesis and biomineralization in early sponge animals

Qing Tang[1], Bin Wan[2], Xunlai Yuan[2,3], A.D. Muscente[4], Shuhai Xiao[1]

[1]*Department of Geosciences and Global Change Center, Virginia Tech, Blacksburg, Virginia 24061, USA*

[2]*State Key Laboratory of Palaeobiology and Stratigraphy, Center for Excellence in Life and Paleoenvironment, Nanjing Institute of Geology and Palaeontology, Chinese Academy of Sciences, Nanjing 210008, China*

[3]*University of Chinese Academy of Sciences, Beijing 100049, China*

[4]*Department of Geological Sciences, University of Texas, Austin, Texas 78712, USA*

5.1 Abstract

Sponges are sister group to all other extant animals and most have siliceous/calcareous spicules. Molecular clocks and biomarkers indicate sponge classes diverged in the Cryogenian, but the oldest sponge spicules are Cambrian in age. It was hypothesized that sponges evolved biomineralization long after their origin or Precambrian spicules are not amenable to fossilization. However, paleontological data needed to test these hypotheses are limited. Here we report early Cambrian sponges that, like some other early Paleozoic sponges, had weakly biomineralized spicules with large axial filaments and disproportionately large amounts of organic material. Thus, early sponges had weakly biomineralized spicules. This conclusion implies that Precambrian sponges may have also had weakly biomineralized spicules or even lacked spicules, hence their poor fossil record. In either case, our work offers an explanation for apparently

conflicting molecular clock, biomarker, and fossil data, and also provides a new search image for Precambrian sponge fossils.

5.2 Introduction

Biomarker fossils suggest that sponge classes may have diverged no later than the Cryogenian Period (Gold et al., 2016). Molecular clock studies (Erwin et al., 2011), including recent ones with improved taxonomic sampling of sponges and independent of the aforementioned biomarkers as a calibration (Dohrmann and Wörheide, 2017; Schuster et al., 2018), point to a similar antiquity of sponge classes. It has been postulated that the last common ancestor of sponges (or that of silicean sponges) may have had biomineralized spicules (Sperling et al., 2010; Botting and Muir, 2018), yet the Precambrian fossil record of biomineralized sponge spicules is ambiguous at best (Antcliffe et al., 2014; Muscente et al., 2015). Previous attempts to resolve this 'missing glass problem' were focused on taphonomic phenomena that might limit the preservation of Precambrian sponge spicules (Sperling et al., 2010). However, emerging phylogenetic data do not require the presence of biomineralized spicules in the last common ancestor of demosponges (and that of siliceans) (Erpenbeck et al., 2012; Hill et al., 2013; Schuster et al., 2018), suggesting that spicules may have evolved independently among sponge classes (Erwin and Valentine, 2013) and necessitating a paleontological investigation of spiculogenesis in early sponges. Here we present a comprehensive analysis of early Cambrian (Stage 2) sponge fossils from the Hetang Formation in South China (Fig. 5.1). These fossils have siliceous spicules with large axial filaments and high organic content. When considered together with a compilation of Phanerozoic sponge spicule microstructures, the Hetang fossils indicate that early sponges may have had only weakly mineralized spicules with low fossilization

potential. Together with Ediacaran non-mineralized filaments that may be precursors of axial filaments, the Hetang fossils indicate that, although sponge classes may have diverged in the Cryogenian Period or earlier on the basis of biomarker fossils and molecular clocks, biomineralized spicules may have evolved later and independently among sponge clades.

5.3 Materials and Methods

A total of nineteen sponge body fossils, currently reposited in the Virginia Polytechnic Institute Geosciences Museum (VPIGM, Blacksburg, Virginia, USA), were recovered from the stone coal unit of the Hetang Formation at the Xiaoxi section (29°52.541'N, 118°03.626'E) in the Lantian area (Fig. 5.1). A full description of the geological and stratigraphic background and age constraints of the Hetang Formation in the Lantian area, Anhui Province, South China, was published in Xiao et al. (2005). The Hetang Formation conformably overlies siliceous rock of the terminal Ediacaran Piyuancun Formation and underlies the early Cambrian limestone of the Dachenling Formation (Fig. 5.1). Regionally, the Hetang Formation consists of four lithostratigraphic units, in ascending order, (1) a ~68 m thick mudstone unit rich in phosphorite at the base; (2) a ~30 m thick interval of stone coal (combustible organic-rich mudstone); (3) a ~110 m thick shale and mudstone unit; and (4) a ~110 m thick unit of shale with carbonate nodules (Zhou and Jiang, 2009). Abundant articulated sponge fossils have been recovered from the stone coal unit which was deposited in ferruginous basinal environment (Xiao et al., 2005; Yuan et al., 2014). Regional litho- and biostratigraphic correlation on the basis of small shelly fossils, acritarchs, and trilobites of the Hetang Formation indicate the fossiliferous stone coal unit of the Hetang Formation is early Cambrian Stage 2 (~529−521 Ma) in age (see Xiao et al., 2005 for more details).

Specimens were initially examined and photographed on an Olympus SZX7 stereomicrscope connected with an Infinity 1 camera. Well-preserved specimens were then coated with a ~20 nm conductive gold-palladium layer and analyzed using an array of electron microscopic instruments in the Virginia Tech Institute of Critical Technology and Applied Science Nanoscale Characterization and Fabrication Laboratory (VT-ICTAS-NCFL). Secondary electron and backscattered electron scanning electron microscopy (SE-SEM and BSE-SEM), energy dispersive X-ray spectroscopy (EDS), and EDS element mapping were conducted on a FEI Quanta 600FEG environmental SEM, with a pole piece backscattered electron (BSE) solid-state detector (SSD), a secondary electron (SE) Everhart-Thornley detector (ETD), and a Bruker EDX with a silicon drifted detector (Muscente and Xiao, 2015b). The operating voltage in BSE-SEM, SE-SEM, and EDS modes was 5−20 kV in high-vacuum condition. Selected Hetang spicules were subsequently FIB-sectioned on a FEI Helios 600 NanoLab focused ion bean electron microscope (FIB-EM) equipped with a gallium ion beam column for controlled excavation and a high-resolution Elstar Schottky FEG for SEM (Schiffbauer and Xiao, 2009).

The distance from the presumed osculum to the aboral end of sponge body fossils was measured and reported as sponge body fossil length; for specimens without a distinguishable osculum, the maximum dimension of sponge body fossils was measured. These measurements are reported in Table 5.1. The diameters of sponge spicules (d_s) and axial filaments (d_{af}) were measured on the tunnels (i.e., external molds of spicules) and inner core, respectively. When preserved, the maximum thickness of the outer lamella of the cylindrical structure was measured as an approximation of the thickness of the organic layer (t_{ol}). The relative thickness of the axial filament as a percentage of the spicule diameter was calculated as (d_{af} / d_s) * 100%, and the relative thickness of the organic cylindrical structure as ((2 * t_{ol} + d_{af}) / d_s) * 100% (i.e., organic

proportion). Measurements reported in Table 5.2 are based on published extant and fossil spicules. The relative proportion of the organic structures as a percentage of the spicule diameter was represented by a ratio: when the axial filaments and/or organic layer are preserved, this ratio was calculated as $(d_{af} + (t_{ol} + t_{os}) * 2) / d_s * 100\%$ (where t_{os} represents the thickness of the outer sheath); when only the axial canal is preserved, this ratio was calculated as $(d_{ac} + (t_{ol} + t_{os}) * 2) / d_s * 100\%$ (where d_{ac} represents the diameter of the axial canal).

5.4 Results

5.4.1 Description

The fossils are millimeters in size (Table 5.1) and are preserved as discoidal or elliptical carbonaceous compressions. In some specimens, the disc or ellipsoid has a neck-like extension and a central cavity (Fig. 5.2a−c), which are interpreted as possible osculum and spongocoel, respectively. They each contain abundant monaxons, diaxons, and triaxons that are randomly distributed in the organic remains. Most spicules are non-mineralized, demineralized, or partially demineralized (Muscente and Xiao, 2015a), resulting in cylindrical tunnels that represent the external molds (Fig. 5.2d, e). These tunnels are micrometers in diameter (Table 5.1) and typically contain a cylindrical structure that is located centrally (Fig. 5.2d) or eccentrically due to secondary dislocation (Fig. 5.2e). The cylindrical structures are straight or slightly sinuous (Fig. 5.2h, i). Some cylindrical structures are incompletely preserved or fragmented due to degradation (Fig. 5.2e−g). Although some cylindrical structures may be monaxons, others are clearly stauractines (Fig. 5.2f), pentactines (Fig. 5.2h), and hexactines with orthogonal rays (Fig. 5.2i, j). The overall shape of the cylindrical structures is consistent with the hosting spicules.

The cylindrical structures are variable in diameter, accounting for ~10% to nearly 100% of the spicule diameter (Fig. 5.3a and Table 5.1). Some of them consist of two parts, a solid inner core and a concentric outer lamella (Figs. 5.2g and 5.4a−c). The inner core also has hexactine-based rays, which may taper distally (Fig. 5.2h, i) or be aborted to form a short protuberance (arrows in Fig. 5.2h, j). The core is circular in cross section (Figs. 5.4a−c and 5.5a, b, and 5.6a), accounting for much of the cylindrical structure and sometimes being the only component of the cylindrical structure when the outer lamella is not developed or preserved (Figs. 5.2d, e, h−j and 5.4e, f). The core consists of elongate nanoparticles loosely compacted with nanoporous structures, which can be observed on both transverse sections (Fig. 5.4c, d) and on the surface (Fig.5.4e). The surface of the core is sometimes ornamented with ridges (Fig. 5.4e−g) and tubercles (Figs. 5.4h). The ridges are longitudinally or obliquely oriented, with an angle of 0–57° relative to the longitudinal axis of the core. They are broadly similar to the ridges on the core or middle layer of some spicules of the Cambrian sponge *Lenica* sp. from the Hetang Formation (see figures 1B and 2A in Botting et al., 2012).

The outer lamella of the cylindrical structure is a concentric layer enclosing the inner core (Figs. 5.4a−c and 5.5 and 5.6a). It is typically coarse and uneven on its outer surface (Figs. 5.4a and 5.5e), and consists of porous amorphous nanoparticles (Fig. 5.4d). The gaps between the inner core and outer lamella and between the outer lamella and the matrix are variable (Figs. 5.4a−c and 5.5e, i and 5.6a). In some specimens, the inner core is tightly enveloped by the outer lamella, and the entire spicule is fully occupied by the cylindrical structure without any appreciable gaps (Fig. 5.5a, b). A few longitudinally exposed specimens show variable preservation: segments of the cylindrical structure are well preserved with a very narrow gap

(Fig. 5.5c, d, f−h) whereas the rest of the cylindrical structure has wider gaps because the outer lamella is lost (Fig. 5.5e, f, i).

Energy dispersive X-ray spectroscopy (EDS) analyses indicate the cylindrical structures, including the inner core and outer lamella, are mainly composed of organic carbon (Fig. 5.6). EDS point analyses show that the inner core and outer lamella have higher C peaks but lower Al and Si peaks than the surrounding matrix (Fig. 5.6a, b). EDS elemental maps (Fig. 5.6b) confirm the organic nature of the cylindrical structures. In addition, a few cylindrical structures consist of an inner core rich in organic carbon and an outer siliceous layer rich in Si and O (Fig. 5.6c, d). This outer siliceous layer may represent the remnant of siliceous spicule that survived diagenetic demineralization (Muscente and Xiao, 2015a).

5.4.2 Interpretation

The presence of hexactine-based spicules, as well as putative oscula and spongocoels, indicates that the Hetang specimens are sponge body fossils. The concentric arrangement of the inner core and outer lamella (or outer siliceous layer), as well as the ridges on the best-preserved inner cores, suggests that these represent structural components of the spicules rather than secondary overgrowth. The inner core and outer lamella are interpreted as the axial filament and concentric organic layer, respectively. Their concentric arrangement is consistent with the appositional growth of extant sponge spicules (Wang et al., 2012). The carbonaceous composition, size, and central location of the inner core are also consistent with an axial filament interpretation. Finally, the nanoporous and nanoparticle structures in the inner core are similar to those in the axial filaments of extant silicean sponges (Croce et al., 2004), for example *Suberites domuncula* (see figure 2L in Wang et al., 2012).

The outer lamella in Hetang spicules is interpreted as a concentric organic layer surrounding the axial filament. An interpretive analog is found among extant silicean spicules that develop organic layers intercalated with silica lamellae (Wang et al., 2012). Similar to the axial filament, these organic layers are predominately composed of silicatein-collagen complex and play important roles in mediating the formation of biosilica lamellae (Wang et al., 2012). Concentric organic layers have also been reported from the Ordovician silicean *Cyathophycus loydelli*, whose spicules typically consist of intercalated silica lamellae and organic layers (Botting and Muir, 2013).

The concentric gaps present in some Hetang spicules are probably related to diagenetic demineralization (Muscente and Xiao, 2015a). The narrow gap between the inner core and outer lamella (Fig. 5.5d, f) may represent a mineralic layer that was subsequently demineralized, suggesting that these spicules may have originally had a mineral layer between the axial filament and outer organic layer (Fig. 5.7). This mineralic layer likely consisted of biosilica, given the preservation of a siliceous layer surrounding the axial filament of partially demineralized spicules (Fig. 5.6c) and the fact that extant hexactine-based spicules are always siliceous. The gap between the outer lamella and matrix may represent another demineralized layer of biosilica or shrinkage of the outer lamella.

5.5 Discussion

The Hetang axial filaments stand out in their cylindrical shape. The cross-sectional symmetry of axial filaments is an important character for class-level identification of extant sponges, with hexactinellids characterized by quadrangular axial filaments and demosponges by triangular or hexagonal ones (Uriz, 2006). However, axial filaments are rare in the fossil record.

Some spicule fossils preserve a cylindrical axial canal (Botting and Muir, 2013), but this is an unreliable morphological proxy for the axial filament (Botting et al., 2012; Botting and Muir, 2013), because it can be reshaped and enlarged by mineral dissolution (Bertolino et al., 2017). Organically preserved axial filaments, on the other hand, provide more reliable information about their biological precursors. Cylindrical axial filaments in the Hetang sponges and other Cambrian-Ordovician siliceans, such as *Cyathophycus loydelli* (figure 3I of Botting and Muir, 2013) and *Lenica* (figure 5 in Botting et al., 2012), indicate that cylindrical axial filaments existed in multiple early Paleozoic sponges.

The Hetang axial filaments are also distinguished from their modern counterparts by their relatively larger but variable diameters as well as by the relatively thick organic layers that surround them. Overall, the axial filaments are 0.7–9.4 μm in diameter (representing 6–94% of spicule diameter) and the surrounding organic layers are 0.2–3.8 μm in thickness (Table 5.1). For comparison, the corresponding measurements of modern silicean spicules are 0.1–2 μm (or 3–6% of spicule diameter) and 2−10 nm (e.g., in the hexactinellid *Euplectella* of Weaver et al., 2007), respectively. In addition, there is a positive relationship between spicule diameter and axial filament diameter (Fig. 5.3b), suggesting that the Hetang axial filaments may have grown in size as spicules matured. Thus, the Hetang axial filaments may have functioned as an important structural component of the spicules. A high organic content has also been observed in other Paleozoic sponge spicules. A compilation of fossil and extant sponge spicules shows that the organic proportion of the Hetang spicules and several other early Paleozoic sponge spicules is much higher than that of younger ones, despite that the latter values are generally maximum estimates based on axial canal measurements (Fig. 5.8 and Table 5.2). Indeed, some Cambrian sponges, such as *Vauxia* (Ehrlich et al., 2013), have organic fibrous skeletons, whereas post-

Ordovician and extant sponge spicules also show relatively low organic content, except ontogenetically immature ones (Maldonado and Riesgo, 2007).

As examples of early sponges, the Hetang sponges with organic-rich spicules may indicate that early sponges, including those in the Precambrian, may have had weakly mineralized spicules or entirely organic skeletons. We prefer the interpretation that they descended from Precambrian sponges that produced axial filaments, but not biomineralized spicules, because (a) one would expect that weakly biomineralized spicules would be preserved somewhere in Precambrian rocks; (b) fossils with weakly biomineralized skeletons (e.g., *Cloudina*) are common and widespread in the terminal Ediacaran Period (Wood et al., 2017); and (c) biomineralization evolved many times in animals, as certain organic templates were repeatedly and independently recruited for the process (Knoll, 2003).

Indeed, a number of Ediacaran fossils have been interpreted as non-mineralized sponge animals, although such interpretations have not been widely accepted (Antcliffe et al., 2014), partly because they do not have mineralized spicules. A non-exhaustive list includes *Coronacollina* [which has been reconstructed as a sponge animal with a conical body possessing either organic filaments or biomineralized spicules (Clites et al., 2012)], as well as *Cucullus*, *Liulingjitaenia*, and *Sinospongia* [which are tubular fossils apparently consisting of organic filaments (Xiao et al., 2002)). Notably, phosphatized microfossils in the Ediacaran Doushantuo Formation contain filamentous microstructures (up to several microns in diameter) that resemble monaxonal filaments and were originally interpreted as cylindrical siliceous sponge spicules (Li et al., 1998). Subsequent analyses have shown that they are organic in composition and quadrangular (rectangular) in cross section (Muscente et al., 2015), thus decisively falsifying the original interpretation that they represent cylindrical siliceous spicules (Li et al., 1998). However,

this does not mean that these filaments cannot be remnants of Ediacaran sponge animals; indeed, Muscente et al. (2015) explicitly stated that these filaments could be “axial filaments of early hexactinellids”. Given that it is very odd for microbial filaments or otherwise abiotically formed filaments to have a rectangular cross section, and that a typical axial filament of a modern hexactinellidis characterized by a square cross-section (or rectangular cross-section when obliquely cut) (Reiswig, 1971; Reitner and Mehl, 1996), it is possible that these organic filaments may represent Ediacaran precursors of axial filaments before hexactinellids acquired biomineralized spicules in the Cambrian. In any case, the lack of biomineralized spicules may be a real signal among Precambrian sponges. If so, it strips a convenient diagnostic feature that can be easily preserved in the rock record, making it more challenging to explore the Precambrian sponge fossil record because the lack of biomineralized spicules is not sufficient to exclude a grouping with total-group sponges.

The Hetang spicules can help us reconstruct the sequence of character acquisitions in early sponge evolution (Fig. 5.9). Because organic axial filaments are essential for the formation of silicean spicules (Wang et al., 2012), they are inferred to have predated siliceous spicules. It is thus plausible that the last common ancestor of poriferans and perhaps stem-group siliceans may have had only organic filaments, which originally served a function but were later independently recruited to facilitate spiculogenesis, ultimately evolving into the axial filaments in siliceans. The Hetang spicules may represent an evolutionary grade after this recruitment, possessing large axial filaments and thick organic layers, that latter of which may be homologous to the organic lamellae in siliceous spicules and organic sheaths in calcareous spicules. Considering their cylindrical axial filaments, the Hetang sponges likely represent poriferans that are phylogenetically outside crown-group hexactinellids and demosponges. Instead, they may be

stem-group hexactinellids, stem-group siliceans, or even stem-group poriferans, given that it is uncertain whether hexactines and siliceous spicules are synapomorphies of hexactinellids (Botting and Muir, 2018).

This interpretation supports the possibility that early spiculate sponges, including stem-group siliceans and stem-group poriferans, may have weakly biomineralized spicules or even entirely organic skeletons. This possibility may also be true for many stem-group hexactinellids, demosponges, and calcareans. The evolution of fully biomineralized spicules did not occur until the Cambrian, perhaps independently in several sponge classes and driven by top-down ecological forces such as predation (Marshall, 2006).

5.6 Conclusions

Biomarker fossils indicate that sponge classes may have diverged in the Cryogenian Period or earlier, and independent molecular clock analyses support this estimate. However, there have been no convincing biomineralized sponge spicules in the Precambrian. Early Cambrian sponge spicules described in this paper, as well as some other early Paleozoic sponge spicules, have a relatively large proportion of organic material, indicating that early sponges may have had weakly mineralized spicules or entirely organic skeletons. The biomarker, molecular clock, and spicular data suggest that, although sponge classes may have diverged in the Precambrian, they independently evolved biomineralized spicules at the Precambrian-Cambrian transition.

This hypothesis offers a new search image for Precambrian sponge body fossils. Perhaps early sponges are not preserved as biomineralized spicules, but as carbonaceous remains. In this regard, it is important not to exclude Ediacaran fossils as sponge animals simply because they

lack biomineralized spicules, and it is equally important to revisit Ediacaran sponge-like carbonaceous macrofossils that had been previously disregarded as sponges because of the lack of biomineralized spicules. In the end, molecular clocks, biomarker fossils, and spicular fossils must tell a coherent story about the early evolution of sponge animals.

5.7 Acknowledgments

The authors thank J. Wang, Dr. S.K. Pandey, and Y. Shao for field assistance, and Dr. H. Tang for assistance in light photography. This research was supported by National Science Foundation (EAR 1528553), NASA Exobiology and Evolutionary Biology Program (NNX15AL27G), National Natural Science Foundation of China (41130209), and Chinese Academy of Sciences (QYZDJ-SSW-DQC009).

5.8 Tables and table captions

Table 5.1. Measurements of the Hetang sponge body fossils and their constituent spicules. "0" in the column of "organic layer thickness" denotes that an organic layer is not preserved or developed. s.d. = standard deviation; d_s = spicule diameter; d_{af} = axial filament diameter; t_{ol} = organic layer thickness; r_{op} = organic proportion. Axial filament as a proportion of spicule diameter is represented by a ratio = (d_{af} / d_s) * 100%. The relative organic proportion of the spicules is represented by a ratio r_{op} = ((d_{af} + 2 * t_{ol}) / d_s) * 100% (plotted as blue symbols in Fig. 5.8).

Summary of measurements				
Category	**range**	**mean**	**number**	**s.d.**
body size in maximum dimension	2.5–12.4 mm	5.6	19	2.2
tunnel (=spicule) diameter	2-22 μm	7.3	141	3.5
cylindrical structure diameter	1-15 μm	4.9	141	2.6
inner core (= axial filament) diameter	0.7-9.4 μm	2.9	141	1.8
outer lamella (= organic layer) thickness	0.2-3.8 μm	1.2	113	0.7
nanoparticle length	0.2-0.8 μm	0.4	8	0.2
nanoparticle width	0.06-0.2 μm	0.13	8	0.04
ridge with	0.04-0.4 μm	0.2	18	0.1
ridge height	0.2-0.4 μm	0.3	9	0.06
ridge spacing	0.2-1.4 μm	0.4	23	0.3
tubercle width	0.6-4.0 μm	1.5	7	1.2
tubercle height	0.5-2.0 μm	0.9	6	0.6
number of spicules per body fossil	5,000 −20, 000			

sponge body fossils (n = 19)	**length or maximum dimension (mm)**
16-HT-T5-9-8-BSED-20KV-1	2.5
16-HT-T5-7-3-BSEM-20KV-1-2	3.3
16-HT-T6-1-SZX7-2-1.25X-4	3.8
16-HT-T5-9-3-ETD-20KV-1	3.8
16-HT-T5-9-3-SZX7-1.25X-2	3.9
16-HT-T4-27-2-3.2X-3	4.0
16-HT-T5-1-1-SZX7-1.25X-5	4.1

16-HT-T5-9-2-SZX7-1X-1	5.1
16-HT-T5-9-1-SZX7-1X-3	5.3
16-HT-T6-1-SZX7-4-0.8X-4	5.3
16-HT-T5-1-1-5KV-1	5.7
16-HT-T6-1-SZX7-1-0.8X-6	5.7
16-HT-T5-1-1-SZX7-1X-5	5.8
16-HT-T6-1-SZX7-3-0.8X-5	6.0
16-HT-T5-7-6-SZX7-1X-5	6.8
16-HT-T5-6-1-SZX7-1X-2	7.1
16-HT-T5-7-4-SZX7-0.8X-1	7.3
16-HT-T4-31-1	7.7
16-HT-T3-77-1-1X-3	12.4

spicules (n = 141)	**d_s (µm)**	**d_{af} (µm)**	**d_{af} / d_s (%)**	**t_{ol} (µm)**	**r_{op} (%)**
16-HT-T6-2-T5-1-20KV-2-1	14.5	1.9	13%	0.0	13%
16-HT-T6-2-T5-1-20KV-3-1	7.2	2.6	35%	1.6	79%
16-HT-T6-2-T5-1-20KV-4-1	7.3	2.0	28%	1.3	63%
16-HT-T6-2-T5-1-20KV-5-1	4.7	2.7	57%	0.3	72%
16-HT-T6-2-T5-1-20KV-6-1	6.4	1.8	28%	1.0	60%
16-HT-T6-2-T5-1-20KV-7-1	3.9	1.5	39%	0.3	57%
16-HT-T6-2-T5-1-20KV-8-1	15.0	6.2	41%	3.7	90%
16-HT-T6-2-T5-1-20KV-9-1	3.6	1.6	43%	0.6	78%
16-HT-T6-2-T5-3-20KV-2-1	10.4	5.0	48%	2.2	92%
16-HT-T6-2-T5-3-20KV-3-1	4.5	2.4	54%	0.8	90%
16-HT-T6-2-T5-3-20KV-4-2	5.4	2.7	50%	0.7	76%
16-HT-T6-2-T5-3-20KV-5-1	13.7	8.6	63%	2.2	96%
16-HT-T6-2-T5-3-20KV-6-1	6.1	4.3	70%	0.4	83%
16-HT-T6-2-T5-3-20KV-7-1	5.7	2.7	47%	0.0	47%
16-HT-T6-2-T5-3-20KV-9-1	8.8	2.3	26%	0.0	26%
16-HT-T6-2-T5-4-20KV-2-1	9.7	2.9	30%	0.0	30%
16-HT-T6-2-T5-4-20KV-4-1	8.9	5.7	63%	1.2	90%
16-HT-T6-2-T5-4-20KV-5-1	7.2	2.4	33%	1.5	74%
16-HT-T6-2-T5-4-20KV-7-1	5.7	2.0	35%	1.4	85%
16-HT-T6-2-T5-4-20KV-9-1	8.3	5.5	66%	1.2	95%
16-HT-T6-2-T5-5-20KV-2-1	6.9	3.2	47%	1.1	79%
16-HT-T6-2-T5-5-20KV-3-1	7.4	3.5	48%	1.2	80%
16-HT-T6-1V-T1-1-20KV-2-1	4.4	1.4	32%	0.5	55%
16-HT-T6-1V-T1-1-20KV-4-1	7.8	3.9	50%	1.4	87%

16-HT-T6-1V-T1-1-20KV-4-2	2.3	1.3	55%	0.0	55%
16-HT-T6-1V-T1-1-20KV-8-1	3.3	1.3	39%	0.5	68%
16-HT-T6-1V-T1-1-20KV-11-1	5.9	1.9	32%	1.8	92%
16-HT-T6-1V-T1-2-20KV-2-1	5.5	2.3	42%	1.2	84%
16-HT-T6-1V-T1-2-20KV-3-1	8.2	5.3	64%	0.7	81%
16-HT-T6-1V-T1-3-20KV-2-1	5.6	2.6	46%	0.8	73%
16-HT-T6-1V-T1-3-20KV-3-1	6.1	3.9	64%	1.0	97%
16-HT-T6-1V-T1-3-20KV-4-1	10.1	6.3	62%	1.0	82%
16-HT-T6-1V-T1-3-20KV-5-1	4.1	1.0	25%	0.8	64%
16-HT-T6-1V-T1-4-20KV-2-1	8.9	5.5	61%	1.1	85%
16-HT-T6-1V-T1-4-20KV-3-1	7.2	3.1	43%	2.0	99%
16-HT-T6-1V-T1-4-20KV-4-1	7.7	4.3	56%	1.0	81%
16-HT-T6-1V-T1-4-20KV-5-1	12.1	5.6	47%	1.3	68%
16-HT-T6-1V-T1-4-20KV-6-1	9.0	4.4	49%	0.9	69%
16-HT-T6-1V-T1-5-20KV-2-1	10.8	3.8	35%	1.7	67%
16-HT-T6-1V-T1-6-20KV-2-1	11.1	3.5	31%	0.9	48%
16-HT-T6-1V-T1-6-20KV-3-1	9.2	2.7	29%	0.8	46%
16-HT-T6-1V-T1-6-20KV-5-1	7.6	2.1	28%	1.7	74%
16-HT-T6-1V-T1-7-20KV-2-1	19.5	4.6	23%	2.4	48%
16-HT-T6-1V-T1-8-20KV-2-1	21.4	1.4	6%	3.7	41%
16-HT-T6-1V-T1-8-20KV-4-1	9.8	2.9	29%	1.9	69%
16-HT-T6-1V-T1-9-20KV-2-1	10.0	1.5	15%	1.6	46%
16-HT-T6-1V-T1-10-20KV-2-1	11.8	5.5	47%	2.5	89%
16-HT-T6-1V-T2-1-20KV-2-1	5.5	2.4	44%	0.8	74%
16-HT-T6-1V-T2-2-20KV-2-1	7.3	3.8	52%	1.4	91%
16-HT-T6-1V-T3-2-20KV-4-2	5.5	3.1	56%	1.1	97%
16-HT-T6-1V-T3-2-20KV-2-1	5.3	2.0	38%	0.5	55%
16-HT-T6-1V-T3-2-20KV-5-1	9.6	2.1	22%	0.4	30%
16-HT-T6-1V-T3-3-20KV-2-3	7.3	2.6	35%	1.1	67%
16-HT-T6-1V-T3-3-20KV-3-1	4.3	1.1	25%	1.2	79%
16-HT-T6-1V-T3-3-20KV-3-1-2	4.7	1.6	33%	1.0	76%
16-HT-T6-1V-T3-3-20KV-5-1	13.6	7.7	57%	1.7	82%
16-HT-T6-1V-T3-4-20KV-2-1	5.0	1.0	19%	1.2	68%
16-HT-T6-1V-T3-3-20KV-7-1	4.8	2.2	45%	0.9	83%
16-HT-T6-1V-T3-4-20KV-3-1	12.4	1.1	9%	0.0	9%
16-HT-T6-1V-T3-5-20KV-2-1	9.8	5.8	59%	0.7	74%
16-HT-T6-1V-T3-5-20KV-5-1	13.0	3.3	25%	1.9	54%
16-HT-T6-1V-T4-3-20KV-2-1	13.9	4.5	32%	3.8	87%
16-HT-T4-33-V-1-20KV-1-1	2.6	1.6	59%	0.0	59%

16-HT-T4-33-V-2-20KV-3-1	6.7	3.5	52%	1.2	88%
16-HT-T4-33-V-3-20KV-4-1	4.6	2.0	43%	0.8	76%
16-HT-T4-33-V-4-20KV-2-1	6.6	1.8	28%	0.9	55%
16-HT-T4-33-V-4-20KV-3-1	4.3	2.0	47%	0.9	88%
16-HT-T4-33-V-4-20KV-5-3	9.6	5.4	56%	0.0	56%
16-HT-T4-33-V-4-20KV-6-1	6.6	2.4	36%	0.9	62%
16-HT-T4-33-V-5-20KV-2-2	6.6	1.2	18%	2.2	84%
16-HT-T4-33-V-5-20KV-3-2	5.9	1.3	22%	1.3	67%
16-HT-T4-33-V-5-20KV-4-1	2.3	1.3	57%	0.2	72%
16-HT-T4-33-V-5-20KV-5-2	8.1	2.1	26%	1.6	65%
16-HT-T4-33-V-5-20KV-5-3	5.4	2.5	47%	0.8	77%
16-HT-T4-33-V-5-20KV-5-4	2.5	0.7	30%	0.5	67%
16-HT-T4-33-V-5-20KV-6-1	2.5	0.6	26%	0.5	65%
16-HT-T4-33-V-5-20KV-8-1	5.0	1.5	30%	1.2	79%
16-HT-T4-33-V-5-20KV-9-1	5.7	1.2	21%	1.6	77%
16-HT-T4-33-V-5-20KV-10-1	3.8	0.8	20%	1.5	99%
16-HT-T5-2-15-20KV-2-1	6.2	3.0	48%	0.6	68%
16-HT-T5-2-15-20KV-6-1	16.7	4.5	27%	1.6	46%
16-HT-T5-2-15-20KV-8-1	3.2	2.3	72%	0.0	72%
16-HT-T5-2-15-20KV-11-1	4.0	2.9	73%	0.0	73%
16-HT-T5-2-15-20KV-12-1	5.1	3.5	68%	0.0	68%
16-HT-T5-2-15-20KV-14-1	5.2	2.9	56%	0.0	56%
16-HT-T5-2-16-20KV-2-1	3.5	2.4	70%	0.0	70%
16-HT-T5-2-16-20KV-3-1	6.2	2.1	34%	1.0	65%
16-HT-T5-2-17-20KV-3-1	12.1	3.6	30%	1.1	47%
16-HT-T5-2-17-20KV-4-1	2.6	1.5	57%	0.0	57%
16-HT-T5-2-18-20KV-1-1	2.6	1.6	62%	0.0	62%
16-HT-T5-2-19-20KV-3-1	2.4	1.6	69%	0.0	69%
16-HT-T5-2-19-20KV-7-1	5.6	2.4	44%	0.0	44%
16-HT-T5-2-19-20KV-8-1	4.3	4.3	100%	0.0	100%
16-HT-T5-2-19-20KV-10-1	9.8	7.9	81%	0.0	81%
16-HT-T5-2-19-20KV-11-1	7.3	7.3	100%	0.0	100%
16-HT-T5-2-19-20KV-14-1	6.0	2.2	36%	1.0	70%
16-HT-T5-2-19-20KV-18-1	4.6	1.2	26%	0.0	26%
16-HT-T5-2-19-20KV-18-1-2	6.0	2.7	45%	0.0	45%
16-HT-T5-2-19-20KV-21-1	5.9	1.5	26%	1.3	69%
16-HT-T5-2-19-20KV-22-1	6.6	2.5	38%	1.5	83%
16-HT-T5-2-20-20KV-7-1	7.5	7.5	100%	0.0	100%
16-HT-T5-2-20-20KV-8-1	11.0	2.7	24%	1.4	50%

16-HT-T5-2-20-20KV-11-1	13.2	3.2	25%	2.6	64%
16-HT-T5-2-20-20KV-14-1	6.7	1.8	27%	1.2	62%
16-HT-T5-2-20-20KV-15-1	9.5	2.6	28%	1.4	58%
16-HT-T5-2-20-20KV-17-1	7.3	4.0	56%	0.4	67%
16-HT-T5-2-21-20KV-2-1	3.5	1.5	43%	1.0	100%
16-HT-T5-2-21-20KV-3-1	6.0	2.8	46%	1.7	46%
16-HT-T5-2-21-20KV-5-1	5.6	1.7	31%	0.0	31%
16-HT-T5-2-21-20KV-6-1	9.0	2.2	25%	0.0	25%
16-HT-T5-2-21-20KV-8-1	4.2	1.5	37%	0.6	64%
16-HT-T5-2-21-20KV-11-1	9.8	2.0	20%	0.0	20%
16-HT-T5-2-22-20KV-2-1	6.8	2.5	37%	0.4	49%
16-HT-T5-2-22-20KV-3-1	6.2	1.9	30%	1.5	77%
16-HT-T5-3-1-20KV-2-2	14.0	3.1	22%	2.0	51%
16-HT-T5-3-1-20KV-3-1	12.5	4.1	33%	1.5	57%
16-HT-T5-3-1-20KV-4-1	16.4	9.3	57%	2.8	92%
16-HT-T5-3-1-20KV-5-1	6.8	1.0	15%	0.0	15%
16-HT-T5-3-1-20KV-6-1	6.6	1.5	22%	0.0	22%
16-HT-T5-2-11-20KV-2-4	9.8	4.7	48%	1.8	84%
16-HT-T5-2-11-20KV-4-1	6.0	1.2	20%	1.5	70%
16-HT-T5-2-11-20KV-8-1	10.3	2.9	29%	1.6	60%
16-HT-T5-2-12-20KV-2-1	5.4	1.9	35%	1.1	75%
16-HT-T5-2-12-20KV-6-1	5.9	1.6	27%	0.6	48%
16-HT-T5-2-12-20KV-7-1	6.0	3.9	66%	0.0	66%
16-HT-T5-2-12-20KV-8-1	8.7	1.8	21%	1.8	62%
16-HT-T5-2-12-20KV-9-1	6.5	1.8	28%	0.5	43%
16-HT-T5-2-12-20KV-11-1	5.2	1.9	37%	0.0	37%
16-HT-T5-2-12-20KV-17-1	8.6	2.5	29%	1.3	58%
16-HT-T5-2-13-20KV-3-1	9.4	9.4	100%	0.0	100%
16-HT-T5-2-13-20KV-6-1	6.3	2.5	40%	0.9	70%
16-HT-T5-2-13-20KV-7-1	11.9	2.5	21%	0.0	21%
2016-HT-T4-33-1-10-2-3	3.0	1.1	36%	0.6	78%
2016-HT-T4-33-1-10-2-4	6.2	1.7	28%	0.7	52%
2016-HT-T4-33-1-10-5-2	4.1	1.7	42%	1.2	98%
2016-HT-T4-33-1-10-7-2	2.0	1.2	63%	0.3	89%
2016-HT-T4-33-1-10-11-1	3.3	1.1	33%	0.4	59%
2016-HT-T4-33-1-10-17-1	4.2	1.2	28%	0.8	66%
2016-HT-T4-33-1-10-20-2	6.9	2.0	29%	1.0	56%
2016-HT-T4-33-1-10-22-1	3.2	1.2	37%	0.4	62%
2016-HT-T4-33-1-10-28-1	8.5	3.7	43%	1.5	78%

Table 5.2. Measurements of fossil and extant spicules of representative poriferan groups/classes. d_s = spicule diameter; d_{af} = axial filament diameter; t_{ol} = organic layer thickness; t_{os} = outer sheath thickness; d_{ac} = axial canal diameter; r_{op} = organic proportion. "×" denotes that the structure is not developed or preserved; "√" denotes that the structure is present but unable to measure due to poor preservation or illustrations. The relative organic proportion of sponge spicules is quantified as a ratio: when the axial filaments are preserved, this ratio was calculated as $r_{op} = (d_{af} + (t_{ol} + t_{os}) * 2) / d_s * 100\%$ (plotted as red symbols in Fig. 5.8); when only the axial canal is preserved, this ratio was calculated as $r_{op} = (d_{ac} + (t_{ol} + t_{os}) * 2)/d_s * 100\%$ (plotted as gray symbols in Fig. 5.8). Because axial canals can be enlarged by mineral dissolution (Bertolino et al., 2017), the latter method and the gray symbols in Fig. 5.8 represent maximum estimates of organic proportion in sponge spicules. The absolute age of fossil occurrences is an average between the maximum and minimum age constraints unless otherwise available in the referred publications. For example, the Hetang Formation is regarded as Cambrian Stage 2 (~529−521 Ma) and the Hetang sponge fossils are estimated to be ~525 Ma.

Age	**Formation/Location**	**Group/Taxon**	**d_s (µm)**	**d_{af} (µm)**	**t_{ol} (µm)**	**t_{os} (µm)**	**d_{ac} (µm)**	**r_{op}**	**Reference**	
Cambrian, Fortunian, ~539 Ma	Yanjiahe Fm.	Silicea, discrete spicules	61.8	×	×	×	5.7	9%	fig. 3G	(Chang et al., 2017)
			6.8	×	×	×	1.7	25%	fig. 3K1	
			69.9	×	×	×	7.3	10%	fig. 3N	
Cambrian, Fortunian ~535 Ma	Soltanieh Fm.	Hexactinellida, discrete spicules	35.3	×	×	×	10.7	30%	fig. 12D	(Antcliffe et al., 2014)
			45.5	×	×	×	10.5	23%	fig. 12 E	

Cambrian, Stage 2, ~525 Ma	Hetang Fm.	Silicea, *Lenica* sp.	574.2	40.5	×	28.2	×	17%	fig. 5	(Botting et al., 2012)
			508	119.9	×	√	×	>24%	fig. 1E	
			358.8	×	×	23.2	×	13%	fig. 1B	
Cambrian, Stage 3, ~518 Ma	Buen Fm.	Silicea, *Lenica* cf. *unicca*	1,800	×	×	200	×	22%	fig. 5A	(Botting and Peel, 2016)
			1,900	×	×	200	×	21%		
			2,000	×	×	200	×	20%		
			700	×	×	100	×	29%	fig. 5B	
			600	×	×	100	×	33%	fig. 5D	
Early Cambrian, ~515 Ma	Forteau Fm.	Hexactinellida, Organic-walled spicules	18.1	×	×	√	×	√	fig. 1o	(Harvey, 2010)
			20	×	×	√	×	√	fig. 1o	
			16.7	×	×	√	×	√	fig. 1o	
			16.7	×	×	√	×	√	fig. 1f	
Cambrian, ~508 Ma	Burgess Shale Fm.	Heteractinida, *Eiffelia globosa*	353.2	×	×	7.1	×	4%	fig. 2B–C	(Botting and Butterfield, 2005)
Middle Cambrian, ~508 Ma	Burgess Shale Fm.	Takakkawiidae, *Takakkawia lineata*	11.8	×	×	√	×	√	fig. 1E	(Botting, 2012)
			17.1	×	×	√	×	√	fig. 1E	
			22.3	×	×	√	×	√	fig. 1E	
Middle Cambrian, ~508 Ma	Burgess Shale Fm.	Protomonaxonida, *Pirania Muricata*	200.5	22.1	×	√	×	>11%	fig. 4.5	(Botting and Muir, 2014)
			191.1	16.8	×	√	×	>9%	fig. 4.5	
			176.8	14.7	×	√	×	>8%	fig. 4.6	
			195.1	16.3	×	√	×	>8%	fig. 4.6	
			200.1	19.2	×	√	×	>10%	fig. 4.6	
Middle	Beetle Creek Fm.	Silicea,	58.1	×	×	×	7.2	12%	pl. 5.3	(Mehl, 1998)

Cambrian, ~508 Ma		discrete spicules	45.3	×	×	×	8.9	20%	pl. 5.4	
			31.6	×	×	×	6.9	22%	pl. 5.5	
			36.6	×	×	×	9.1	25%		
			37.6	×	×	×	2.7	7%	pl. 5.8	
			34	×	×	×	5	15%	pl. 5.9	
			35.2	×	×	×	5	14%	pl. 5.10	
Ordovician, Early Tremadocian, ~482 Ma	Dol-cyn-Afon Fm.	Protomonaxonida, *Choia*	210	×	×	√	×	√	fig. 5d	(Botting et al., 2015)
			152	×	×	√	×	√	fig. 5e	
Ordovician, Sandbian, ~456 Ma	Llanfawr Mudstones Fm.	Silicea, *Cyathophycus loydelli*	17.9	3.1	×	×	×	17%	fig. 3D	(Botting and Muir, 2013)
			11.8	5.2	×	×	×	44%	fig. 3I	
			10.4	2.8	×	×	×	26%	fig. 3E	
			42.8	2.2	11.7	×	×	60%	fig. 4A	
			28.4	3	2.1	×	×	25%	fig. 4G	
			22.5	1.7	4.7	×	×	50%	fig. 6A	
			22.2	2.6	1.9	×	×	29%	fig. 6B	
			48.8	6.9	3.4	×	×	28%	fig. 6C	
Ordovcian, Floian−Darriwilian, ~468 Ma	Valhallfonna Fm. & Cow Head and Table Head groups & Vinini Fm.	Silicea, discrete spicules	22.2	×	×	×	6.4	29%	fig. 3A	(Carrera and Maletz, 2014)
			30.1	×	×	×	5.7	19%	fig. 3C	
			43.2	×	×	×	14.5	34%	fig. 4F	
			82.3	×	×	×	15.4	19%	fig. 4M	
			75.2	×	×	×	24	32%	fig. 5B	
			72.3	×	×	×	13.9	19%	fig. 6B	
			64.3	×	×	×	7.5	12%	fig. 6C	

			42.3	×	×	×	6.1	14%	fig. 6D	
			18.8	×	×	×	3.9	21%	fig. 6K	
			44.3	×	×	×	8	18%	fig. 8J	
Ordovician, Darriwilian, ~463 Ma	San Juan Fm.	Demospongiae, discrete spicules	190.9	×	×	×	20.6	11%	fig. 4.1	(Carrera, 2007)
			240.9	×	×	×	17.6	7%		
			257	×	×	×	33.7	13%		
			224.3	×	×	×	27.1	12%	fig. 4.2	
			292.6	×	×	×	28	10%		
			273.2	×	×	×	20	7%	fig. 4.3	
			140.9	×	×	×	20.3	14%	fig. 4.4	
			156	×	×	×	19.3	12%		
			168.4	×	×	×	33.4	20%		
			79.6	×	×	×	20.8	26%	fig. 4.5	
			157.8	×	×	×	18.4	12%	fig. 4.6	
			220.1	×	×	×	9.5	4%		
Ordovician, Darriwilian, ~463 Ma	Table Cove Fm.	Silicea, discrete spicules	97.1	×	×	×	15.5	16%	fig. 4.12	(Zhang and Pratt, 2000)
			48.7	×	×	×	4.1	8%	fig. 4. 13	
			141.7	×	×	×	20.7	15%	fig. 4.14	
			73.2	×	×	×	12.1	17%	fig. 4.15	
			155.9	×	×	×	37.3	24%	fig. 5.5	
			72.6	×	×	×	6.2	9%	fig. 5.5	
			82.9	×	×	×	10.2	12%	fig. 5.11	
Ordovician,	Builth Volcanic	Protomonaxonid	64.6	×	×	√	×	√	fig. 3D	(Muir and

Darriwilian, ~462 Ma	Gr.	a, Unnamed taxon	65.1	×	×	√	×	√	fig. 3D	Botting, 2015)
Late Ordovician, ~451 Ma	Malongulli Fm.	Hexactinellida, discrete spicules	217.4	×	×	×	24.8	11%	fig. 5.16	(Webby and Trotter, 1993)
Ordovician, Hirnantian, ~444 Ma	Wenchang Fm.	Silicea, *Cyathophycus* sp. & hexactinellid-like sponge	69	×	×	√	×	√	fig. 2E	(Botting et al., 2017)
			61	×	×	√	×	√	fig. 2E	
			93	×	×	√	×	√	fig. 2H	
			106	×	×	√	×	√	fig. 2H	
Silurian, Telychian, ~436 Ma	pebble accumulations	Silicea, Lyssacinosida? Indet. A	142.2	×	×	×	74.1	52%	pl. 21.4	(Rhebergen and Botting, 2014)
			116.3	×	×	×	28.6	25%		
			120	×	×	×	27.1	23%		
			145.9	×	×	×	37.2	25%		
			264.5	×	×	×	26.6	10%	pl. 21.7	
			123.7	×	×	×	23.2	19%		
Devonian, Late Frasnian, ~378 Ma	Domanik Fm.	Hexactinellida, discrete spicules	14.9	×	×	×	2.8	19%	pl. 132.7	(Afanasieva, 2000)
			89.1	×	×	×	19.4	22%	pl. 133.5	
			18.8	×	×	×	5.2	28%	pl. 134.10	
			26.7	×	×	×	1.8	7%	pl. 134.11	
			13.3	×	×	×	2.8	21%	pl. 135.6	

			21	×	×	×	1.9	9%	pl. 135.8	
			9.4	×	×	×	1.8	19%	pl. 135.10	
Devonian, Frasnian−Famennian, ~371 Ma	Late Frasnian beds	Silicea, discrete spicules	137	×	×	×	52.3	38%	fig. 10F	(Vishnevskaya et al., 2002)
Carboniferous, Bashkirian, ~319 Ma	San Emiliano Fm.	Hexactinellida, discrete spicules	156	×	×	×	31	20%	fig. 11.3	(García-Bellido and Rigby, 2004)
			114	×	×	×	25	22%		
			114	×	×	×	31	27%		
			139	×	×	×	37	27%	fig. 11.4	
			88	×	×	×	19	22%		
			101	×	×	×	19	19%		
Late Carboniferous, ~311 Ma	Itarare Fm.	Hexactinellida, discrete spicules	10.2	×	×	×	3.1	30%	pl. 176. 1	(Kling and Reif, 1969)
			9.9	×	×	×	2.8	28%		
			17.8	×	×	×	2.9	16%	pl. 176. 5	
			17.4	×	×	×	3.1	18%		
Late Carboniferous, ~311 Ma	Ottweiler Subgroup	Demospongiae, discrete spicules	13.1	×	×	×	2.1	16%	fig. 5A	(Schindler et al., 2008)
			12.6	×	×	×	2.3	18%		
			8.2	×	×	×	2.5	30%		
			10.9	×	×	×	2.7	25%		
			20.1	×	×	×	2.5	12%	fig. 5B	
			10.1	×	×	×	2.2	22%		

			12.4	×	×	×	1.9	15%		
			8.2	×	×	×	1.9	23%	fig. 5C	
			17.9	×	×	×	2.5	14%	fig. 5D	
			15	×	×	×	2.3	15%		
			11.1	×	×	×	2.3	21%	fig. 5E	
			5.1	×	×	×	1.2	24%		
			10.8	×	×	×	2.6	24%		
Permian, Asselian−Sakmarian, 295 Ma	Rio do Sul Fm.	Hexacinellida, *Microhemidiscia greinerti*	38.4	×	×	3.3	×	>17%	fig. 5	(Mouro et al., 2014)
			24.7	×	×	2.6	×	>21%		
			31.9	×	×	2.7	×	>17%		
			40.4	×	×	2.2	×	>11%		
			24.2	×	×	2.3	×	>19%		
Permian, Leonardian, ~276 Ma	Bone Spring Fm.	Hexactinellida, *Docoderma papillosum*	1255.6	×	×	×	213.1	17%	pl. 41.3	(Finks, 1969)
			901.5	×	×	×	386.6	43%		
Permian, Wordian, ~267 Ma	Word Fm.	Hexactinellida, *Carphites plectus*	181.8	×	×	×	36.5	20%	pl. 43.6	
			317.7	×	×	×	48.9	15%		
		Hexactinellida, *Acanthocoryna stauroma*	601	×	×	×	131.3	22%	pl. 44.5	
			777	×	×	×	198.5	26%		
Permian, Guadalupian, ~266 Ma	Bancheng Fm.	Silicea, discrete spicules	45.7	×	×	×	2.4	5%	fig. 6.7	(Tsuyoshi et al., 2013)
			34	×	×	×	4.9	14%	fig. 6.17	

Early Triassic, ~250 Ma	Thaynes Fm.	Hexactinellida, *Cypellospongia fimbriartis*	131.8	×	×	×	18.4	14%	fig. 5.7	(Rigby and Gosney, 1983)
			55.3	×	×	×	8.1	15%		
Middle Triassic, Mschelkalk, ~235 Ma	Karchowice Beds	Hexactinellida, discrete spicules	430.2	×	×	×	37.6	9%	pl. 3.7	(Pisera and Bodzioch, 1991)
			185.2	×	×	×	36.7	20%	pl. 3.8	
			166.6	×	×	×	31.6	19%	pl. 3.9	
Triassic, Carnian, ~232 Ma	Sina volcanic Fm.	Silicea, discrete spicules	93.8	×	×	×	3.6	4%	pl. 4.2	(Donofrio, 1991)
Jurassic, Hettangian, ~200 Ma	Schnoll Fm.	Hexactinellida, unnamed specimen	92.4	×	×	×	19.5	21%	fig. 10E	(Delecat and Reitner, 2005)
			67.8	×	×	×	14.2	21%		
			56.4	×	×	×	11.5	20%		
Jurassic, Hettangian, ~200 Ma	Sunrise Fm.	Silicea, discrete spicules	87.9	×	×	×	18.8	21%	fig. 4D	(Ritterbush et al., 2014)
			127.4	×	×	×	26	20%	fig. 4E	
			49.5	×	×	×	5.8	12%	fig. 6C	
	Aramachay Fm.		54.6	×	×	×	12.3	23%	fig. 9F	
			98.8	×	×	×	18.6	19%	fig. 10C	
			116.2	×	×	×	15.6	13%		
			108	×	×	×	19.3	18%		
			67.7	×	×	×	8.2	12%		
Jurassic, Hettangian−S	Aramachay Fm.	Silicea, discrete spicules	81.1	×	×	×	11.6	14%	fig. 6A	(Ritterbush et al., 2015)
			47.4	×	×	×	11	23%		

inemurian, ~196 Ma			55.2	×	×	×	6.1	11%	fig. 6B	
			71	×	×	×	9.2	13%		
			71.9	×	×	×	10.1	14%		
			112.8	×	×	×	17.6	16%	fig. 6F	
Jurassic, Toarcian, ~179 Ma	Zegri Fm.	Hexactinellida, discrete spicules	28.1	×	×	×	2.7	10%	fig. 6A	(Reolid, 2014)
Late Jurassic, ~155 Ma	Oxfordian to Kimmeridgian sequences in Swabian Alb	Silicea, discrete spicules	109.8	×	×	×	17.3	16%	pl. 48.2	(Pisera, 1997)
			121	×	×	×	15.3	13%	pl. 48.3	
			64.2	×	×	×	14.3	22%	pl. 50.3	
			44.7	×	×	×	5.8	13%	pl. 50.6	
			90.3	×	×	×	10.6	12%	pl. 50.8	
			43.3	×	×	×	7.8	18%	pl. 50.11	
			188.9	×	×	×	37.4	20%	pl. 51.25	
			211.2	×	×	×	56.6	27%	pl. 51.26	
			41.1	×	×	×	5.2	13%	pl. 53.13	
			31.5	×	×	×	6	19%	pl. 53.14	
			100	×	×	×	13.7	14%	pl. 54.7	
			99.8	×	×	×	20.3	20%	pl. 54.8	
			109.4	×	×	×	23.3	21%		
			34.1	×	×	×	4.3	13%	pl. 54.9	
			62.3	×	×	×	6.9	11%	pl. 54.10	
			72.5	×	×	×	6.5	9%	pl. 54.11	
			102.4	×	×	×	10	10%	pl. 54.13	

			158.8	×	×	×	11.8	7%	pl. 54.14	
			139.1		×	×	12.1	9%	pl. 54.16	
Cretaceous, Cenomanian − Lower Turonian, 97 Ma	Wellheim Fm.	Hexactinellida, *Laocoetis* cf. *tenuis*	129	×	×	×	24.6	19%	fig. 8C	(Schneider et al., 2013)
		Hexactinellida, *Brachiolites fenestratus*	79.2	×	×	×	8.5	11%	fig. 8F	
			73.1	×	×	×	18	25%		
			79.7	×	×	×	17	21%		
			127.1	×	×	×	21.2	17%		
			122.5	×	×	×	26.1	21%		
Cretaceous, early Campanian, 80 Ma	Miechow Synclinorium	Demospongiae. *Homalodoriana tuberosa*	72.5	×	×	×	11.3	16%	fig. 17E	(Świerczewska-Gładysz, 2016)
			189.6	×	×	×	14.5	8%		
			67	×	×	×	8	12%		
			88.5	×	×	×	11.2	13%		
			127.9	×	×	×	13.1	10%		
			80.9	×	×	×	10.8	13%		
		Demospongiae, *Homalodoriana ficus*	88.3	×	×	×	9.7	11%	fig. 19E	
			85.4	×	×	×	7.7	9%		
			35.4	×	×	×	6.5	18%	fig. 19F	
			65.8	×	×	×	7.6	12%		
			39.6	×	×	×	3.7	9%		
Cretaceous,	Rzezusnia section	Hexactinellida,	126.2	×	×	×	47.3	37%	fig. 2c	(Świerczewsk

Campanian, ~78 Ma		discrete spicules	143.2	×	×	×	44.6	31%		a-Gładysz and Jurkowska, 2013)
		Hexactinellida, *Chaunoplectella* sp.	367	×	×	√	×	√	fig. 4a	
			381	×	×	√	×	√		
			425	×	×	√	×	√	fig. 4b	
			341	×	×	√	×	√		
			326	×	×	√	×	√		
		Hexactinellida, unnamed specimen	419	×	×	√	×	√	fig. 4c	
			323	×	×	√	×	√		
			432	×	×	√	×	√		
			440	×	×	√	×	√		
			822	×	×	√	231	28%	fig. 4d	
		Hexactinellida, root tuftss type 1	998	×	×	√	×	√	fig. 5b	
			735	×	×	√	×	√		
Paleogene, late paleocnene to early Eocene, ~57 Ma	Tutuiri Greenland outcrops	Demospongiae, discrete spicules	20	×	×	×	1.8	9%	fig. 4A	(Kelly and Buckeridge, 2005)
			20.1	×	×	×	1.1	5%		
			20	×	×	×	1.7	9%		
			91	×	×	×	4.4	5%	fig. 4B	
			25.1	×	×	×	2.3	9%	fig. 4D	
			25.9	×	×	×	1.7	7%		
			24.3	×	×	×	2	8%		
			29.2	×	×	×	1.5	5%		
			26.6	×	×	×	1.7	6%		

Paleogene, early to middle Eocene, ~49 Ma	DSDP Site 605	Silicea, discrete spicules	14.8	×	×	×	4.8	32%	pl. 1.1	(McCartney, 1987)
			10.9	×	×	×	4.6	42%	pl. 1.3	
			8.3	×	×	×	1.5	18%	pl. 2.3	
			4.9	×	×	×	0.8	16%	pl. 2.6	
			8.7	×	×	×	1.5	17%	pl. 2.7	
			7.2	×	×	×	0.7	10%	pl. 2.9	
			16.7	×	×	×	3.5	21%	pl. 2.10	
			6.3	×	×	×	0.1	2%	pl. 3.4	
			18	×	×	×	4.5	25%	pl. 3.7	
			8.7	×	×	×	2.4	28%	pl. 3.8	
			11.4	×	×	×	1.6	14%	pl. 4.8	
			10.5	×	×	×	1.8	17%		
			7.7	×	×	×	1.6	21%	pl. 5.2	
			7.3	×	×	×	1.1	15%	pl. 5.3	
			7.7	×	×	×	1	13%	pl. 5.6	
			10.5	×	×	×	1.9	18%	pl. 5.7	
			6	×	×	×	1.3	22%	pl. 5.8	
			4.6	×	×	×	0.8	17%	pl. 5.9	
			9.3	×	×	×	1.4	15%	pl. 6.4	
			5.8	×	×	×	2.2	38%	pl. 6.5	
			6.4	×	×	×	0.7	11%	pl. 6.10	
Paleogene, Eocene, ~45 Ma	Castle Hayne Fm.	Hexactinellida, *Exanthesis ovatus*	142.5	×	×	×	26	18%	pl. 53.1	(Finks et al., 2011)

Paleogene, middle Eocene, ~43 Ma	Messel, Germany	Demospongiae, discrete spicules	30.5	×	×	×	2.3	8%	fig. 16A3	(Pronzato et al., 2017)
			23.6	×	×	×	1.9	8%	fig. 16A4	
			13.6	×	×	×	3.4	25%	fig. 16A5	
Paleogene, Late Eocene, ~38 Ma	Blanche Fm. & Pallinup Fm.	Silicea, discrete spicules	31.7	×	×	×	4	13%	fig. 4G	(Łukowiak, 2015)
			26.1	×	×	×	3.1	12%		
			40.2	×	×	×	8	20%	fig. 4V	
			31.7	×	×	×	5.7	18%	fig. 13F	
			33.4	×	×	×	5.7	17%	fig. 13G	
			39.5	×	×	×	5.9	15%	fig. 15K	
			27	×	×	×	4.8	18%	fig. 24R	
			13	×	×	×	4.7	36%	fig. 24S	
			17.6	×	×	×	2.2	13%	fig. 24T	
			20.9	×	×	×	1.6	8%	fig. 24U	
			30.6	×	×	×	3.8	12%	fig. 25A	
			18.7	×	×	×	3.4	18%		
			24.4	×	×	×	4.4	18%	fig. 25E	
			20.4	×	×	×	4.1	20%		
			30.8	×	×	×	3.3	11%	fig. 25H	
			36.9	×	×	×	6.6	18%	fig. 33E	
			25.6	×	×	×	5.9	23%	fig. 33S	
			58.5	×	×	×	6.3	11%	fig. 33T	
Paleogene, Oligocene, ~29 Ma	Site 628 & 627	Silicea, discrete spicules	17.2	×	×	×	3.6	21%	pl. 1.2	(Palmer, 1988)
			33.7	×	×	×	4.3	13%		
			13.1	×	×	×	2.8	21%		

			15.7	×	×	×	4.4	28%		
			29.6	×	×	×	4.9	17%	pl. 4.1	
			24	×	×	×	5.4	23%	pl. 4.2	
Neogene, upper Oligocene–middle Miocene, ~20 Ma	ODP Site 628 & 627	Silicea, discrete spicules	38	×	×	×	9.2	24%	pl. 1.1	(Palmer, 1988)
			28.5	×	×	×	4	14%		
			32.8	×	×	×	4.2	13%		
			41	×	×	×	4.7	11%		
			25.9	×	×	×	3.8	15%	pl. 2.4	
			21.7	×	×	×	4.4	20%		
			17.4	×	×	×	3.9	22%		
Neogene, middle Miocene, ~14 Ma	Hole 918D	Silicea, discrete spicules	16.4	×	×	×	1.8	11%	pl. 1.1	(Lurvey et al., 1998)
			18.8	×	×	×	2.3	12%	pl. 1.2	
			13.6	×	×	×	1.3	10%	pl. 1.3	
			8.9	×	×	×	0.9	10%	pl. 1.4	
			12	×	×	×	0.6	5%	pl. 1.5	
			9.1	×	×	×	3.4	37%	pl. 1.6	
			12.9	×	×	×	0.9	7%	pl. 1.7	
			22.2	×	×	×	1	5%	pl. 1.8	
			9.9	×	×	×	0.6	6%	pl. 1.9	
			10.9	×	×	×	1.3	12%	pl. 1.10	
			6.3	×	×	×	1.2	19%	pl. 2.11	
			8.3	×	×	×	1	12%		
			6.6	×	×	×	1.3	20%		

			7.1	×	×	×	1	14%		
			6.4	×	×	×	2	31%		
			5.8	×	×	×	1.1	19%		
			6.3	×	×	×	1.4	22%	pl. 2.12	
Neogene, Serravalian, ~13 Ma	Mem Moniz marls	Silicea, discrete spicules	40.9	×	×	×	4.6	11%	fig. 3D	(Pisera et al., 2006)
			28.5	×	×	×	7	25%	fig. 3F	
			39.5	×	×	×	6.1	15%	fig. 5D	
			25.3	×	×	×	3.5	14%	fig. 6C	
			30	×	×	×	4.7	16%	fig. 10E	
			63.8	×	×	×	3.9	6%	fig. 10G	
Neogene, Miocene, ~14 Ma	Lacustrine deposit at Oviatt Creek	Silicea, discrete spicules	2.9	×	×	×	0.4	14%	fig. 22A	(Pronzato et al., 2017)
			9.6	×	×	×	3.7	39%	fig. 22B	
			14	×	×	×	5	36%	fig. 22O	
			5.7	×	×	×	1.2	21%	fig. 22V	
			7.4	×	×	×	1.7	23%	fig. 22W	
			8.1	×	×	×	2.2	27%	fig. 22X	
			8.8	×	×	×	1.7	19%	fig. 22Y	
			2.8	×	×	×	0.5	18%	fig. 22Z	
Neogene, late Miocene, ~9Ma	DSDP Site 604	Silicea, discrete spicules	21.3	×	×	×	4.3	20%	pl. 2.2	(McCartney, 1987)
			8.2	×	×	×	2	24%	pl. 5.1	
Quaternary, ~1.5 Ma	ODP Leg 180	Silicea, discrete spicules	8.8	×	×	×	3.9	44%	pl. 1.1	(Andri et al., 2001)
			8.2	×	×	×	3.2	39%		
			8	×	×	×	3.3	41%		

			9.3	×	×	×	3.8	41%	pl. 1.2	
			6.5	×	×	×	2.2	34%	pl. 1.3	
			8.8	×	×	×	3.9	44%	pl. 1.4	
			8.2	×	×	×	3.2	39%		
			8	×	×	×	3.3	41%		
			13.9	×	×	×	1	7%	pl. 1.5	
			7.6	×	×	×	1.2	16%	pl. 1.8	
			6.6	×	×	×	2.3	35%	pl. 1.9	
Quaternary, Holocene, ~0.01 Ma	peaty sediments in Taquarussu region, Brazil	Silicea, discrete spicules	29.9	×	×	×	5.8	19%	fig, 4A	(Parolin et al., 2007)
			22.8	×	×	×	3.1	14%	fig. 4A2	
			8.2	×	×	×	1.5	18%	fig. 4B	
			5	×	×	×	0.8	16%	fig. 4C	
			4.9	×	×	×	0.6	12%	fig. 4C1	
			13.8	×	×	×	2.8	20%	fig. 4E	
			11.6	×	×	×	3.8	33%	fig. 4E1	
			5.4	×	×	×	1	19%	fig. 4E2	
			43.1	×	×	×	2.2	5%	fig. 5	
Extant	Demospongiae, *Suberites domuncula*		1.9	0.4	×	×	×	21%	fig. 2J	(Wang et al., 2012)
			1.6	0.3	×	×		19%	fig. 2K	
			2.4	0.4	×	×	×	15%	fig. 2N	
			2.3	0.5	×	×		22%	fig. 2O	
Extant	Demospongiae, *Crambe crambe*		6.2	1.3	×	×		21%	fig. 3A	(Uriz et al., 2000)
Extant	Demospongiae, *Suberites domuncula*		2.4	×	√	×	0.7	27%	fig. 1A	(Schröder et al., 2007)
			3.1	√	0.4	×	0.4	>13%	fig. 1B	

		2.5	0.3	0.1	×		19%	fig. 1E	
		3.8	×	√	×	0.9	31%	fig. 1F	
		3.7	×	√	×	0.9	32%	fig. 1G	
Extant	Demospongiae, *Corticium candelabrum*	3.2	×	0.2	×	×	9%	fig. 8e	(Maldonado and Riesgo, 2007)
Extant	Demospongiae, *Leiodermatium pfeifferae*	2.5	×	×	×	0.7	28%	fig. 3F	(Maldonado et al., 2015)
Extant	Demospongiae, *Ephydatia fossilis*	9.4	×	×	×	0.7	7%	fig. 21B1	(Pronzato et al., 2017)
		6.8	×	×	×	0.5	7%	fig. 21B2	
		9.1	×	×	×	0.5	5%	fig. 21B3	
		7.1	×	×	×	0.6	8%	fig. 21B4	
Extant	Demospongiae, *Eunapius mackayi*	10.3	×	×	×	1.4	14%	fig. 8g	(Ricciardi and Reiswig, 1993)
		14.1	×	×	×	1.9	13%	fig. 8M	
Extant	Demospongiae, *Trochospongilla horida*	12.4	×	×	×	1.2	10%	fig. 14M	
Extant	Demospongiae, *Trochospongilla pennsylvanica*	11.2	×	×	×	1.8	16%	fig. 15g	
		5.5	×	×	×	0.9	16%	fig. 15ga	
Extant	Hexactinellida, *Monorhaphis chuni*	39.1	0.3	0.3	×	×	2%	fig. 1B	(Müller et al., 2008)
		12.1	1.3	√	×	×	>10%	fig. 1D	
		1.6	0.3	√	×	×	>19%	fig. 1H	
Extant	Hexactinellida, *Monorhaphis internedia*	√	√	0.2	×	×	√	fig. 1F	
Extant	Hexactinellida, *Hyalonema sieboldi*	>70.6	1.1	0.4	×	×	<3%	fig. 2F	(Schröder et al., 2008)

Extant	Hexactinellida, *Euplectella aspergillum*	√	0.1	0.01	×	×	√	fig. 3D	(Weaver et al., 2007)
Extant	Calcarea, *Clathrina wistariensis*	8.8	×	×	0.7	×	17%	fig. 7b	(Sethmann and Wörheide, 2008)
Extant	Calcarea, *Leucetta villosa*	9.3	×	×	0.2	×	5%	fig. 9	
Extant	Calcarea, *Sycon*	√	×	×	√	×	√	fig. 2	(Ledger and Jones, 1977)
Extant	Calcarea, *Leucandra*	√	×	×	√	×	√	fig. 5−6	

5.9 Figures and figure legends

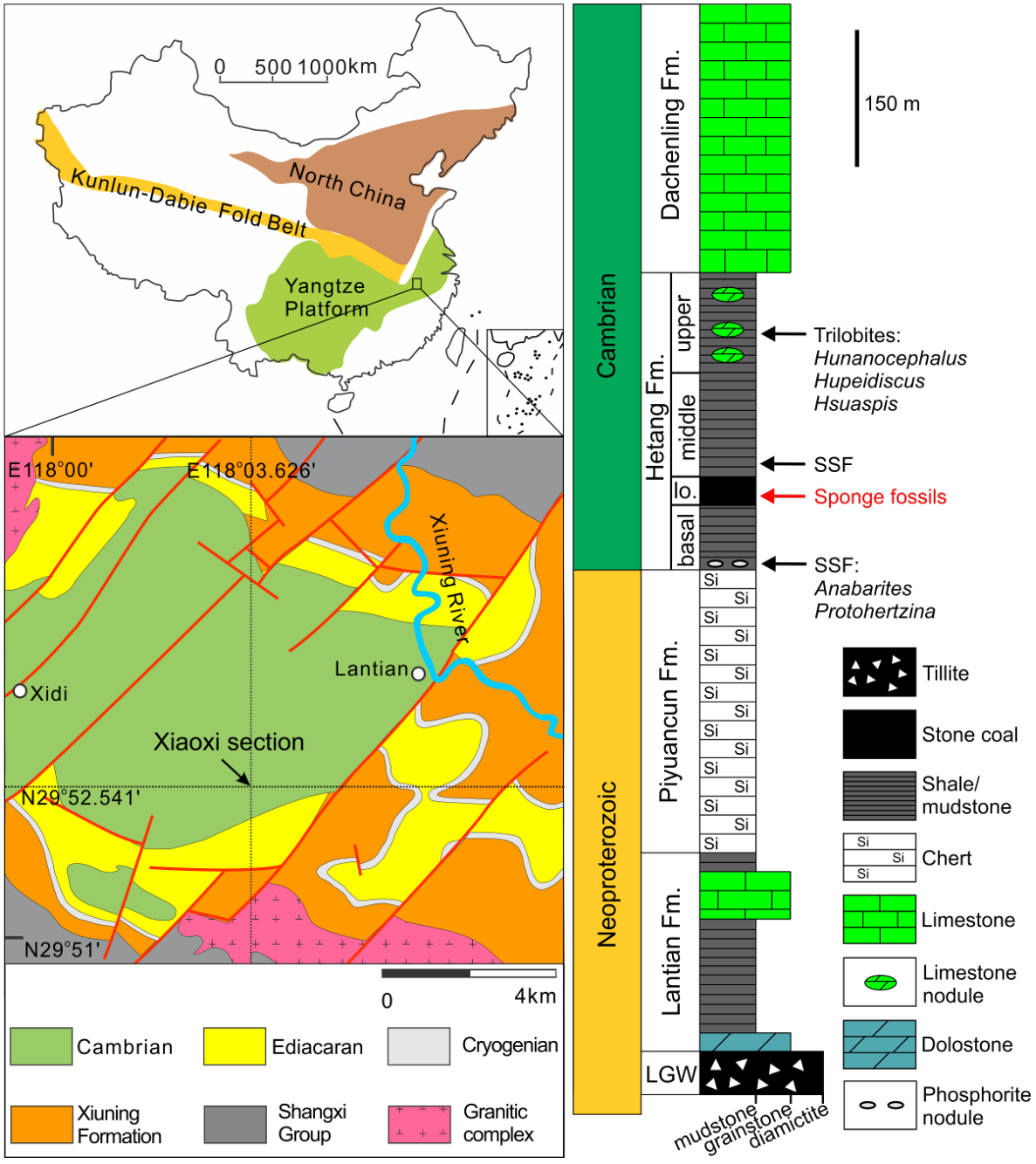

Fig. 5. 1. Geological map and stratigraphic column of Neoproterozoic–lower Cambrian at Lantian area, South China. Modified from Xiao et al. (2005). LGW: Leigongwu Formation, SSF: small shelly fossil, Fm.: Formation.

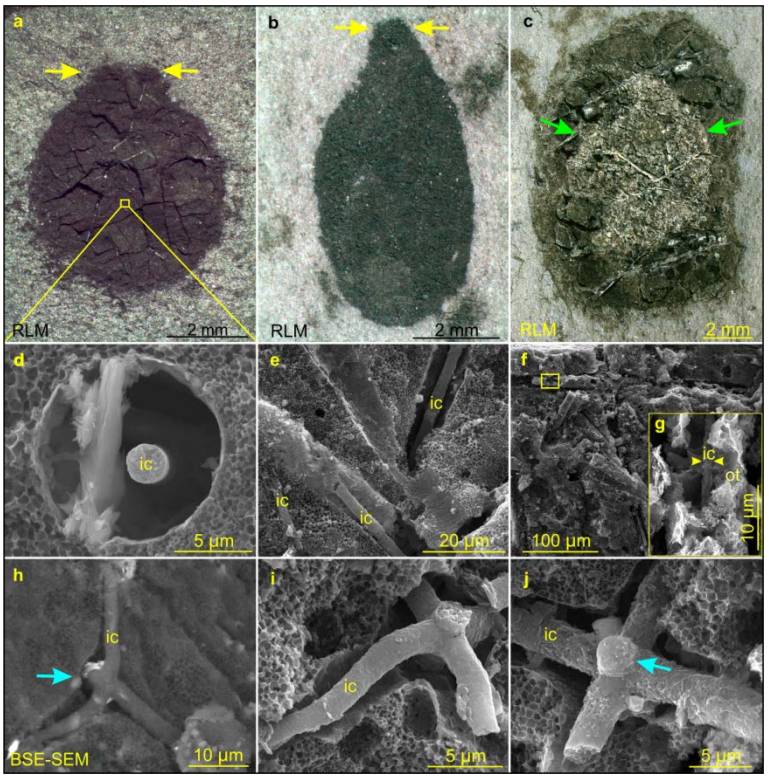

Fig. 5. 2. Sponge fossils from the Hetang Formation. a−c Carbonaceous compressions of sponge body fossils. Yellow and green arrows bracket putative osculum and spongocoel, respectively. Polygonal cracks in a are manifested as black in color. VPIGM-4699 (16-HT-T6-1-1), VPIGM-4700 (16-HT-T5-6-1), and VPIGM-4701 (16-HT-T3-77-1), respectively. d−j Demineralized spicules. d and g are magnifications of rectangles in a and f, respectively. Blue arrows in h and j point to protuberances or aborted rays. e, f VPIGM-4702 and VPIGM-4703, respectively; h−j VPIGM-4704, VPIGM-4705, and VPIGM-4706, respectively. a−c are reflected light micrographs (RLM) and h is backscattered electron scanning electron microscopy (BSE-SEM) micrograph. All other images in this and other figures are secondary electron scanning electron microscopy (SE-SEM) micrographs unless otherwise noted. ic: inner core; ot: outer lamella.

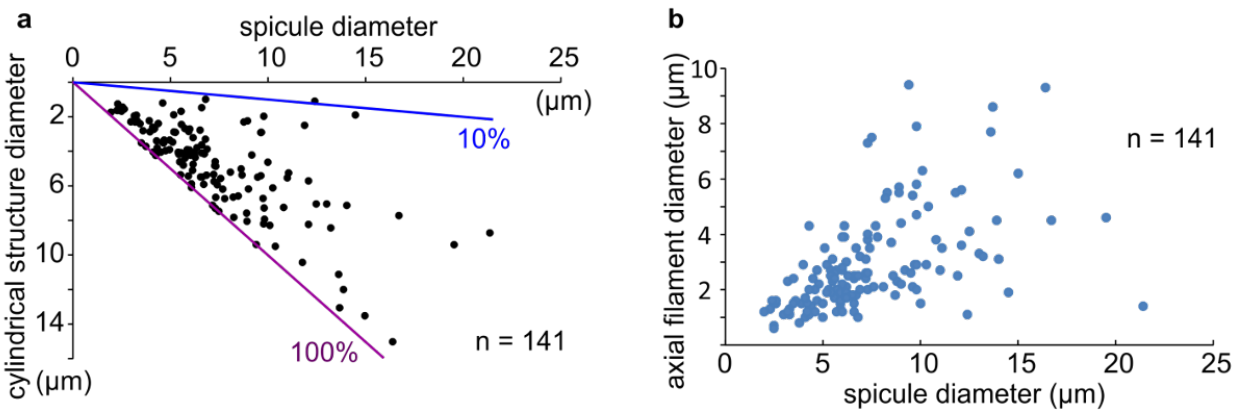

Fig. 5. 3. Biometric data of Hetang spicules. a Cross-plot of spicule diameter and cylindrical structure diameter (= inner core diameter + 2 * outer lamella thickness). Organic cylindrical structure accounts for ~10–100% of spicule diameter. b Cross-plot of spicule diameter and axial filament diameter.

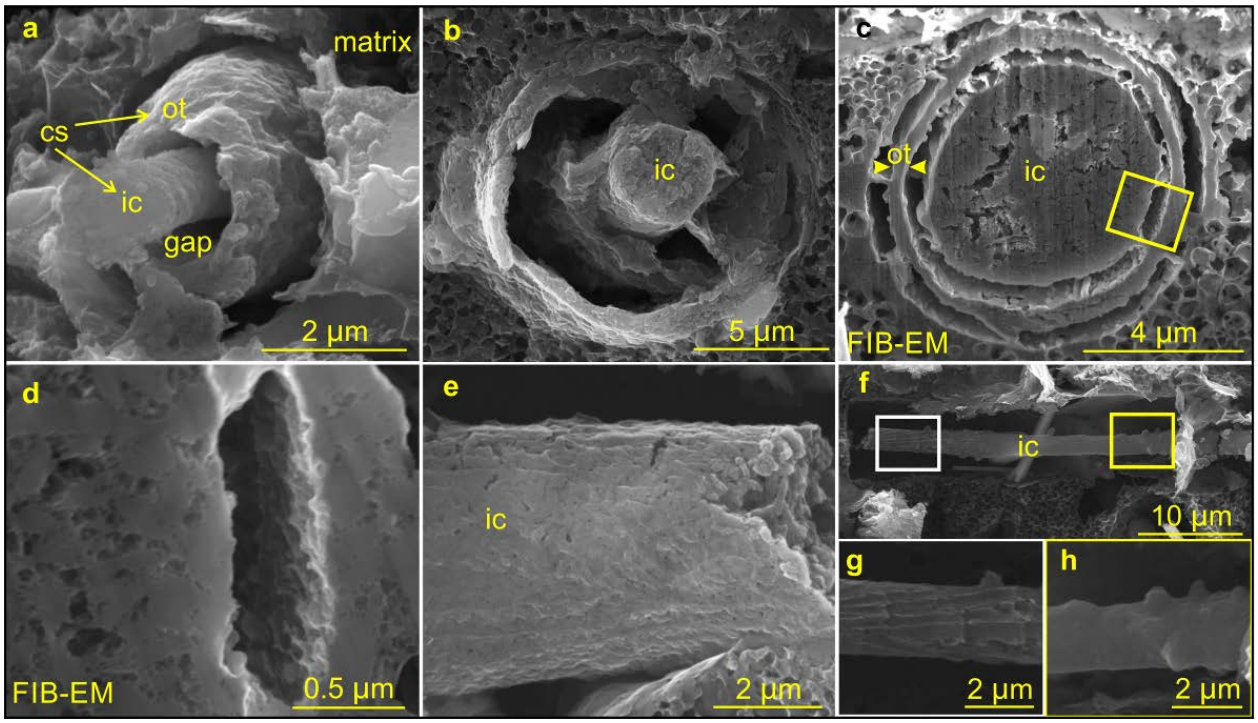

Fig. 5. 4. Demineralized spicules from the Hetang sponges. a–d Cross-sectional views of spicules with inner core and outer lamella. VPIGM-4707, VPIGM-4708, VPIGM-4709, respectively. d is a magnification of the rectangle in c. e, f Lateral views of axial filaments. VPIGM-4710 and VPIGM-4711, respectively. g, h Magnifications of white and yellow rectangles in f, respectively. cs: cylindrical structure; ot: outer lamella; ic: inner core.

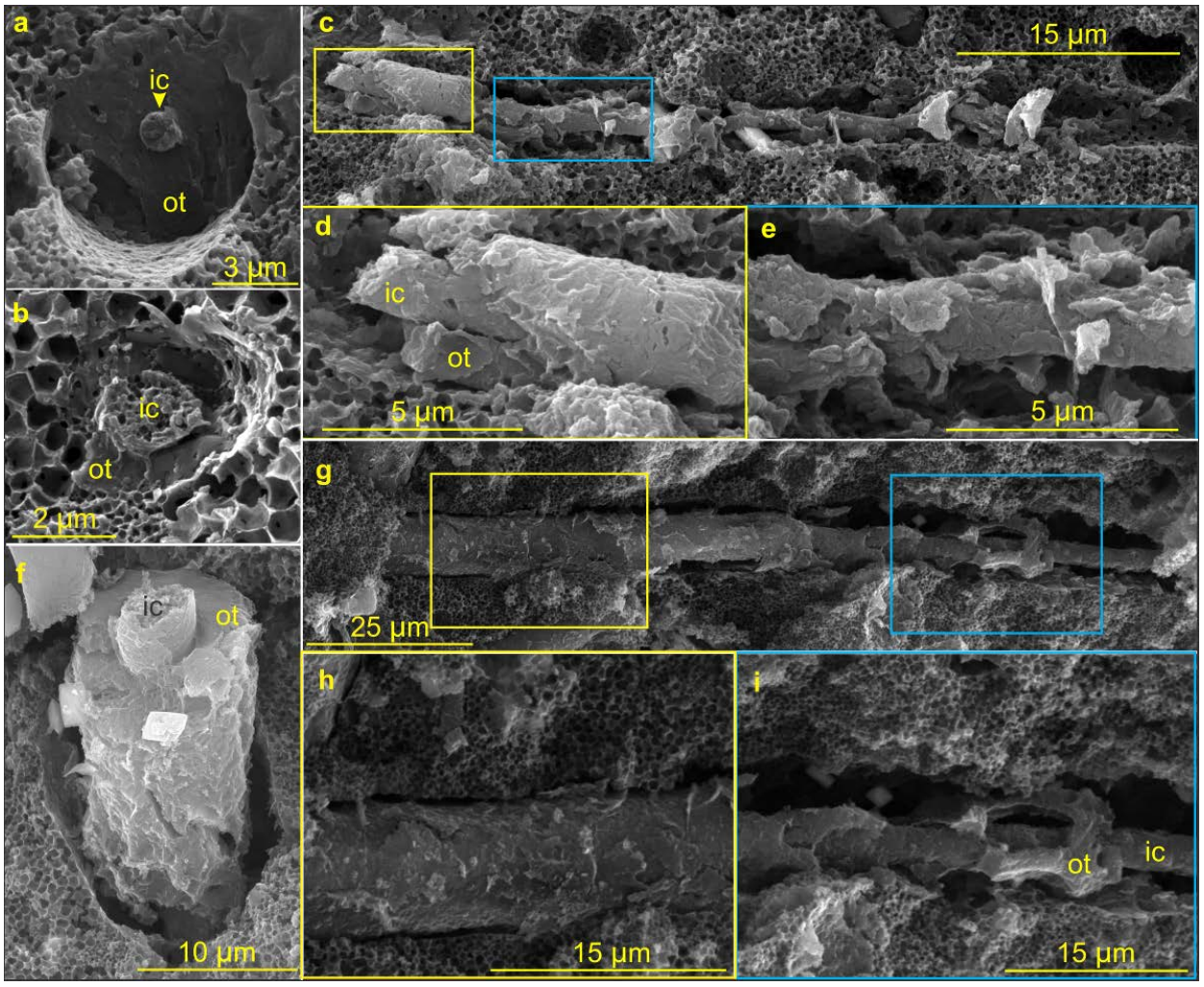

Fig. 5. 5. Cylindrical structures with inner core and outer lamella. a, b Cross-sectional views. VPIGM-4712 and VPIGM-4713, respectively. c, f, g Lateral views. VPIGM-4714, VPIGM-4715, and VPIGM-4716, respectively. d, h Magnifications of the yellow frames in c and g, respectively, showing well-preserved outer lamellae. e, i Magnifications of the blue frames in c and g, respectively, showing partially degraded outer lamellae. ic: inner core; ot: outer lamella.

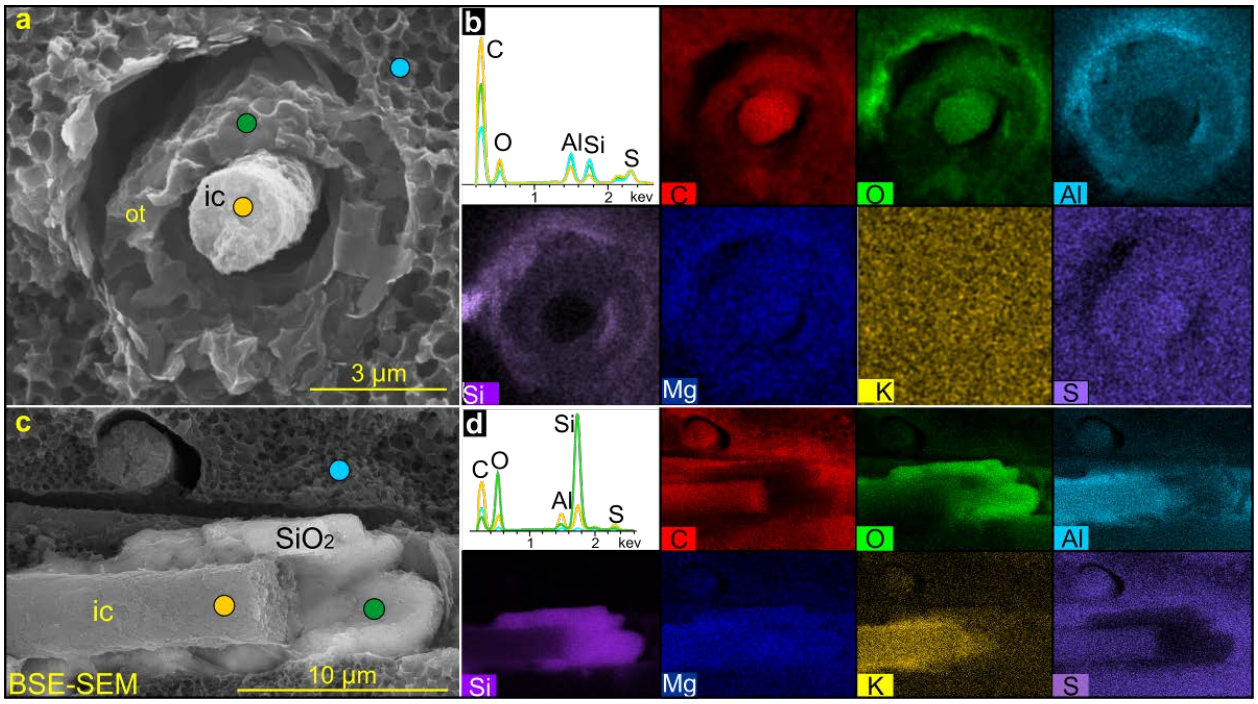

Fig. 5. 6. Preservation of organic and biosilica structures. a Demineralized spicule. VPIGM-4717. b EDS point analysis and element maps of a. c BSE-SEM micrograph of partially demineralized spicule. VPIGM-4718. d EDS point analysis and element maps of c, showing organic axial filament enveloped by a silica lamella. Colored dots in a and c denote the location of EDS point analyses shown in b and d, respectively. ic: inner core; ot: outer lamella; SiO_2: siliceous layer.

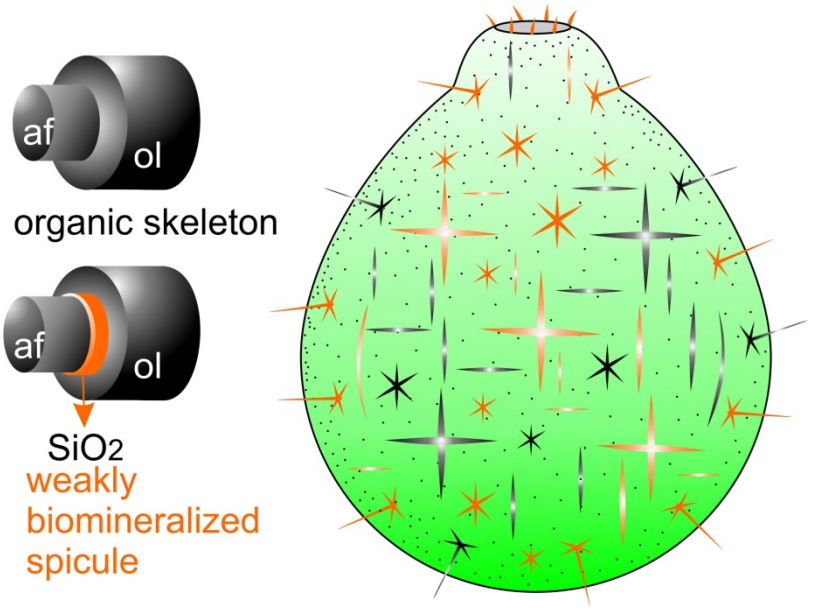

Fig. 5. 7. Spiculogenesis and morphological reconstruction. Schematic reconstructions of early sponges with weakly biomineralized spicules and entirely organic skeletons as inferred from Hetang sponge fossils. Pattern of spicule/skeleton distribution and orientation is conjectural but based on Cambrian reticulosan sponges (Botting and Muir, 2018). Organic skeletons and weakly biomineralized spicules in the sponge body reconstruction are colored in black and orange, respectively. af: axial filament; ol: organic layer; SiO_2: siliceous layer.

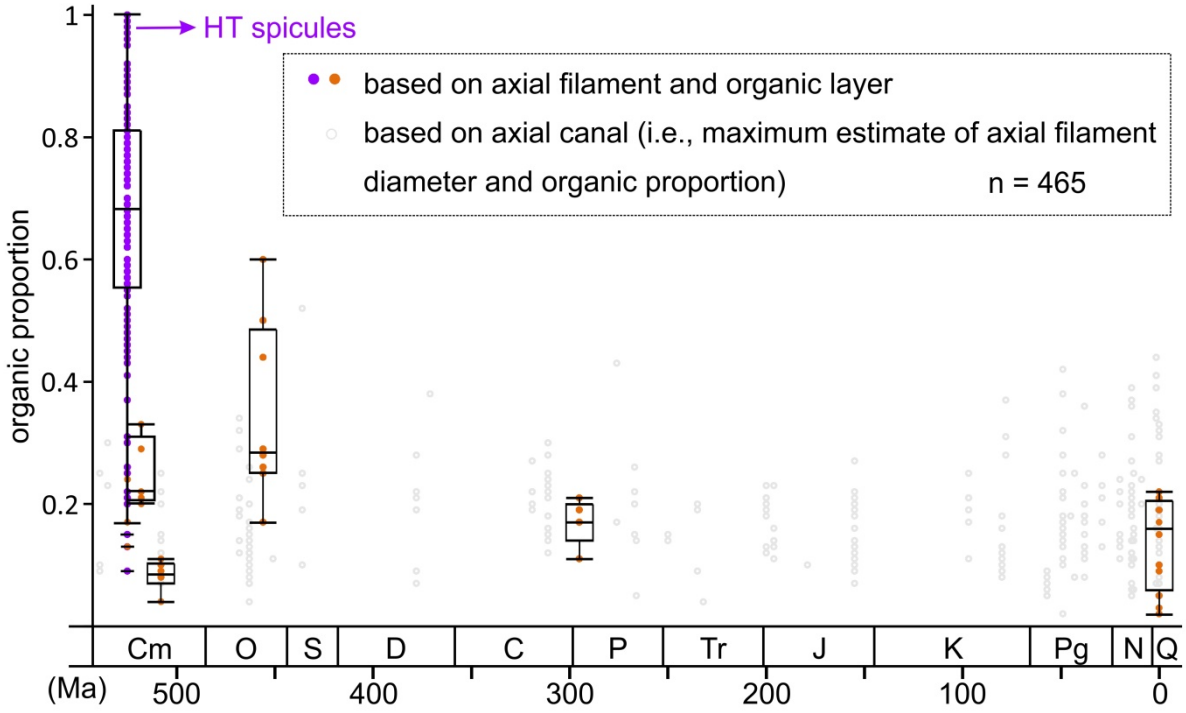

Fig. 5. 8. Relative organic proportion in fossil and extant sponge spicules. Measured as the relative thickness of combined organic structures (including axial filament, organic layer, and outer sheath) in spicules. See Supplementary Tables 1, 2 for details. HT spicules: Hetang spicules; Cm: Cambrian; O: Ordovician; S: Silurian; D: Devonian; C: Carboniferous; P: Permian; Tr: Triassic; J: Jurassic; K: Cretaceous; Pg: Paleogene; N: Neogene; Q: Quaternary and extant.

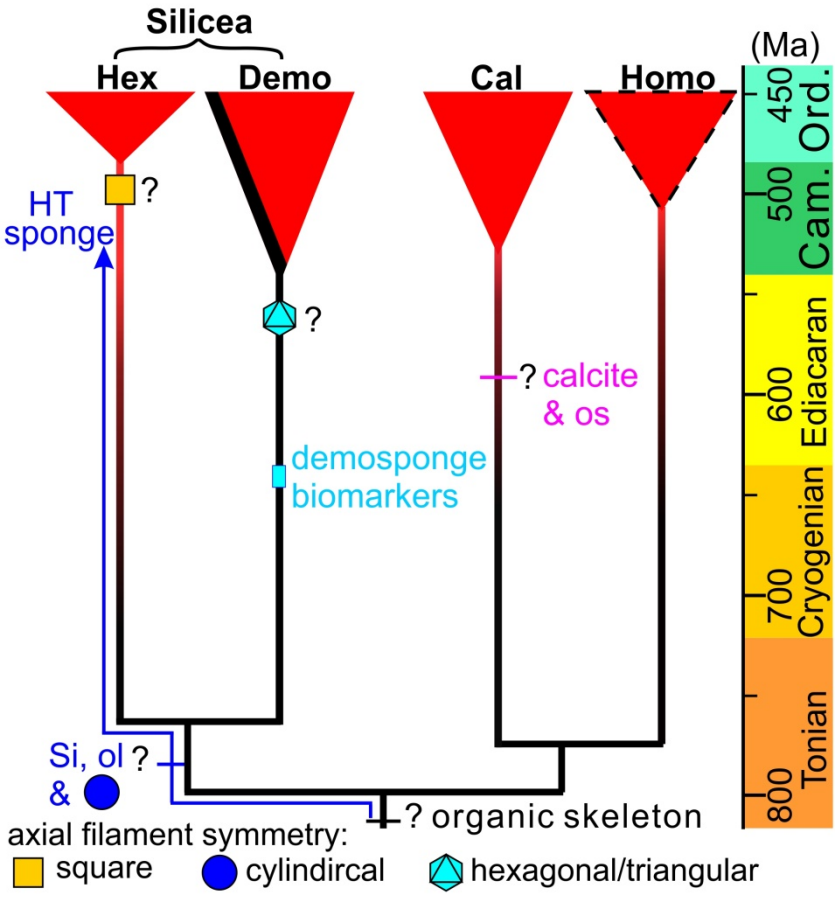

Fig. 5. 9. Phylogenetic interpretations of the Hetang sponges. The phylogenetic tree is simplified and time-calibrated using molecular clock estimates (Dohrmann and Wörheide, 2017). It omits eumetazoans and ctenophores so that it stands regardless the monophyly (Philippe et al., 2009; Feuda et al., 2017; Littlewood, 2017) vs. paraphyly (Sperling et al., 2010) of the poriferans and the phylogenetic placement of the ctenophores (Ryan et al., 2013; Pisani et al., 2015; Feuda et al., 2017; Littlewood, 2017). Although a few molecular phylogenetic analyses give spurious support for the paraphyly of the Silicea (Hill et al., 2013), most other analyses give decisive support for the monophyly of the Silicea (Philippe et al., 2009; Feuda et al., 2017; Littlewood, 2017) – a topology adopted here. A cylindrical axial filament is indicated as a plesiomorphy on the tree,

because it is also present in the Paleozoic sponges *Cyathophycus loydelli* (Botting and Muir, 2013) and *Lenica* (Botting et al., 2012). It is alternatively possible that a cylindrical axial filament could be an autapomorphy of these sponges. This uncertainty, however, does not affect the main conclusion that early sponges may have had weakly biomineralized sponge spicules, which is inferred from the presence of organic carbon in many Paleozoic spicules and juvenile spicules of extant sponges (Maldonado and Riesgo, 2007). Cyan bar denotes the possible age of the demosponge biomarker fossil (Love et al., 2009). Crown-group classes are denoted by triangles (except the aspiculate demonsponges which are colored in black) and their earliest fossil representatives are based on Botting and Muir (2018). Dashed triangle indicates the lack of crown-group fossil record in early Paleozoic. Question marks denote uncertain age constraint or phylogenetic placement of characters. ol: organic layer; Si: biosilica lamella; os: organic sheath; Hex: Hexactinellida; Demo: Demospongiae; Cal: Calcarea; Homo: Homoscleromorpha; HT sponge: Hetang sponge; Cam: Cambrian; Ord: Ordovician.

5.10 References

Afanasieva, M.S., 2000, Atlas of Paleozoic Radiolaria of the Russian Platform. Scientific World Publishing House, Moscow, 480 p.

Andri, E., Gerbaudo, S., and Testa, M., 2001, Quaternary siliceous sponge spicules in the western Woodlark Basin, southwest Pacific (ODP Leg 180). *In* Huchon, P., Taylor, B., and Klaus, A., eds., Proceedings of the Ocean Drilling Program, Scientific Results. College Station, TX, Ocean Drilling Program, p. 1–8.

Antcliffe, J.B., Callow, R.H.T., and Brasier, M.D., 2014, Giving the early fossil record of sponges a squeeze: Biological Review, v. 89, p. 972−1004.

Bertolino, M., Cattaneo-Vietti, R., Pansini, M., Santini, C., and Bavestrello, G., 2017, Siliceous sponge spicule dissolution: In field experimental evidences from temperate and tropical waters: Estuarine, Coast Shelf Science, v. 184, p. 46−53.

Botting, J.P., 2012, Reassessment of the problematic Burgess Shale sponge *Takakkawia lineata* Walcott, 1920: Canadian Journal of Earth Sciences, v. 49, p. 1087−1095.

Botting, J.P., and Butterfield, N.J., 2005, Reconstructing early sponge relationships by using the Burgess Shale fossil *Eiffelia globosa*, Walcott: Proceedings of the National Academy of Sciences of the United States of America, v. 102, p. 1554−1559.

Botting, J.P., and Muir, L.A., 2013, Spicule structure and affinities of the Late Ordovician hexactinellid-like sponge *Cyathophycus loydelli* from the Llanfawr Mudstones Lagerstätte, Wales: Lethaia, v. 46, p. 454−469.

Botting, J.P., and Muir, L.A., 2014, Relationship of the Cambrian Protomonaxonida (Porifera): Palaeontologia Electronica, v. 16, p. 1−23.

Botting, J.P., and Muir, L.A., 2018, Early sponge evolution: A review and phylogenetic framework: Palaeoworld, v. 27, p. 1−29.

Botting, J.P., Muir, L.A., Jordan, N., and Upton, C., 2015, An Ordovician variation on Burgess Shale-type biotas: Scientific Reports, v. 5, p. 9947.

Botting, J.P., Muir, L.A., Xiao, S., Li, X., and Lin, J.-P., 2012, Evidence for spicule homology in calcareous and siliceous sponges: biminerallic spicules in *Lenica* sp. from the Early Cambrian of South China: Lethaia, v. 45, p. 463–475.

Botting, J.P., Muir, L.A., Zhang, Y., Ma, X., Ma, J., Wang, L., Zhang, J., Song, Y., and Fang, X., 2017, Flourishing sponge-based ecosystems after the end-Ordovician mass extinction: Currrent Biology, v. 27, p. 556–562.

Botting, J.P., and Peel, J.S., 2016, Early Cambrian sponges of the Sirius Passet Biota, North Greenland: Papers in Palaeontology, v. 2, p. 463–487.

Carrera, M.G., 2007, The oldest hindiid demosponge from the Darriwilian (Middle Ordovician) of the Argentine Precordillera: evolutionary implications for the tricranocladines: Journal of Paleontology, v. 81, p. 754−759.

Carrera, M.G., and Maletz, J., 2014, Ordovician sponge spicules from Spitsbergen, Nevada and Newfoundland: new evidence for hexactinellid and demosponge early diversification: Journal of Systematic Palaeontology, v. 12, p. 961−981.

Chang, S., Feng, Q., Clausen, S., and Zhang, L., 2017, Sponge spicules from the lower Cambrian in the Yanjiahe Formation, South China: The earliest biomineralizing sponge record: Palaeogeography, Palaeoclimatology, Palaeoecology, v. 474, p. 36–44.

Clites, E.C., Droser, M.L., and Gehling, J.G., 2012, The advent of hard-part structural support among the Ediacara biota: Ediacaran harbinger of a Cambrian mode of body construction: Geology, v. 40, p. 307−310.

Croce, G., Frache, A., Milanesio, M., Marchese, L., Causà, M., Viterbo, D., Barbaglia, A., Bolis, V., Bavestrello, G., Cerrano, C., Benatti, U., Pozzolini, M., Giovine, M., and Amenitsch, H., 2004, Structural characterization of siliceous spicules from marine sponges: Biophysical Journal, v. 86, p. 526−534.

Delecat, S., and Reitner, J., 2005, Sponge communities from the Lower Liassic of Adnet (Northern Calcareous Alps, Austria): Facies, v. 51, p. 385–404.

Dohrmann, M., and Wörheide, G., 2017, Dating early animal evolution using phylogenomic data: Scientific Reports, v. 7, p. 3599.

Donofrio, D.A., 1991, Radiolaria and Porifera (spicula) from the Upper Triassic of Aghdarband (NE-Iran): Abh. Geol. B.-A., v. 38, p. 205–222.

Ehrlich, H., Rigby, J.K., Botting, J.P., Tsurkan, M.V., Werner, C., Schwille, P., Petrášek, Z., Pisera, A., Simon, P., Sivkov, V.N., Vyalikh, D.V., Molodtsov, S.L., Kurek, D., Kammer, M., Hunoldt, S., Born, R., Stawski, D., Steinhof, A., Bazhenov, V.V., and Geisler, T.,

2013, Discovery of 505-million-year old chitin in the basal demosponge *Vauxia gracilenta*: Scientific Reports, v. 3, p. 3497.

Erpenbeck, D., Sutcliffe, P., Cook, S.d.C., Dietzel, A., Maldonado, M., van Soest, R.W.M., Hooper, J.N.A., and Wörheide, G., 2012, Horny sponges and their affairs: On the phylogenetic relationships of keratose sponges: Molecular Phylogenetics and Evolution, v. 63, p. 809−816.

Erwin, D.H., Laflamme, M., Tweedt, S.M., Sperling, E.A., Pisani, D., and Peterson, K.J., 2011, The Cambrian conundrum: Early divergence and later ecological success in the early history of animals: Science, v. 334, p. 1091–1097.

Erwin, D.H., and Valentine, J.W., 2013, The Cambrian Explosion: The Construction of Animal Biodiversity. Roberts and Company Publishers, Greenwood Village, 416 p.

Feuda, R., Dohrmann, M., Pett, W., Philippe, H., Rota-Stabelli, O., Lartillot, N., Wörheide, G., and Pisani, D., 2017, Improved modeling of compositional heterogeneity supports sponges as sister to all other animals: Current Biology, v. 27, p. 3864–3870.e3864.

Finks, R.M., 1969, Late Paleozoic sponge faunas of the Texas region: the siliceous sponges: Bulletin of American Museum of Natural History, v. 120, p. 1–60.

Finks, R.M., Hollocher, K., and Thies, K., 2011, A major Eocene sponge fauna (Castle Hayne Formation, North Carolina): Journal of North Carolina Academy of Science, v. 127, p. 39–175.

García-Bellido, D.C., and Rigby, J.K., 2004, Devonian and Carboniferous sponges from Spain: Journal of Paleontology, v. 78, p. 431–455.

Gold, D.A., Grabenstatter, J., de Mendoza, A., Riesgo, A., Ruiz-Trillo, I., and Summons, R.E., 2016, Sterol and genomic analyses validate the sponge biomarker hypothesis: Proceedings of the National Academy of Sciences of the United States of America, v. 113, p. 2684–2689.

Harvey, T.H.P., 2010, Carbonaceous preservation of Cambrian hexactinellid sponge spicules: Biology Letters, v. 6, p. 834-837.

Hill, M.S., Hill, A.L., Lopez, J., Peterson, K.J., Pomponi, S., Diaz, M.C., Thacker, R.W., Adamska, M., Boury-Esnault, N., Cárdenas, P., Chaves-Fonnegra, A., Danka, E., De Laine, B.-O., Formica, D., Hajdu, E., Lobo-Hajdu, G., Klontz, S., Morrow, C.C., Patel, J., Picton, B., Pisani, D., Pohlmann, D., Redmond, N.E., Reed, J., Richey, S., Riesgo, A., Rubin, E., Russell, Z., Rützler, K., Sperling, E.A., di Stefano, M., Tarver, J.E., and Collins, A.G., 2013, Reconstruction of family-level phylogenetic relationships within Demospongiae (Porifera) using nuclear encoded housekeeping genes: PLoS ONE, v. 8, p. e50437.

Kelly, M., and Buckeridge, J.S., 2005, An early Paleogene sponge fauna, Chatham Island, New Zealand: New Zealand Journal of Marine and Freshwater Research, v. 39, p. 899–914.

Kling, S.A., and Reif, W.-E., 1969, The Paleozoic history of amphidisc and hemidisc sponges: New evidence from the Carboniferous of Uruguay: Journal of Paleontology, v. 43, p. 1429–1434.

Knoll, A.H., 2003, Biomineralization and evolutionary history: Reviews in Mineralogy and Geochemistry, v. 54, p. 329–356.

Ledger, P.W., and Jones, W.C., 1977, Spicule formation in the calcareous sponge *Sycon ciliatum*: Cell Tissue Research, v. 181, p. 553−567.

Li, C., Chen, J., and Hua, T., 1998, Precambrian sponges with cellular structures: Science, v. 279, p. 879–882.

Littlewood, D.T.J., 2017, Animal evolution: Last word on sponges-first?: Current Biology, v. 27, p. R259–R261

Love, G.D., Grosjean, E., Stalvies, C., Fike, D.A., Grotzinger, J.P., Bradley, A.S., Kelly, A.E., Bhatia, M., Meredith, W., Snape, C.E., Bowring, S.A., Condon, D.J., and Summons, R.E., 2009, Fossil steroids record the appearance of Demospongiae during the Cryogenian period: Nature, v. 457, p. 718–721.

Łukowiak, M., 2015, Late Eocene siliceous sponge fauna of southern Australia: reconstruction based on loose spicules record: Zootaxa, v. 3917, p. 1–65.

Lurvey, L.K., McCartney, K., and Wei, W., 1998, Siliceous sponge spicules, silicoflagellates, and ebridians from Hole 918D, continental rise of the Greenland margin. *In* Saunders,

A.D., Larsen, H.C., and Wise, S.W., Jr., eds., Proccedings of the Ocean Drilling Program, Scientific Results. College Station, TX, Ocean Drilling Program, p. 191–199.

Müller, W.E.G., Boreiko, A., Schloßmacher, U., Wang, X., Eckert, C., Kropf, K., Li, J., and Schröder, H.C., 2008, Identification of a silicatein(-related) protease in the giant spicules of the deep-sea hexactinellid *Monorhaphis chuni*: Journal of Experimental Biology, v. 211, p. 300–309.

Maldonado, M., Aguilar, R., Blanco, J., García, S., Serrano, A., and Punzón, A., 2015, Aggregated clumps of lithistid sponges: A singular, reef-like bathyal habitat with relevant paleontological connections: PLoS ONE, v. 10, p. e0125378.

Maldonado, M., and Riesgo, A., 2007, Intra-epithelial spicules in a homosclerophorid sponge: Cell Tissue Research, v. 328, p. 639–650.

Marshall, C.R., 2006, Explaining the Cambrian “explosion” of animals: Annal Review of Earth and Planetary Science, v. 34, p. 355−384.

McCartney, K., 1987, Siliceous sponge spicules from Deep Sea Drilling Project Leg 93. *In* Van Hinte, J.E., Wise, S.W., Jr., and abbot, D.S., eds., Initial Reports, Deep Sea Drilling Project. Washington, U.S. Govt. Printing Office, p. 818–824.

Mehl, D., 1998, Porifera and Chancelloriidae from the Middle Cambrian of the Georgina Basin, Australia: Palaeontology, v. 41, p. 1153-1182.

Mouro, L., Fernandes, A., Rogerio, D., and Fonseca, V., 2014, First articulated sponge from the Paleozoic of Brazil, and a new organization of the order Hemidiscosa: Journal of Paleontology, v. 88, p. 171−178.

Muir, L.A., and Botting, J.P., 2015, An outline of the distribution and diversity of Porifera in the Ordovician Builth Inlier (Wales, UK): Palaeoworld, v. 24, p. 176−190.

Muscente, A.D., Michel, M.F., Dale, J.G., and Xiao, S., 2015, Assessing the veracity of Precambrian 'sponge' fossils using in situ nanoscale analytical techniques: Precambrian Research, v. 263, p. 142−156.

Muscente, A.D., and Xiao, S., 2015a, New occurrences of *Sphenothallus* in the lower Cambrian of South China: Implications for its affinities and taphonomic demineralization of shelly fossils: Palaeogeography, Palaeoclimatology, Palaeoecology, v. 437, p. 141–164.

Muscente, A.D., and Xiao, S., 2015b, Resolving three-dimentional and subsurficial features of carbonaceous compressions and shelly fossils using backscattered electron scanning electron microscopy (BSE-SEM): PALAIOS, v. 30, p. 462−481.

Palmer, A.A., 1988, Paleoenvironmental significance of siliceous sponge spicules from Site 627 and 628, Little Bahama Bank, Ocean Drilling Program Leg 101. *In* Austin, J.A., Jr. and Schlager, W., eds., Proceedings of the Ocean Drilling Program, Scientific Results. College Station, TX, Ocean Drilling Program, p. 159–168.

Parolin, M., Volkmer-Ribeiro, C., and Stevaux, J.C., 2007, Sponge spicules in peaty sediments as paleoenvironmental indicators of the Holocene in the upper Paraná river, Brazil: Revista Brasileira Paleontology, v. 10, p. 17–26.

Philippe, H., Derelle, R., Lopez, P., Pick, K., Borchiellini, C., Boury-Esnault, N., Vacelet, J., Renard, E., Houliston, E., Quéinnec, E., Da Silva, C., Wincker, P., Le Guyader, H., Leys, S., Jackson, D.J., Schreiber, F., Erpenbeck, D., Morgenstern, B., Wörheide, G., and Manuel, M., 2009, Phylogenomics revives traditional views on deep animal relationships: Current Biology, v. 19, p. 706–712.

Pisani, D., Pett, W., Dohrmann, M., Feuda, R., Rota-Stabelli, O., Philippe, H., Lartillot, N., and Wörheide, G., 2015, Genomic data do not support comb jellies as the sister group to all other animals: Proceedings of the National Academy of Sciences of the United States of America, v. 112, p. 15402−15407.

Pisera, A., 1997, Upper Jurassic siliceous sponges from the Swabian Alb: Taxonomy and Paleocology: Palaeontologia Polonica, v. 57, p. 1–216.

Pisera, A., and Bodzioch, A., 1991, Middle Triassic lyssacinosan sponges from Upper Silesia (southern Poland), and the history of hexactinosan and lychniscosan sponges: Acta Geologica Polonica, v. 41, p. 193–207.

Pisera, A., Cachao, M., and Marques Da Silva, C., 2006, Siliceous sponge spicule from the Miocene Mem Moniz Marls (Portugal) and their environmental significance Rivista Italiana di Paleontologia e Stratigrafia, v. 112, p. 287–299.

Pronzato, R., Pisera, A., and Manconi, R., 2017, Fossil freshwater sponges: Taxonomy, geographic distribution, and critical review: Acta Paleontologica Polonica, v. 62, p. 467–495.

Reiswig, H.M., 1971, The axial symmetry of sponge spicules and its phylogenetic significance.: Cahiers de Biologie Marine, v. 12, p. 505–514.

Reitner, J., and Mehl, D., 1996, Monophyly of the Porifera: Verhandlungen des Naturwissenschaftlichen Vereins in Hamburg, v. (NF) 36, p. 5–32.

Reolid, M., 2014, Pyritized radiolarians and siliceous sponges from oxygen-restricted deposits (Lower Toarcian, Jurassic): Facies, v. 60, p. 789–799.

Rhebergen, F., and Botting, J.P., 2014, A new Silurian (Llandovery, Telychian) sponge assemblage from Gotland, Sweden: Fossil and Strata, v. 60, p. 1–87.

Ricciardi, A., and Reiswig, H.M., 1993, Freshwater sponges (Porifera, Spongillidae) of eastern Canada: taxonomy, distribution, and ecology: Canadian Journal of Zoology, v. 71, p. 665–682.

Rigby, J.K., and Gosney, T.C., 1983, First reported Triassic lyssakid sponges from North America: Journal of Paleontology, v. 57, p. 787–796.

Ritterbush, K.A., Bottjer, D.J., Corsetti, F.A., and Rosas, S., 2014, New evidence on the role of siliceous sponges in ecology and sedimentary facies development in eastern Panthalassa following the Triassic–Jurassic mass extinction: PALAIOS, v. 29, p. 652–668.

Ritterbush, K.A., Rosas, S., Corsetti, F.A., Bottjer, D.J., and West, A.J., 2015, Andean sponges reveal long-term benthic ecosystem shifts following the end-Triassic mass extinction: Palaeogeography, Palaeoclimatology, Palaeoecology, v. 420, p. 193–209.

Ryan, J.F., Pang, K., Schnitzler, C.E., Nguyen, A.-D., Moreland, R.T., Simmons, D.K., Koch, B.J., Francis, W.R., Havlak, P., Smith, S.A., Putnam, N.H., Haddock, S.H.D., Dunn, C.W., Wolfsberg, T.G., Mullikin, J.C., Martindale, M.Q., and Baxevanis, A.D., 2013, The genome of the Ctenophore *Mnemiopsis leidyi* and its implications for cell type evolution: Science, v. 342, p. 1242592.

Schiffbauer, J.D., and Xiao, S., 2009, Novel application of focused ion beam electron microscopy (FIB-EM) in preparation and analysis of microfossil ultrastructures: A new view of complexity in early eukaryotic organisms: PALAIOS, v. 24, p. 616–626.

Schindler, T., Wuttke, M., and Poschmann, M., 2008, Oldest record of freshwater sponges (Porifera: Spongillina)—spiculite finds in the Permo-Carboniferous of Europe: Paläontologische Zeitschrift, v. 82, p. 373–384.

Schneider, S., Jager, M., Kroh, A., Mitterer, A., Niebuhr, B., Vodrazka, R., Wilmsen, M., Wood, C.J., and Zagorsk, K., 2013, Silicified sea life–Macrofauna and palaeoecology of the Neuburg Kieselerde Member (Cenomanian to Lower Turonian Wellheim Formation, Bavaria, southern Germany): Acta Geologica Polonica, v. 63, p. 555−610.

Schröder, H.C., Natalio, F., Shukoor, I., Tremel, W., Schlossmacher, U., Wang, X., and Müller, W.E.G., 2007, Apposition of silica lamellae during growth of spicules in the demosponge

Suberites domuncula: Biological/biochemical studies and chemical/biomimetical confirmation: Journal of Structural Biology, v. 159, p. 325–334.

Schröder, H.C., Wang, X., Tremel, W., Ushijima, H., and Müller, W.E.G., 2008, Biofabrication of biosilica-glass by living organisms: Natural Product Reports, v. 25, p. 455−474.

Schuster, A., Vargas, S., Knapp, I.S., Pomponi, S.A., Toonen, R.J., Erpenbeck, D., and Wörheide, G., 2018, Divergence times in demosponges (Porifera): first insights from new mitogenomes and the inclusion of fossils in a birth-death clock model: BMC Evolutionary Biology, v. 18, p. 114.

Sethmann, I., and Wörheide, G., 2008, Structure and composition of calcareous sponge spicules: A review and comparison to structurally related biominerals: Micron, v. 39, p. 209−228.

Sperling, E.A., Robinson, J.M., Pisani, D., and Peterson, K.J., 2010, Where's the glass? Biomarkers, molecular clocks, and microRNAs suggest a 200-Myr missing Precambrian fossil record of siliceous sponge spicules: Geobiology, v. 8, p. 24−36.

Świerczewska-Gładysz, E., 2016, Early Campanian (Late Cretaceous) Pleromidae and Isoraphiniidae (lithistid Demospongiae) from the Łódź-Miechów Synclinorium (central and southern Poland): new data and taxonomic revision: Papers in Palaeontology, v. 2, p. 189−233.

Świerczewska-Gładysz, E., and Jurkowska, A., 2013, Occurrence and paleoecological significance of lyssacinosid sponges in the Upper Cretaceous deposits of southern Poland: Facies, v. 59, p. 763–777.

Tsuyoshi, I., Zhang, L., Feng, Q., and Atsushi, M., 2013, Guadalupian (Middle Permian) radiolarian and sponge spicule faunas from the Bancheng Formation of the Qinzhou allochthon, South China: Journal of Earth Science, v. 24, p. 145–156.

Uriz, M.-J., 2006, Mineral skeletogenesis in sponges: Canadian Journal of Zoology, v. 84, p. 322−356.

Uriz, M.J., Turon, X., and Becerro, M.A., 2000, Silica deposition in Demosponges: spiculogenesis in *Crambe crambe*: Cell Tissue Research, v. 301, p. 299−309.

Vishnevskaya, V., Pisera, A., and Racki, G., 2002, Siliceous biota (radiolarians and sponges) and the Late Devonian biotic crisis: The Polish reference: Acta Paleontologica Polonica, v. 47, p. 211–226.

Wang, X., Schröder, H.C., Wang, K., Kaandorp, J.A., and Müller, W.E.G., 2012, Genetic, biological and structural hierarchies during sponge spicule formation: from soft sol-gels to solid 3D silica composite structures: Soft Matter, v. 8, p. 9501−9518.

Weaver, J.C., Aizenberg, J., Fantner, G.E., Kisailus, D., Woesz, A., Allen, P., Fields, K., Porter, M.J., Zok, F.W., Hansma, P.K., Fratzl, P., and Morse, D.E., 2007, Hierarchical assembly of the siliceous skeletal lattice of the hexactinellid sponge *Euplectella aspergillum*: Journal of Structural Biology, v. 158, p. 93−106.

Webby, B.D., and Trotter, J., 1993, Ordovician sponge spicules from New South Wales, Australia: Journal of Paleontology, v. 67, p. 28–41.

Wood, R., Ivantsov, A.Y., and Zhuravlev, A.Y., 2017, First macrobiota biomineralization was environmentally triggered: Proceedings of the Royal Society of London B, v. 284, p. 20170059.

Xiao, S., Hu, J., Yuan, X., Parsley, R.L., and Cao, R., 2005, Articulated sponges from the Lower Cambrian Hetang Formation in southern Anhui, South China: their age and implications for the early evolution of sponges: Palaeogeography, Palaeoclimatology, Palaeoecology, v. 220, p. 89–117.

Xiao, S., Yuan, X., Steiner, M., and Knoll, A.H., 2002, Macroscopic carbonaceous compressions in a terminal Proterozoic shale: A systematic reassessment of the Miaohe biota, South China: Journal of Paleontology, v. 76, p. 347–376.

Yuan, Y., Cai, C., Wang, T., Xiang, L., Jia, L., and Chen, Y., 2014, Redox condition during Ediacaran–Cambrian transition in the Lower Yangtze deep water basin, South China: constraints from iron speciation and $\delta^{13}C_{org}$ in the Diben section, Zhejiang: Chinese Science Bulletin, v. 59, p. 3638−3649.

Zhang, X., and Pratt, B.R., 2000, A varied Middle Ordovician sponge spicule assemblage from western Newfoundland: Journal of Paleontology, v. 74, p. 386−393.

Zhou, C., and Jiang, S., 2009, Palaeoceanographic redox environments for the lower Cambrian Hetang Formation in South China: Evidence from pyrite framboids, redox sensitive trace elements, and sponge biota occurrence: Palaeogeography, Palaeoclimatology, Palaeoecology, v. 271, p. 279−286.

CHAPTER 6

Closing thoughts on Neoproterozoic eukaryotes and Cambrian animals preserved as carbonaceous compression

QING TANG

Department of Geosciences, Virginia Tech, Blacksburg, VA 24060, USA

6.1 Conclusions

The four case studies of this dissertation report innovative techniques and methods for investigating various groups of carbonaceous fossils from Neoproterozoic microscopic eukaryotes to Cambrian macroscopic metazoans that all with carbonaceous preservation. Specifically, the research in chapter 2 illustrates the application of backscattered electron scanning electron microscopy (BSE-SEM) to unveil hidden biological structures of one of the most common Neoproterozoic carbonaceous compressions; the work in chapter 3 highlights the efficiency of low manipulation maceration technique in extracting well preserved organic-walled microfossils with minimal damage from shale and mudstone; the research in chapter 4 and 5 draws attention to *in situ* mciro- to nanoscale analytical technique for studying carbonaceous fossil altrastructures, chemical composition, and mineralogy. These methods and techniques have shown their great potential for studying paleobiological, biostratigraphic and taphonomic hypotheses, thus improving our knowledge on the evolutionary history of early eukaryotes and animals. Following is the synopsis of each chapter:

Chapter 2 describes new data on the paleobiology of a Proterozoic fossil *Chuaria* (Tang et al., 2017). The discovery allows us to critically reappraise various hypotheses about the biological interpretation of *Chuaria* (Sun, 1987; Sharma et al., 2009). Our data indicate that *Chuaria* was a simple multicellular organism, most possibly a eukaryote with a multicellular vegetative stage in its life cycle. The indication raises an interesting question about its relationship with other microorganisms such as *Symplassosphaeridium* and *Synsphaeridium* that are often found in Neoproterozoic rocks (Tang, 2013; Tang et al., 2015). Although these microfossils are featured by simple multicellularity, they represent an evolutionary stage that underlies the greater diversity and complexity as manifested by the many multicellular organisms

that came afterwards in the Cryogenian and Ediacaran Periods (Butterfield, 2007; Ye et al., 2015). More systematic investigation of *Chuaria* and other carbonaceous compressions using BSE-SEM holds promise to further illuminate the evolution of multicellularity in the Tonian Period.

Chapter 3 reports a diverse organic-walled microfossil assemblage from the Gouhou Formation in North China (Tang et al., 2015). There are totally 22 taxa have been identified, including a new species—*Dictyosphaera tacita* n. sp. More importantly, the co-occurrence of *Trachyhystrichosphaera aimika* and *Valeria lophostriata* from the lower Gouhou Formation indicates that the lower Gouhou Formation is Tonian in age. Given that the middle Gouhou Formation has been dated as early Cambrian deposit (He et al., 2017), the Precambrian-Cambrian (P-C) boundary in Huaibei region might be located between the lower and middle Gouhou Formation, indicating a >200 myr depositional gap (i.e., the Great Unconformity) at the P-C boundary. The magnitude of this unconformity suggests that a major tectonostratigraphic event occurred in the southeastern margin of North China between Tonian and early Cambrian periods.

Chapter 4 reports a new animal species with carbonaceous preservation from the early Cambrian Hetang Formation in South China. The new animal species—*Cambrowania ovata* n. gen. n. sp.—is characterized by a subcircular structure with a network of crossbars and some with a V-shaped cleft. It is reconstructed as either a spherical vesicle or more likely a carapace of bivalved arthropod with limited gaping, ornamented with thickened ribs or ridges on the vesicle or carapace. *Cambrowania ovata* is tentatively interpreted as an arthropod with a bivalved carapace. It adds to the taxonomic diversity of the Hetang biota that is otherwise dominated by benthic sponges.

Finally, chapter 5 provides new insights on spiculogenesis and biomineralization in early sponge animals. The study, using a series of *in situ* micro- and nanoscale analytical technique—including secondary electron scanning electron microscopy (SE-SEM), Backscattered electron scanning electron miscroscopy (BSE-SEM), focused ion beam electron microscopy (FIB-EM), energy dispersive X-ray spectroscopy (EDS), and EDS element mapping, tests sponge fossils with carbonaceous preservation from the early Cambrian Hetang Formation in South China. The data from these analyses show relatively large proportions of organic materials preserved in sponge spicules, indicating that early sponges may have had weakly mineralized spicules or entirely organic skeletons with low preservation potential. Therefore, the biomarker, molecular clock, and spicular data can be reconciled and suggest that although sponge classes may have diverged in the Precambrian, they independently evolved biomineralized spicules later during the Precambrian-Cambrian transition.

6.2 References

Butterfield, N.J., 2007, Macroevolution and macroecology through deep time: Palaeontology, v. 50, p. 41–55.

He, T., Zhou, Y., Vermeesch, P., Rittner, M., Miao, L., Zhu, M., Carter, A., Pogge von Strandmann, P.A.E., and Shields, G.A., 2017, Measuring the 'Great Unconformity' on the North China Craton using new detrital zircon age data: Geological Society, London, Special Publications, v. 448, p. 145–159.

Sharma, M., Mishra, S., Dutta, S., Banerjee, S., and Shukla, Y., 2009, On the affinity of *Chuaria-Tawuia* complex: A multidisciplinary study: Precambrian Research, v. 173, p. 123–136.

Sun, W., 1987, Palaeontology and biostratigraphy of Late Precambrian macroscopic colonial algae: *Chuaria* Walcott and *Tawuia* Hofmann: Palaeontographica Abt. B, v. 203, p. 109–134.

Tang, Q., 2013, Organic-walled microfossils from the early Neoproterozoic Liulaobei Formation in the Huainan region of North China and their biostratigraphic significance: Precambrian Research, v. 236, p. 157–181.

Tang, Q., Pang, K., Yuan, X., Wan, B., and Xiao, S., 2015, Organic-walled microfossils from the Tonian Gouhou Formation, Huaibei region, North China Craton, and their biostratigraphic implications: Precambrian Research, v. 266, p. 296–318.

Tang, Q., Pang, K., Yuan, X., and Xiao, S., 2017, Electron microscopy reveals evidence for simple multicellularity in the Proterozoic fossil *Chuaria*: Geology, v. 45, p. 75–78.

Ye, Q., Tong, J., Xiao, S., Zhu, S., An, Z., Tian, L., and Hu, J., 2015, The survival of benthic macroscopic phototrophs on a Neoproterozoic snowball Earth: Geology, v. 43, p. 507–510.